Distribution Agreement

In presenting this thesis or dissertation as a partial fulfillment of the requirements for an advanced degree from Emory University, I hereby grant to Emory University and its agents the non-exclusive license to archive, make accessible, and display my thesis or dissertation in whole or in part in all forms of media, now or hereafter known, including display on the world wide web. I understand that I may select some access restrictions as part of the online submission of this thesis or dissertation. I retain all ownership rights to the copyright of the thesis or dissertation. I also retain the right to use in future works (such as articles or books) all or part of this thesis or dissertation.

Signature:

_____ _____

Yunlong Zhang Date

Hierarchical Self-assembly of Novel DNA Nanostructures

for Biomedical and Biomimetic Research

By

Yunlong Zhang

Doctor of Philosophy

Chemistry

Yonggang Ke

Advisor

David G. Lynn

Committee Member

Vincent Conticello

Committee Member

Accepted:

Kimberly Jacob Arriola, Ph.D, MPH

Dean of the James T. Laney School of Graduate Studies

Date

Hierarchical Self-assembly of Novel DNA Nanostructures for Biomedical and Biomimetic Research

By

Yunlong Zhang

B.S., Jilin University, 2017

Advisor: Yonggang Ke, Ph.D.

An abstract of
A dissertation submitted to the Faculty of the
James T. Laney School of Graduate Studies of Emory University
in partial fulfillment of the requirements for the degree of
Doctor of Philosophy
in Chemistry
2024

Abstract

Hierarchical Self-assembly of Novel DNA Nanostructures

for Biomedical and Biomimetic Research

By Yunlong Zhang

Structural DNA nanotechnology has been extensively utilized for the self-assembly of an unprecedented number of nanostructures in past decades. However, the pursuit of novel assembly mechanisms and scaling methods of DNA nanostructures has never ended. In this dissertation, we introduce our effort on several challenging projects focusing on this pursuit in structural DNA nanotechnology. Chapter 1 of this dissertation introduces the current state of structural DNA nanotechnology, the challenges that remain unsolved, and the significance of the contribution to solving these challenges. Chapter 2 describes a novel amphiphilic spherical micelle/nanorod assembly from cholesterol-DNA block copolymer. The hierarchical assembly mechanism from spherical micelles to nanorods provides brand new inspiration for future amphiphilic DNA block copolymer design. Chapter 3 describes a simple yet versatile method for the scaling of DNA nanotubes into micrometer-scale rigid DNA bundles. The constructed DNA bundles are reconfigurable and possess high programmability, which allows applications in nanofabrication and biomimetic research. Chapter 4 summarizes the work covered in this dissertation in detail, and also briefly introduces other selected projects that have been conducted during the graduate study.

Hierarchical Self-assembly of Novel DNA Nanostructures for Biomedical and Biomimetic Research

By

Yunlong Zhang

B.S., Jilin University, 2017

Advisor: Yonggang Ke, Ph.D.

A dissertation submitted to the Faculty of the
James T. Laney School of Graduate Studies of Emory University
in partial fulfillment of the requirements for the degree of
Doctor of Philosophy
in Chemistry
2024

Acknowledgements

The pursuance of the Ph.D. title is not an easy task. On the road to Ph.D., no one could accomplish every goal on himself. In my 7 years of PhD study, I received immeasurable support from other people. Without them, it would be impossible for me to finish this long journey.

First, I'd like to thank my advisor, Dr. Yonggang Ke, for his invaluable guidance and support. I'm really lucky to be able to work in Ke lab during my Ph.D. study. Yonggang's innovative way of thinking and his passion for science have always deeply influenced me during my research. His genuineness, humor, and optimism make me feel less stressed and more confident to overcome all the difficulties in both my life and research. I always learn a lot from his extensive knowledge, smart work strategy, and wonderful presentation skills. By the end of my Ph.D. life, I would say this confidently: Joining the Ke lab is one of the best decisions I have ever made, and the experience has benefited me forever.

Secondly, I'd like to thank my graduate committee members, Dr. Vincent Conticello and Dr. David Lynn. During the several rounds of annual qualifying exams, I always got instructive feedback from them, and they have always been encouraging me to think more critically. I also want to thank them for their understanding when I needed to make several last-minute changes to schedules. There is still a long way for me to be fully qualified, but I really appreciate the advice they gave to make me start moving.

Next, I'd like to thank all the group members and alumni in Ke lab. The list may be too long, but I still want to announce their name for respect: Lei Yu, Chunyang Zhou, Kun Zhao, Han Wu, Ruizi Peng, Fengyuan Xu, Yingwei Zhang, Victor Pan, Travis Meyer, Pengfei Wang, Palash Dutta, Kun Zhou, Vicky Zhao, Jack Wang, Yuxin Duan, Dongfang Wang, Shikufa

Mousavi, Sierra Sterling, Tianyi Zhang, Qinyi Lu, Shuang Wang, Luyao Shen. I really thank them for making this challenging journey more colorful and fun, as we have always helped and supported each other to overcome hardship. Among these members, I especially want to thank Kun Zhou and Pengfei Wang, who taught me a lot about doing experiments and led me into the gate of DNA nanotechnology. Without them, it would be much harder for me to learn everything by myself. I really appreciate their selfless contribution to my projects.

I would also like to thank all my collaborators: Dr. Stefan Zauscher, Dr. Gaurav Arya, Dr. Pengfei Wang, Dr. Dong Moon Shin, Dr. Periasamy Selvaraj, Dr. Tianquan Lian. Without them, I would not have a chance to take part in various research projects. Together we put much effort into discovery and publications, and the knowledge I learnt from them has made me a more prepared novice for future complex scientific research.

Finally, I want to thank all my friends in the US, who made my life here more colorful and prevented me from drowning in the failures I got along the road. I especially want to thank Yuxin Duan, Bo Wei, and Zhiyao Zhu, as we had a lot of brilliant memories all over the territory of the US. Without them, my life here would be darker and much more difficult to come through. I also want to thank all my old friends back in China. Although we are not together, I know they are always sincerely wishing me all good. And last but not least, I would like to give my biggest thanks to my family. They have always been supporting me on the other end of the earth in their own way, and without their support, I would not be able to come to the US for post-graduation study. They give me all the courage, motivation, and confidence to keep going. It will never be enough for me to express my love and appreciation to them.

Table of Content

List of Figures and Tables

List of Abbreviations

Abbreviation	Full Name
DNA	Deoxyribonucleic acid
C	Sytosine
G	Guanine
A	Adenine
T	Thymine
DX	Double-crossover
2D	Two dimensional
3D	Three dimensional
RNA	Ribonucleic acid
mRNA	Messenger RNA
SELEX	Systematic evolution of ligands by exponential enrichment
DBC	DNA block copolymer
1D	One dimensional
Chol-DNA	Cholesterol-DNA
TEG	Triethylene glycol
TEM	Transmission electron microscopes
AFM	Atomic force microscopes
HPLC	High-performance liquid chromatography
DI	Deionized
IDT	Integrated DNA Technologies
PBS	Phosphate-buffered saline

UF	Uranyl formate
PAGE	Polyacrylamide gel electrophoresis
TE	Tris-EDTA buffer
CLSM	Confocal laser scanning microscopy
AuNP	Gold nanoparticle
STV	Streptavidin
I	Inhibitor
AI	Anti-inhibitor
DANP	DNA-aptamer nanoparticle
Tdt	Terminal deoxynucleotidyl polymerase
RNAi	RNA interference
siRNA	Small interfering RNA
shRNA	Small hairpin RNA
ssRNP	Single-stranded RNA nanoparticle

Chapter 1. Introduction of structural DNA nanotechnology

1.1 Structural DNA nanotechnology

1.1.1 Introduction

In nature, deoxyribonucleic acid (DNA) is the main genetic information carrier for most living organisms. However, at the end of last century, DNA was found to be more than just the secret of life: In the 1980s, researchers started to employ DNA as the basic material to build newly developed nano- to micro-scale structures (1). Since then, the era of structural DNA nanotechnology has begun.

Structural DNA nanotechnology refers to the field where DNA is used as basic building blocks to construct artificial nanostructures through self-assembly pathways (2). The establishment of structural DNA nanotechnology lies in the unique characteristics of DNA. For example, the canonical binding pattern of the DNA biopolymers, known as Watson-Crick base pairing, is simple, predictable, and versatile among all kinds of DNA molecules (3). This simple rule indicates that DNA is a kind of biopolymer made of 4 kinds of deoxynucleotides, which are differentiated by four nucleobases: Cytosine (C), guanine (G), adenine (A), and thymine (T). In a normal Watson-Crick base pairing pattern, A mainly pairs to T through 2 hydrogen bonds, and C mainly pairs to G through 3 hydrogen bonds. This simple yet predictable constitution makes the interaction between DNA molecules highly programmable, which is a highly preferred characteristic compared with other materials such as peptides. Moreover, most DNA molecules employ a double helix conformation that is known as B-form DNA. B-form DNA double helix has a well-defined nanoscale morphology, with a diameter of 2 nm and a helical turn of 3.4nm in average. This uniformity of DNA molecular structure allows the versatile application of DNA as the building material towards various utilities.

The concept of structural DNA nanotechnology can be traced back to Nadrian Seeman's hypothesis of using DNA to assist the crystallization of proteins and peptides (4). From then on, over decades of development, structural DNA nanotechnology has become a major research topic nowadays, and DNA has been proved to be a designer molecule for the construction of unprecedented numbers of nanostructures. These nanostructures can be both static or dynamic, constructed with unparallel complexity and unique properties. Besides, these DNA nanostructures are increasingly utilized on their own or with other materials for a variety of applications, including nanofabrication, nanomachine, and drug delivery (5-7). In the following sections, we will briefly introduce the designing and assembly methods of structural DNA nanotechnology. Representative examples will be covered to show the advantages and merits of DNA nanostructures. Further on, the application of DNA nanostructures related to the projects discussed in this thesis will be briefly introduced, along with the challenges and perspectives of these applications.

1.1.2 Methods for DNA nanostructure construction

Most strategies to construct DNA nanostructures can be categorized into two basic strategies: DNA tile and DNA origami. In this section, these two strategies will be briefly reviewed, and representative examples will be presented.

DNA tiles are defined as a set of small artificial DNA structures consisting of several DNA single strands. These DNA single strands with uniquely designed sequences first assemble into DNA tiles, then hierarchically assemble into large DNA nanostructures. The first DNA tile structure, named immobile 4-way junction, was designed to resemble the naturally occurring Holiday junctions (Figure 1-1a) (1). Based on this first work, DNA tiles with other numbers of strands were successfully assembled (8-10). However, these DNA tiles failed to form higher-order structures due to the high flexibility. The first DNA tile that was able to form large DNA

nanostructure was the DNA double crossover (DX) tile structure, which was assembled by a set of DNA single strands with a specific binding pattern to form two crossover motifs (11). Such 2-arm DX tile structure was able to assemble into two-dimensional (2D) DNA crystals through sticky-end mediated self-assembly (Figure 1-1b). Since then, other more complex DNA tiles have been developed and successfully self-assembled into 2D nanostructures (12-15). Furthermore, in 2009, three-dimensional (3D) DNA crystals were finally achieved and up to now, these DNA tile-based structures are still being heavily investigated (16-19).

However, these DNA tile designs could only produce periodic and symmetric structures, resulting in low programmability and versatility. Thus, DNA brick method was later introduced, where the single-strand DNA was treated as a tile/crick to interact with other tiles/bricks to form 2D or 3D objects through uniquely designed sequences (Figure 1-1c) (20-23). Due to its modularity, this method was able to fulfill the purpose of high-throughput DNA nanostructure building with arbitrary sizes and shapes.

On the other hand, in 2006, DNA origami method was first introduced (24). Origami, originally a Japanese word, refers to the art of folding paper into arbitrarily shaped objects. Similarly, DNA origami is a process of folding DNA into arbitrarily shaped objects: a long single-strand DNA called scaffold strand is folded into prescribed objects with the help of hundreds of short DNA single strands called staple strands. This is made possible by specifically designing the staple strands' sequence to be complementary to different parts of the scaffold strand, thus the staple strands are working as the staples to crosslink spatially far-away segments of the scaffold strand (Figure 1-1d). During the assembly of DNA origami, an appropriate concentration of cations (Mainly Na^+ and Mg^{2+}) is required to reduce the electrostatic repulsion caused by the high compactness of negatively charged DNA strand backbones. DNA origami was first reported by Paul Rothemund, where a set of 2D objects, including the famous smiley face origami, were constructed (24). Further on, 3D DNA origami objects were reported as a hollow

tetrahedron and a hollow cube structure (25, 26). However, these hollow 3D objects were based on the folding of flat 2D sheets, confining the complexity and arbitrability of 3D object design. Thus, in later reports, solid 3D objects and 3D origami objects with curvatures were successfully assembled to resolve this problem (27-30). As these objects were defined as lattice-based DNA origami, wireframe DNA origami was later introduced to produce soft and porous nanostructures (Figure 1-1e) (31, 32). The compactness of DNA strands in wireframe DNA origami was lower than in lattice-based DNA origami, resulting in a lower requirement of cation concentration and may find more potential in intracellular applications.

One advantage of structural DNA nanotechnology is the accessibility of design software and algorithms to assist the DNA sequence design. Two of the most common software are Tiamat for the design of DNA tile structures, and caDNAno for the design of DNA origami structures (31, 33). Besides, other software and algorithms can also assist in the analysis of DNA nanostructures, such as Cando for DNA nanostructure computational feedback and visualization (34). With these tools, the design process of complex DNA nanostructures is largely facilitated.

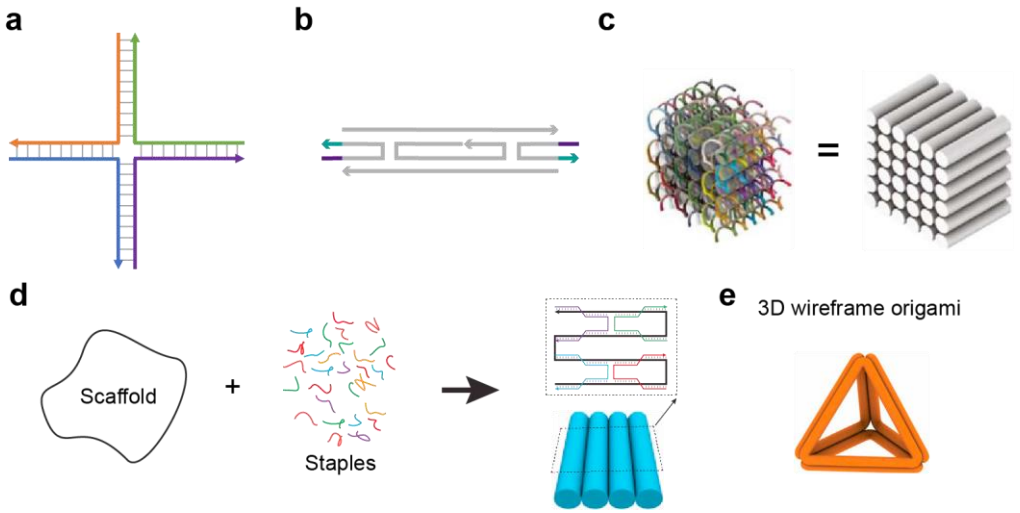

Figure 1-1. Methods for DNA nanostructure construction. (a) Artificial immobile 4-way junction assembled from four DNA single strands. (b) An example of DNA double-crossover (DX) tile. Grey sequences are backbones, and colored sequences are sticky ends used for the connection of DX tiles. (c) DNA bricks for the assembly of 2D and 3D objects. Figures reprinted with permission from reference (22). (d) Basic design strategy and assembly mechanism of DNA origami. Figures reprinted with permission from reference (35). (e) An illustration of 3D wireframe origami structure. Figures reprinted with permission from reference (35).

1.2 Applications of structural DNA nanotechnology

In past decades, DNA nanostructures have been utilized in various applications and investigations. Here, selected applications that are closely related to the projects in this thesis will be briefly reviewed.

1.2.1 Dynamic DNA nanostructures

The ability to design complex morphology precisely gives structural DNA nanotechnology the potential to construct nanodevices and nanomachines that may employ dynamic processes, such as motion or conformational change. Constructing dynamic DNA nanostructures relies on the integration of mechanical and chemical properties of DNA molecules, such as flexibility and biochemical addressability. Up to now, a wide range of dynamic DNA nanodevices, either 2D or 3D, have been constructed. They are capable of various dynamic processes, including programmed motion, conformational change, and tunable distribution of molecular states.

Representative examples of dynamic DNA nanostructures include DNA motors and walkers (36-38), containers with responsive lids (39), reconfigurable strand systems (40-42), and mechanical joints (43-46). Common triggers for the dynamic process include DNA or RNA strands (Figure 1-2a) (47), other molecules (48), solution condition change (49), and temperature and light change (50, 51). One ultimate goal for these DNA nanodevices is to serve as the biomimetic analogs to natural biological processes, such as the mimic of myosin and actin rotor (52, 53). We believe that with further development, these dynamic DNA nanostructures will largely contribute to the understanding of molecular processes and the establishment of artificial cells.

1.2.2 Nanofabrication

Owing to the high specificity, addressability, and programmability of DNA nanostructures, they have been widely used as the breadboard to organize a variety of other molecules and materials for nanofabrication. DNA nanotructure has been utilized as template structures for the organization of both synthetic nanomaterial components and biomolecules, as molds for nanoparticle synthesis, as masks for nanolithography, and as scaffolds for artificial enzyme cascades, etc (35). The fabricated structures and devices have been further utilized for numerous other applications, including nanoplasmonics, biosensing, and drug delivery.

To classify these works according to the nanomaterials fabricated, three main classifications are the fabrication of inorganic materials, synthetic molecules and polymers, and biomaterials. For inorganic material fabrication, silica, metal particles, and semiconductors are always hot topics in this area due to their close relationship to quantum science (Figure 1-2b) (54). The fabrication of molecular catalysts was also demonstrated to be capable of tuning the catalysis reaction for organic synthesis (55). Finally, the nanofabrication of nucleic acids, enzymes, and other biopolymers has led to complex spatial and temporal arrangement of biomolecules on DNA nanostructure base, which further led to enhanced biomedical activity and new biological functionality (56, 57). However, there are still some challenges in this field, such as the size limitation of the DNA nanostructure base. Further advances in DNA nanostructure construction method are also required for the actual application of these fabricated structures.

1.2.3 Drug delivery

Nowadays, advanced disease therapeutics usually require the targeted delivery of drugs to abnormal cells and tissues. This can increase therapeutic efficiency while also reducing side effects. To fulfill this requirement, various materials, including synthetic polymers, metal nanoparticles, and biopolymers, have been utilized for the construction of drug delivery agents. Among these materials, DNA nanostructure is one of the most promising options owing to its

high biocompatibility, high programmability, and the capability for targeted and controlled payload release. A number of studies have been conducted to construct various DNA nanostructures and fabrication schemes to load, deliver, and release molecular drugs for cancer treatment, gene silencing, and immune stimulation. Besides, the payloads loaded on the DNA nanostructures are also capable of the target location and responsive release to complete designated tasks.

The most common application of DNA nanostructures in drug delivery is the delivery of anticancer drugs. This concept was first realized in 2012 by Bogberg and Ding groups, where doxorubicin was loaded onto DNA origami and internalized into breast cancer cells to induce cancer apoptosis (58). Further on, various therapeutic payloads, including small molecule drugs (59), quantum dots (60), antibodies (61), and therapeutic oligonucleotides (Figure 1-2c) (62), have all been successfully delivered and showed certain levels of improved therapeutic effects on cancer cells both *in vitro* and *in vivo*. However, certain drawbacks of using DNA nanostructures for drug delivery still remain to be resolved, such as the cost of preparation, requirement of high cation concentration, and biological barrier penetration (35).

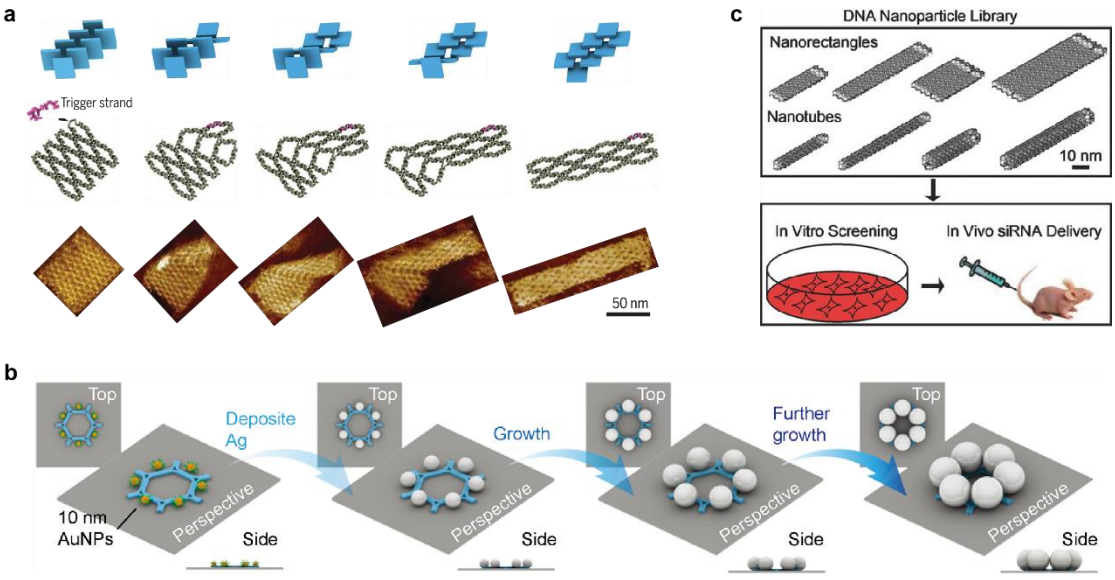

Figure 1-2. Representative examples of DNA nanostructure applications from Ke lab. (a) An example of dynamic DNA nanostructure: Reconfiguration of DNA Molecular Arrays Driven by Information Relay. Figures reprinted with permission from reference (63). (b) An example of nanofabrication: Magnetic Plasmon Networks Programmed by Molecular Self-Assembly. Figures reprinted with permission from reference (64). (c) An example of DNA nanostructure-based drug delivery: Systemic Delivery of Bcl2-Targeting siRNA by DNA Nanoparticles Suppresses Cancer Cell Growth. Figures reprinted with permission from reference (62).

1.3 Challenges and perspectives of structural DNA nanotechnology

Although structural DNA nanotechnology is already powerful in various applications, there are still many challenges and perspectives that remain to be solved. In this section, we will cover several challenges and perspectives that are closely related to the projects in this thesis.

1.3.1 Scaling up DNA nanostructures

Up to now, nearly all arbitrary morphology in nanometer scale can be realized by structural DNA nanotechnology. However, scaling up the assembled structure from nano-scale to micro-scale or higher is still challenging. For example, in the assembly of DNA origami, a long DNA scaffold strand is folded into a 3D structure that is held in its desired shape by multitude of staple strands. However, the maximum size of a DNA origami object is limited by its scaffold strand length, which becomes prone to shearing beyond a certain length (54, 65). Researchers have tried to create larger structures by assembling single origamis together, but efficiently linking them to each other has been challenging (66, 67). Thus far, these roadblocks have prevented the creation of DNA nanostructures above the sub-micron range, which would significantly expand their usability in real-world applications.

Along with the strategy to link the already assembled DNA nanostructures together, another strategy is to construct higher-scale DNA structures from the bottom. However, this is also not easy to realize, since higher-scale structures will require more DNA strands, and in order to guarantee the orthogonality of these strands, the workload on DNA strand sequence design would be near-exponentially growing. Several groups have successfully realized this strategy. For example, Yin and coworkers constructed a set of gigadalton-sized 3D nanostructures using DNA bricks, of which the assembly model closely resembles Lego blocks (23). These successful results are truly elegant and stunning, vividly reflecting the robustness of this

strategy. However, a module with simple constitution and low cost while retaining the potential to construct complex DNA macro-structures is still in demand.

We envision that a method that could allow the assembly of DNA structures with the size above micrometer while also avoiding the drawbacks of previous methods would be extremely beneficial for potential applications in material science, biomedical science, and surface engineering.

1.3.2 Optimization on drug delivery systems

DNA nanostructures have some critical characteristics to be utilized as an effective delivery vehicle. For example, good biocompatibility, high addressability, and precise control of morphology and surface chemistry (65). However, certain drawbacks still exist that hinder the actual application of DNA nanostructures for drug delivery. First of all, for DNA origami, a fast, economical, and environment-friendly production method of scaffold and staple strands are still in urgent demand to reduce the overall cost of DNA nanostructure preparation. Secondly, the *in vitro* and *in vivo* stability of DNA nanostructures is another main issue due to the lack of high cation concentration (Na^+ and Mg^+) required by the assembly in physiological conditions. Finally, to effectively reach the spot of interest for targeted delivery and drug release, DNA nanostructures need to penetrate a set of biological barriers, such as the blood vessel barrier penetration after administration and evasion from the cleanse of immune systems. To solve these problems, extensive study is still highly demanded.

Besides the hindrance, new discoveries also put forward higher demands for DNA nanostructure-based drug delivery systems. Historically, traditional drug delivery systems focused on simple shape construction, such as nanospheres and nanotubes (68). During the last decades, a number of research have revealed that delivery systems with prescribed shapes, like tetrahedrons, can lead to prolonged in vivo circulation time, enhanced biological barrier

penetration efficiency, well-controlled slow-release function, and reduced overall cytotoxicity (69, 70). Furthermore, these delivery systems usually possess higher drug loading capacity and enable the precise incorporation of an accurate number of payloads at the specified position. By forming a bridge between same or different targets, these delivery systems can increase the target local concentration and enhance the immune checkpoint activation (71, 72). As such geometry and multi-valency effect proved to largely contribute to the improvement of overall therapeutic effect, we envision that the enrollment of these knowledge to create next-generation drug delivery agents will be a promising direction to pursue.

1.3.3 From multi-stranded to single-stranded, from DNA to RNA

In addition to tile-based DNA nanostructure and DNA origami, single-stranded DNA nanostructures are another toolset that holds promising potential. As its name indicated, single-stranded DNA nanostructures are assembled from one lone single strand DNA. Compared to conventional multi-stranded methods, single-stranded DNA nanostructures are more resistant to enzymatic degradation due to the decreased number of 5' and 3' ends on a single DNA strand. Besides, the modularity of single-stranded DNA nanostructures is higher, as a set of single strand DNA could serve as a canvas for building a large number of different higher-ordered objects. However, single-stranded DNA nanostructures also have their drawbacks, including the difficulty on sequence design, the low yield of correct nanostructures, and higher requirements on cation concentrations. Not many labs have successfully realized this kind of novel DNA nanostructures (73, 74); However, this method is certainly still a promising one.

Nanostructures made from DNA are already potent platforms for various applications. However, in recent years, researchers have started to pay more attention on using RNA to self-assemble into nanostructures. Compared to DNA self-assembly, RNA self-assembly has several advantages. For instance, RNA can be readily bulk-produced by transcription or

bacteria, which provides the potential to largely decrease the cost of DNA production. Besides, RNA nanostructures are believed to be more compatible with physiological environments with higher thermal stability *in vivo* (75). However, unlike the guidance by the simple Watson-crick base pairing rule, RNA's conformation is largely influenced by noncanonical binding patterns, hence much more challenging to predict and design. Besides, RNA is known to be more vulnerable to nuclease degradation, which largely hinders the use of RNA nanostructures in physiological conditions. In recent years, both multi-stranded and single-stranded RNA origami have been successfully assembled, showing certain improved properties over their DNA counterparts (76-78). We believe that further investigation on RNA nanostructures will allow the settlement of the drawbacks and make them a valuable complementary toolset for structural DNA nanotechnology.

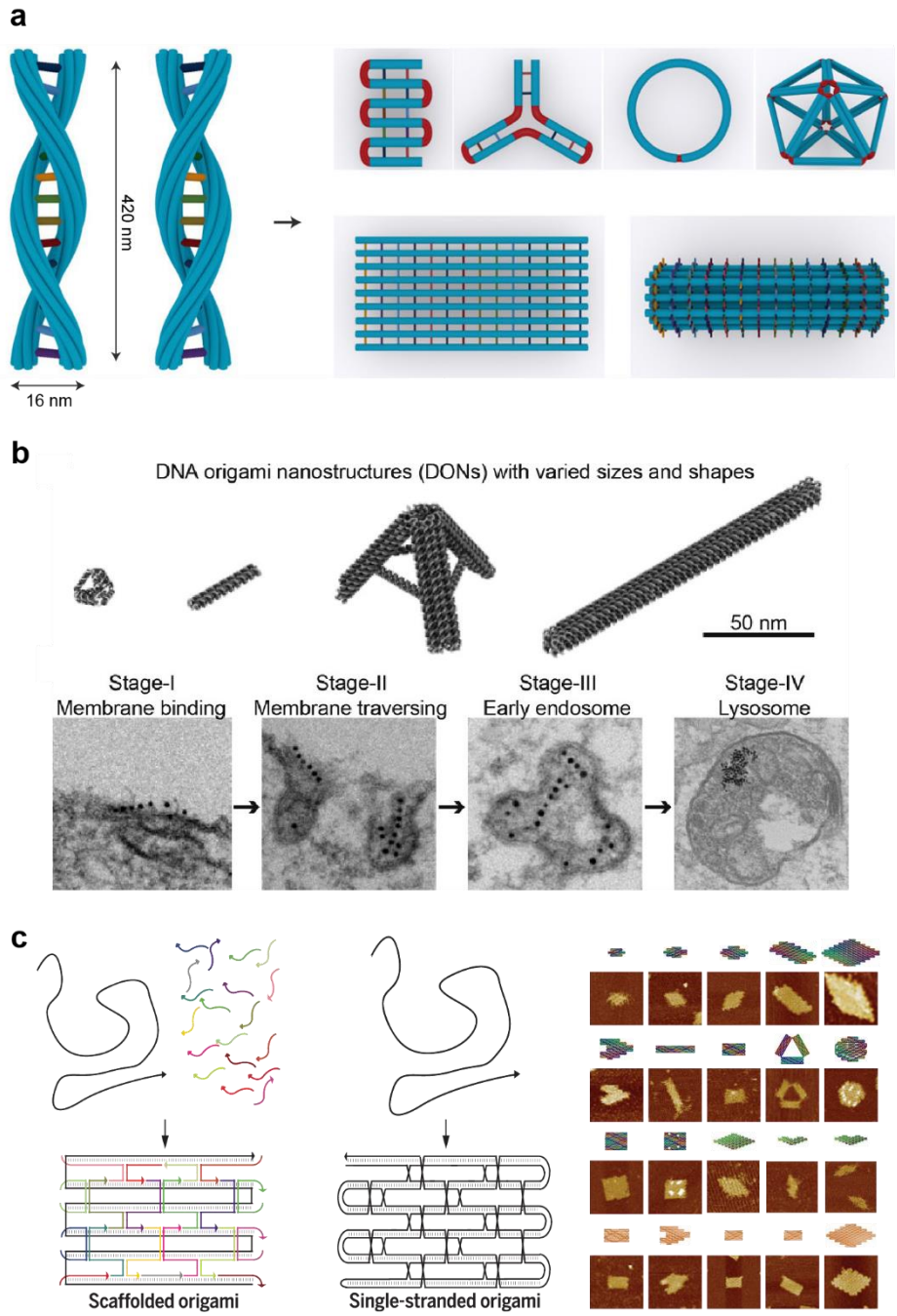

Figure 1-3. Challenges and perspectives of structural DNA nanotechnology. (a) An example of the scaling of DNA nanostructures: Meta-DNA structures. Figures reprinted with permission from reference (66). (b) An example of the optimization on drug delivery systems: Visualization of the Cellular Uptake and Trafficking of DNA Origami Nanostructures in Cancer Cells. Figures reprinted with permission from reference (70). (c) Single-stranded DNA and RNA origami. Figures reprinted with permission from reference (74).

1.4 Other nucleic acid-related backgrounds involved in this thesis

One of the merits of structural DNA nanotechnology is its high versatility to combine with other techniques, especially other nucleic acid-related ones. In this section, several DNA or RNA-based techniques will be briefly introduced.

1.4.1 DNA strand displacement

Strand displacement process, where one intruder DNA single strand displaces another single strand from a DNA helix, was initially investigated for its relevance to genetic recombination. After the emergence of the concept of structural DNA nanotechnology, this process has been widely involved in constructing dynamic DNA nanomachines. Strand displacement can happen under various driving force, but the most commonly utilized one is the toehold-mediated strand displacement. Toehold-mediated strand displacement is based on the Watson-Crick hybridization of two complementary strands of DNA and makes use of a process called branch migration (79). It is an enzyme-free molecular tool to exchange one strand of DNA with another strand via the binding of toehold region (Figure 1-4a). The first use of toehold-mediated strand displacement in DNA nanotechnology was in 2000 by Yurke et al., where strand displacement process was employed as the driving force of a dynamic DNA nanomachine (80). Since then, toehold-mediated strand displacement has been utilized with increasing sophistication and towards unprecedented applications (81).

One of the main applications of toehold-mediated strand displacement focuses on the construction of dynamic DNA nanomaterials, including DNA walker and switches, reconfigurable nanostructures and containers, reaction cascade, DNA computing, and patterning and lithography (82-86). Besides, toehold-mediated strand displacement can also find applications in biomedical areas, including biosensors, pathogen detection, and gene editing (87-89). In a word, strand displacement, especially toehold-mediated strand

displacement, is one of the most important foundations for the construction of dynamic DNA nanostructures.

In this thesis, strand displacement process will be involved in the project described in chapter 3.

1.4.2 RNA transcription and Central dogma

Ribonucleic acid (RNA) is one of the most essential biopolymers for most biological functions in nature. Unlike DNA, RNA is assembled as a chain of nucleotides, and the four nucleobases for RNA are cytosine (C), guanine (G), adenine (A), and uracil (U). According to the central dogma (Figure 1-4b), in most living organisms, RNA is mainly produced by the transcription process from DNA. RNA transcription is the process of transferring the information from a segment of DNA into RNA. This process is mainly happening in the cell nucleus, pseudo-nucleus, and organelles containing genetic information. RNA polymerase and other helping enzymes are required to catalyze the reaction. Nowadays, cell-free reaction kits for RNA transcription are widely available and have become a routine method for research labs to obtain high-quality single-stranded RNA samples. This process is referred to as *in-vitro* transcription. However, when transcribing DNA templates with artificially designed sequences, the transcription yield may be largely compromised, especially when the transcribed RNA has large portions of secondary structures (90).

The central dogma of molecular biology is an explanation of the flow of genetic information in a biological system. According to the central dogma, the transcribed RNA that can encode proteins is called messenger RNA (mRNA). In most living organisms, mRNA will be consumed after several rounds of translation into proteins, so that the relationship between template DNA and mRNA is a one-way process. However, some viruses may encode reverse transcriptase, which allows the reverse transcription from RNA back to DNA. Besides, some

virus, like alpha virus, possesses an RNA-to-RNA amplification process owing to the presence of a special replicase (91). These special routes that are not included in the original version of central dogma have found various novel applications, such as the establishment of cDNA library and the self-amplifying mRNA vaccine (92).

In this thesis, RNA-related techniques are involved in one project described in chapter 4.

1.4.3 Aptamer

Over the past hundred years, antibodies, mainly as proteins, have demonstrated decent capability in target sensing, immune blockade, bioassay, etc. However, the response rate, the shelf life, and the development difficulty of antibodies are still far from satisfactory (93). In addition to antibodies, in recent years, synthetic antibodies, particularly DNA and RNA aptamers, started to rise as another family of promising molecules for effecting binding and blockade.

Aptamers are single-stranded DNA or RNA oligonucleotides that bind with high affinity and specificity to target antigens such as small molecules, peptides, proteins, or cell (94). Most aptamers are based on a specific oligomer sequence of 20-100 base, some having chemical modifications for functional enhancements. They typically have complex secondary and tertiary structures as binding spots for the target (Figure 1-4c). The development of aptamers is based on an assay called Systematic evolution of ligands by exponential enrichment (SELEX), during which the best aptamers from the starting oligonucleotide library will be selected after several rounds of binding assay. This method is fast and versatile, thus allowing the selection of aptamers targeting arbitrary antigens to be finished in a short time (95).

Compared to antibodies, DNA aptamers have a wider target range due to the ease of producing a large variety of strands with different lengths and sequences. Besides, due to the nature of the DNA and protein, DNA aptamers exhibit a much longer shelf life than antibodies under

preferred storage condition. According to previous research, aptamers also usually exhibit lower immunogenicity than antibodies (96). However, the actual use of these aptamers is still hindered by their limited in vivo stability and the lack of efficient in vivo delivery systems to overcome biological barriers. To solve these problems, several previous research has proved that structural DNA nanotechnology is a great candidate to deliver aptamers while protecting them from degradation (97, 98).

In this thesis, aptamers will be involved in one project described in chapter 4.

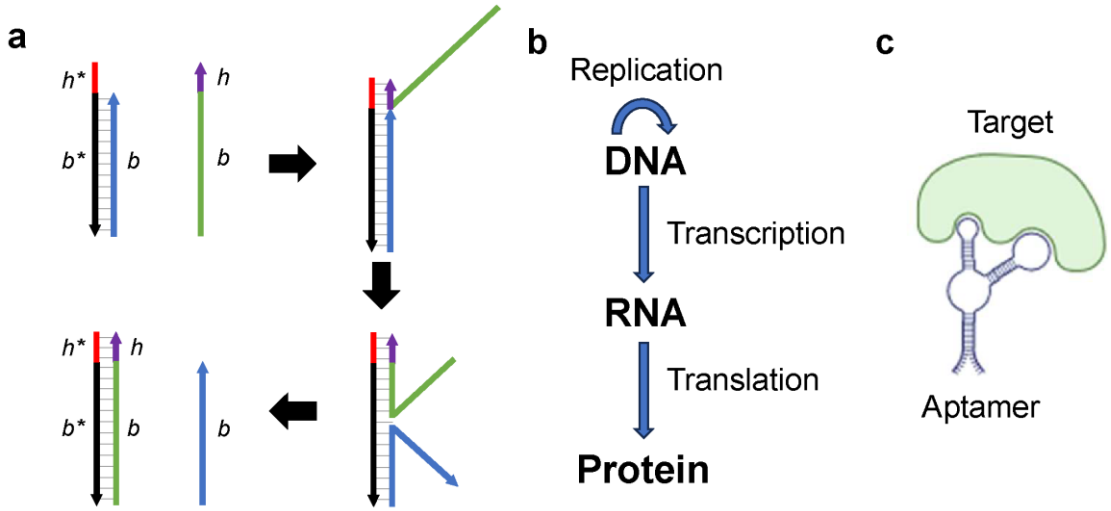

Figure 1-4. Other nucleic acid-related backgrounds involved in this thesis. (a) A typical toehold-mediated strand displacement process. *h* is the toehold. *h* and *h** have complementary sequence, while *b* and *b** have complementary sequence. (b) The original version of the central dogma of molecular biology. Note that the reverse transcription and RNA self-amplification are not included in the original version. (c) An illustration of aptamer binding to its target molecule.

1.5 Aim and scope of this dissertation

Structural DNA nanotechnology is the design and manufacture of artificial nucleic acid structures for technological uses. The use of structural DNA nanotechnology has dramatically improved the complexity, scalability, addressability, and versatility of self-assembled nanostructures. The methods for DNA self-assembly in structural DNA nanotechnology has led to numerous uses in various fields, including nano-electronics and nano-photonics, artificial reaction networks, biomedical research, and so forth. Up to now, structural DNA nanotechnology has become a powerful and indispensable solution in nanotechnology areas (2). However, certain drawbacks and potential improvements still exist for structural DNA nanotechnology. For example, the cost of DNA strand synthesis and the difficulty in design still hinder the scaling up of DNA nanostructures into micrometer or higher scales (35). Besides, newly developed assembly mechanisms and pathways of DNA nanostructures will never be enough for the actual applications of structural DNA nanotechnology.

Thus, this thesis will mainly focus on the development of novel assembly pathways for structural DNA nanotechnology. Our ultimate goal is to fulfill the need for biomedical and biomimetic research with our developed methods and nanostructures. Two main questions are to be answered in this dissertation: Firstly, by tuning the reaction condition, can we use routinely used, most usual molecules to construct novel DNA nanostructures for biomedical research? Secondly, by employing simple model structures, can we develop a direct yet powerful method to scale up DNA self-assembly into micro-meter or even higher scale? To answer these questions, two main projects are introduced and discussed in this dissertation.

In chapter 2, we reported a novel amphiphilic spherical micelle/nanorod assembly from cholesterol-DNA block copolymer. We discovered that under acidic conditions, chol-DNA with certain DNA sequences could form micellular nanostructures, including spherical

micelles and nanorods, through a hierarchical assembly pathway. Extensive study was carried out to confirm that the morphology of the assembly was mainly controlled by salt concentration, solution pH, and DNA sequence. Thinking of the popularity of using DBC to construct amphiphilic nano-vehicle for drug delivery recent years, we believe that our work can find valuable applications in future biomedical research.

In chapter 3, we reported a simple yet versatile method for the scaling of DNA double-crossover tiles into micrometer-scale rigid DNA bundles. The assembly mechanism of this system is a hierarchical pathway mainly enabled by the flanking cohesive linker design. Along with the buffer conditions, such cohesive linker provides capability to better control the major assembly parameters including width, compactness, constitution, and reconfigurability. Through the fabrication of model materials on DNA bundles, we envision that this project can provide strategies for future rational design on constructing macro-sized biomimetic functional materials.

Besides these two main projects, during my Ph.D. study, I also participated in other projects towards the application of structural DNA nanotechnology in biomedical and biomimetic research. These projects were either unfinished, discontinued, or only partially contributed by me. Thus, they are only briefly discussed in chapter 4. However, we still believe that along with the two main projects, all these works will largely contribute to future development of DNA nanotechnology and provide valuable reference to the design of DNA-based building blocks for nanostructure self-assembly. Besides, the close relationship between these projects and the practical biomedical and biomimetic demands will largely benefit the investigation and verification of future therapeutics.

1.6 References

1. Kallenbach NR, Ma RI, Seeman NC. An Immobile Nucleic-Acid Junction Constructed from Oligonucleotides. Nature. 1983;305(5937):829-31.

2. Ke YG, Castro C, Choi JH. Structural DNA Nanotechnology: Artificial Nanostructures for Biomedical Research. Annu Rev Biomed Eng. 2018;20:375-401.

3. Watson JD, Crick FHC. Molecular Structure of Nucleic Acids - a Structure for Deoxyribose Nucleic Acid. Nature. 1953;171(4356):737-8.

4. Seeman NC. Nucleic-Acid Junctions and Lattices. J Theor Biol. 1982;99(2):237-47.

5. Tian Y, Wang T, Liu WY, Xin HL, Li HL, Ke YG, et al. Prescribed nanoparticle cluster architectures and low-dimensional arrays built using octahedral DNA origami frames. Nat Nanotechnol. 2015;10(7):637-+.

6. Zhang C, Ma XY, Zheng XD, Ke YG, Chen KT, Liu DS, et al. Programmable allosteric DNA regulations for molecular networks and nanomachines. Sci Adv. 2022;8(5).

7. Douglas SM, Bachelet I, Church GM. A Logic-Gated Nanorobot for Targeted Transport of Molecular Payloads. Science. 2012;335(6070):831-4.

8. Ma RI, Kallenbach NR, Sheardy RD, Petrillo ML, Seeman NC. Three-arm nucleic acid junctions are flexible. Nucleic Acids Res. 1986;14(24):9745-53.

9. Wang YL, Mueller JE, Kemper B, Seeman NC. Assembly and characterization of five-arm and six-arm DNA branched junctions. Biochemistry. 1991;30(23):5667-74.

10. Wang X, Seeman NC. Assembly and characterization of 8-arm and 12-arm DNA branched junctions. J Am Chem Soc. 2007;129(26):8169-76.

11. Fu TJ, Seeman NC. DNA double-crossover molecules. Biochemistry. 1993;32(13):3211-20.

12. Winfree E, Liu F, Wenzler LA, Seeman NC. Design and self-assembly of two-dimensional DNA crystals. Nature. 1998;394(6693):539-44.

13. Yan H, Park SH, Finkelstein G, Reif JH, LaBean TH. DNA-templated self-assembly of protein arrays and highly conductive nanowires. Science. 2003;301(5641):1882-4.

14. He Y, Chen Y, Liu H, Ribbe AE, Mao C. Self-assembly of hexagonal DNA two-dimensional (2D) arrays. J Am Chem Soc. 2005;127(35):12202-3.

15. He Y, Tian Y, Ribbe AE, Mao C. Highly connected two-dimensional crystals of DNA six-point-stars. J Am Chem Soc. 2006;128(50):15978-9.

16. He Y, Ye T, Su M, Zhang C, Ribbe AE, Jiang W, et al. Hierarchical self-assembly of DNA into symmetric supramolecular polyhedra. Nature. 2008;452(7184):198-201.

17. Zhang C, Su M, He Y, Zhao X, Fang PA, Ribbe AE, et al. Conformational flexibility facilitates self-assembly of complex DNA nanostructures. Proc Natl Acad Sci U S A. 2008;105(31):10665-9.

18. Zhang C, Wu W, Li X, Tian C, Qian H, Wang G, et al. Controlling the chirality of DNA nanocages. Angew Chem Int Ed Engl. 2012;51(32):7999-8002.

19. Zhang C, Ko SH, Su M, Leng Y, Ribbe AE, Jiang W, et al. Symmetry controls the face geometry of DNA polyhedra. J Am Chem Soc. 2009;131(4):1413-5.

20. Ke YG, Ong LL, Shih WM, Yin P. Three-Dimensional Structures Self-Assembled from DNA Bricks. Science. 2012;338(6111):1177-83.

21. Wei B, Dai MJ, Yin P. Complex shapes self-assembled from single-stranded DNA tiles. Nature. 2012;485(7400):623-+.

22. Ke YG, Ong LL, Sun W, Song J, Dong MD, Shih WM, et al. DNA brick crystals with prescribed depths. Nat Chem. 2014;6(11):994-1002.

23. Ong LL, Hanikel N, Yaghi OK, Grun C, Strauss MT, Bron P, et al. Programmable self-assembly of three-dimensional nanostructures from 10,000 unique components. Nature. 2017;552(7683):72-7.

24. Rothemund PW. Folding DNA to create nanoscale shapes and patterns. Nature. 2006;440(7082):297-302.

25. Andersen ES, Dong M, Nielsen MM, Jahn K, Subramani R, Mamdouh W, et al. Self-assembly of a nanoscale DNA box with a controllable lid. Nature. 2009;459(7243):73-6.

26. Ke Y, Sharma J, Liu M, Jahn K, Liu Y, Yan H. Scaffolded DNA origami of a DNA tetrahedron molecular container. Nano Lett. 2009;9(6):2445-7.

27. Ke Y, Douglas SM, Liu M, Sharma J, Cheng A, Leung A, et al. Multilayer DNA origami packed on a square lattice. J Am Chem Soc. 2009;131(43):15903-8.

28. Douglas SM, Dietz H, Liedl T, Hogberg B, Graf F, Shih WM. Self-assembly of DNA into nanoscale three-dimensional shapes. Nature. 2009;459(7245):414-8.

29. Ke Y, Voigt NV, Gothelf KV, Shih WM. Multilayer DNA origami packed on hexagonal and hybrid lattices. J Am Chem Soc. 2012;134(3):1770-4.

30. Dietz H, Douglas SM, Shih WM. Folding DNA into twisted and curved nanoscale shapes. Science. 2009;325(5941):725-30.

31. Han D, Pal S, Yang Y, Jiang S, Nangreave J, Liu Y, et al. DNA gridiron nanostructures based on four-arm junctions. Science. 2013;339(6126):1412-5.

32. Liu W, Halverson J, Tian Y, Tkachenko AV, Gang O. Self-organized architectures from assorted DNA-framed nanoparticles. Nat Chem. 2016;8(9):867-73.

33. Douglas SM, Marblestone AH, Teerapittayanon S, Vazquez A, Church GM, Shih WM. Rapid prototyping of 3D DNA-origami shapes with caDNAno. Nucleic Acids Res. 2009;37(15):5001-6.

34. Kim DN, Kilchherr F, Dietz H, Bathe M. Quantitative prediction of 3D solution shape and flexibility of nucleic acid nanostructures. Nucleic Acids Res. 2012;40(7):2862-8.

35. Wang PF, Meyer TA, Pan V, Dutta PK, Ke YG. The Beauty and Utility of DNA Origami. Chem-Us. 2017;2(3):359-82.

36. Pan J, Li F, Cha TG, Chen H, Choi JH. Recent progress on DNA based walkers. Curr Opin Biotechnol. 2015;34:56-64.

37. Sherman WB, Seeman NC. A precisely controlled DNA biped walking device. (vol 4, pg 1801, 2004). Nano Letters. 2004;4(9):1801-.

38. Jung C, Allen PB, Ellington AD. A stochastic DNA walker that traverses a microparticle surface. Nat Nanotechnol. 2016;11(2):157-63.

39. Zadegan RM, Jepsen MD, Thomsen KE, Okholm AH, Schaffert DH, Andersen ES, et al. Construction of a 4 zeptoliters switchable 3D DNA box origami. ACS Nano. 2012;6(11):10050-3.

40. Zhang Z, Olsen EM, Kryger M, Voigt NV, Torring T, Gultekin E, et al. A DNA tile actuator with eleven discrete states. Angew Chem Int Ed Engl. 2011;50(17):3983-7.

41. Ranallo S, Prevost-Tremblay C, Idili A, Vallee-Belisle A, Ricci F. Antibody-powered nucleic acid release using a DNA-based nanomachine. Nat Commun. 2017;8:15150.

42. Gu H, Yang W, Seeman NC. DNA scissors device used to measure MutS binding to DNA mis-pairs. J Am Chem Soc. 2010;132(12):4352-7.

43. Kuzyk A, Schreiber R, Zhang H, Govorov AO, Liedl T, Liu N. Reconfigurable 3D plasmonic metamolecules. Nat Mater. 2014;13(9):862-6.

44. Sobczak JPJ, Martin TG, Gerling T, Dietz H. Rapid Folding of DNA into Nanoscale Shapes at Constant Temperature. Science. 2012;338(6113):1458-61.

45. Ketterer P, Willner EM, Dietz H. Nanoscale rotary apparatus formed from tight-fitting 3D DNA components. Sci Adv. 2016;2(2).

46. Marras AE, Zhou LF, Su HJ, Castro CE. Programmable motion of DNA origami mechanisms. P Natl Acad Sci USA. 2015;112(3):713-8.

47. Gu H, Chao J, Xiao SJ, Seeman NC. A proximity-based programmable DNA nanoscale assembly line. Nature. 2010;465(7295):202-5.

48. Hudoba MW, Luo Y, Zacharias A, Poirier MG, Castro CE. Dynamic DNA Origami Device for Measuring Compressive Depletion Forces. ACS Nano. 2017;11(7):6566-73.

49. Kuzyk A, Urban MJ, Idili A, Ricci F, Liu N. Selective control of reconfigurable chiral plasmonic metamolecules. Sci Adv. 2017;3(4):e1602803.

50. Gerling T, Wagenbauer KF, Neuner AM, Dietz H. Dynamic DNA devices and assemblies formed by shape-complementary, non-base pairing 3D components. Science. 2015;347(6229):1446-52.

51. Yang YY, Endo M, Hidaka K, Sugiyama H. Photo-Controllable DNA Origami Nanostructures Assembling into Predesigned Multiorientational Patterns. Journal of the American Chemical Society. 2012;134(51):20645-53.

52. Shin JS, Pierce NA. A synthetic DNA walker for molecular transport. J Am Chem Soc. 2004;126(35):10834-5.

53. Marras AE, Zhou L, Su HJ, Castro CE. Programmable motion of DNA origami mechanisms. Proc Natl Acad Sci U S A. 2015;112(3):713-8.

54. Hong F, Zhang F, Liu Y, Yan H. DNA Origami: Scaffolds for Creating Higher Order Structures. Chem Rev. 2017;117(20):12584-640.

55. Alarcon-Correa M, Kilwing L, Peter F, Liedl T, Fischer P. Platinum-DNA Origami Hybrid Structures in Concentrated Hydrogen Peroxide. Chemphyschem. 2023;24(22):e202300294.

56. Fu J, Li T. Spatial Organization of Enzyme Cascade on a DNA Origami Nanostructure. Methods Mol Biol. 2017;1500:153-64.

57. Klein WP, Thomsen RP, Turner KB, Walper SA, Vranish J, Kjems J, et al. Enhanced Catalysis from Multienzyme Cascades Assembled on a DNA Origami Triangle. ACS Nano. 2019;13(12):13677-89.

58. Jiang Q, Song C, Nangreave J, Liu X, Lin L, Qiu D, et al. DNA origami as a carrier for circumvention of drug resistance. J Am Chem Soc. 2012;134(32):13396-403.

59. Zhao YX, Shaw A, Zeng X, Benson E, Nystrom AM, Hogberg B. DNA origami delivery system for cancer therapy with tunable release properties. ACS Nano. 2012;6(10):8684-91.

60. Banerjee A, Pons T, Lequeux N, Dubertret B. Quantum dots-DNA bioconjugates: synthesis to applications. Interface Focus. 2016;6(6):20160064.

61. Wagenbauer KF, Pham N, Gottschlich A, Kick B, Kozina V, Frank C, et al. Programmable multispecific DNA-origami-based T-cell engagers. Nat Nanotechnol. 2023;18(11):1319-26.

62. Rahman MA, Wang P, Zhao Z, Wang D, Nannapaneni S, Zhang C, et al. Systemic Delivery of Bc12-Targeting siRNA by DNA Nanoparticles Suppresses Cancer Cell Growth. Angew Chem Int Ed Engl. 2017;56(50):16023-7.

63. Song J, Li Z, Wang P, Meyer T, Mao C, Ke Y. Reconfiguration of DNA molecular arrays driven by information relay. Science. 2017;357(6349).

64. Wang P, Huh JH, Lee J, Kim K, Park KJ, Lee S, et al. Magnetic Plasmon Networks Programmed by Molecular Self-Assembly. Adv Mater. 2019;31(29):e1901364.

65. Zhan P, Peil A, Jiang Q, Wang D, Mousavi S, Xiong Q, et al. Recent Advances in DNA Origami-Engineered Nanomaterials and Applications. Chem Rev. 2023;123(7):3976-4050.

66. Yao G, Zhang F, Wang F, Peng T, Liu H, Poppleton E, et al. Meta-DNA structures. Nat Chem. 2020;12(11):1067-75.

67. Xin Y, Shen B, Kostiainen MA, Grundmeier G, Castro M, Linko V, et al. Scaling Up DNA Origami Lattice Assembly. Chemistry. 2021;27(33):8564-71.

68. Simone EA, Dziubla TD, Muzykantov VR. Polymeric carriers: role of geometry in drug delivery. Expert Opin Drug Deliv. 2008;5(12):1283-300.

69. Wang P, Ke Y. Attack on the Cell Membrane: The Pointy Ends of DNA Nanostructures Lead the Way. ACS Cent Sci. 2018;4(10):1298-9.

70. Wang P, Rahman MA, Zhao Z, Weiss K, Zhang C, Chen Z, et al. Visualization of the Cellular Uptake and Trafficking of DNA Origami Nanostructures in Cancer Cells. J Am Chem Soc. 2018;140(7):2478-84.

71. van der Schans JJ, van de Donk N, Mutis T. Dual Targeting to Overcome Current Challenges in Multiple Myeloma CAR T-Cell Treatment. Front Oncol. 2020;10:1362.

72. Talevi A. Multi-target pharmacology: possibilities and limitations of the "skeleton key approach" from a medicinal chemist perspective. Front Pharmacol. 2015;6:205.

73. Wei B, Dai M, Yin P. Complex shapes self-assembled from single-stranded DNA tiles. Nature. 2012;485(7400):623-6.

74. Han D, Qi X, Myhrvold C, Wang B, Dai M, Jiang S, et al. Single-stranded DNA and RNA origami. Science. 2017;358(6369).

75. Jasinski D, Haque F, Binzel DW, Guo P. Advancement of the Emerging Field of RNA Nanotechnology. ACS Nano. 2017;11(2):1142-64.

76. Li M, Zheng M, Wu S, Tian C, Liu D, Weizmann Y, et al. In vivo production of RNA nanostructures via programmed folding of single-stranded RNAs. Nat Commun. 2018;9(1):2196.

77. Lee JB, Hong J, Bonner DK, Poon Z, Hammond PT. Self-assembled RNA interference microsponges for efficient siRNA delivery. Nat Mater. 2012;11(4):316-22.

78. Afonin KA, Bindewald E, Yaghoubian AJ, Voss N, Jacovetty E, Shapiro BA, et al. In vitro assembly of cubic RNA-based scaffolds designed in silico. Nat Nanotechnol. 2010;5(9):676-82.

79. Reynaldo LP, Vologodskii AV, Neri BP, Lyamichev VI. The kinetics of oligonucleotide replacements. J Mol Biol. 2000;297(2):511-20.

80. Yurke B, Turberfield AJ, Mills AP, Simmel FC, Neumann JL. A DNA-fuelled molecular machine made of DNA. Nature. 2000;406(6796):605-8.

81. Simmel FC, Yurke B, Singh HR. Principles and Applications of Nucleic Acid Strand Displacement Reactions. Chem Rev. 2019;119(10):6326-69.

82. Simmel FC, Yurke B. Using DNA to construct and power a nanoactuator. Phys Rev E Stat Nonlin Soft Matter Phys. 2001;63(4 Pt 1):041913.

83. Li XY, Liu DR. DNA-Templated organic synthesis: Nature's strategy for controlling chemical reactivity applied to synthetic molecules. Angew Chem Int Edit. 2004;43(37):4848-70.

84. Fan D, Wang J, Wang E, Dong S. Propelling DNA Computing with Materials' Power: Recent Advancements in Innovative DNA Logic Computing Systems and Smart Bio-Applications. Adv Sci (Weinh). 2020;7(24):2001766.

85. Huang FJ, Xu HG, Tan WH, Liang HJ. Multicolor and Erasable DNA Photolithography. Acs Nano. 2014;8(7):6849-55.

86. Chen HR, Weng TW, Riccitelli MM, Cui Y, Irudayaraj J, Choi JH. Understanding the Mechanical Properties of DNA Origami Tiles and Controlling the Kinetics of Their Folding and Unfolding Reconfiguration. Journal of the American Chemical Society. 2014;136(19):6995-7005.

87. Choi HMT, Schwarzkopf M, Fornace ME, Acharya A, Artavanis G, Stegmaier J, et al. Third-generation in situ hybridization chain reaction: multiplexed, quantitative, sensitive, versatile, robust. Development. 2018;145(12).

88. Xing S, Lu Z, Huang Q, Li H, Wang Y, Lai Y, et al. An ultrasensitive hybridization chain reaction-amplified CRISPR-Cas12a aptasensor for extracellular vesicle surface protein quantification. Theranostics. 2020;10(22):10262-73.

89. Li D, Zhou W, Chai Y, Yuan R, Xiang Y. Click chemistry-mediated catalytic hairpin self-assembly for amplified and sensitive fluorescence detection of Cu(2+) in human serum. Chem Commun (Camb). 2015;51(63):12637-40.

90. Cramer P. Organization and regulation of gene transcription. Nature. 2019;573(7772):45-54.

91. Pietila MK, Hellstrom K, Ahola T. Alphavirus polymerase and RNA replication. Virus Res. 2017;234:44-57.

92. Bloom K, van den Berg F, Arbuthnot P. Self-amplifying RNA vaccines for infectious diseases. Gene Ther. 2021;28(3-4):117-29.

93. Yang J, Hu L. Immunomodulators targeting the PD-1/PD-L1 protein-protein interaction: From antibodies to small molecules. Med Res Rev. 2019;39(1):265-301.

94. Crivianu-Gaita V, Thompson M. Aptamers, antibody scFv, and antibody Fab' fragments: An overview and comparison of three of the most versatile biosensor biorecognition elements. Biosens Bioelectron. 2016;85:32-45.

95. Tuerk C, Gold L. Systematic evolution of ligands by exponential enrichment: RNA ligands to bacteriophage T4 DNA polymerase. Science. 1990;249(4968):505-10.

96. Zhang Y, Lai BS, Juhas M. Recent Advances in Aptamer Discovery and Applications. Molecules. 2019;24(5).

97. Lakhin AV, Tarantul VZ, Gening LV. Aptamers: problems, solutions and prospects. Acta Naturae. 2013;5(4):34-43.

98. Hu Q, Li H, Wang L, Gu H, Fan C. DNA Nanotechnology-Enabled Drug Delivery Systems. Chem Rev. 2019;119(10):6459-506.

Chapter 2. Hierarchical Self-Assembly of Cholesterol-DNA Nanorods

2.1 Abstract

During recent decades, DNA has been extensively used as the basic building blocks for nanostructure construction. Most of the work in this area is focused on using pure DNA strands; However, there are certain researches aiming at the self-assembly of DNA conjugated with other molecules. Among these conjugated DNA strands, amphiphilic DNA block copolymer is one example that has been widely utilized in the preparation of self-assembled amphiphilic structures in water-based solutions. These amphiphilic DNA block copolymers usually consist of both hydrophilic DNA parts and specially designed hydrophobic regions. However, in previous work, these amphiphilic DNA block copolymers were mainly self-assembled under near-physiological conditions. In this work, we report a novel self-assembly of cholesterol-DNA block copolymer, which can result in spherical micelles and nanorods under acidic conditions. Comprehensive study was carried out to demonstrate the factors influencing the morphology of the assembly, and the hierarchical assembly pathway from the micelles to nanorod structures was further revealed. We envision that our finding can provide new insights for future amphiphilic DNA block copolymer design, and the assembled structures may find useful in certain biomedical research areas.

2.2 Background

2.2.1 DNA block copolymers in DNA nanotechnology

Structural DNA nanotechnology uses synthetic or biological DNA strands as basic building blocks for the self-assembly of artificially designed nanostructures. Most of the work in this field utilizes sole DNA strands for nanostructure construction. These nanostructures are founded on the specific yet simple interactions between nucleotide molecules, which is known as the Watson-Crick base pairing. This versatile binding rule of DNA strands allowed the

unprecedented blooming of artificial nanostructures with drastic complexity and programmability (1). On the other hand, by conjugating DNA strands to other molecules, polymers, or nanoparticles, these conjugated structures can endow the whole DNA strand with new interactions during assembly, such as hydrophobic, electrostatic, and π- π interactions (2). These conjugated DNA strands are usually referred to as DNA block copolymers (DBC).

Introducing these new interactions onto DNA strands has been proven to demonstrate orthogonal bindings and long-range morphology control in DBS self-assembly. By utilizing DBC, a set of new generation of DNA nanostructures has been developed (3-6). Among these DBCs, one particular kind is the amphiphilic DNA copolymer. In amphiphilic DBCs, DNA strands are mainly serving as hydrophilic parts, while the conjugated molecules are mainly serving as hydrophobic parts. Some typical examples of these hydrophobic molecules include synthetic polymers, fluorescent dyes, and lipids (7, 8). In aqueous solutions, the hydrophilic DNA strands will wrap the hydrophobic molecules inside the shell to prevent the contact of water with hydrophobic core. In this condition, amphiphilic DBCs have been extensively utilized to assemble one-dimensional (1D), two-dimensional (2D), and three-dimensional (3D) nanostructures with highly tunable size and shape (9-11). Besides morphology properties, a lot of previous work has also demonstrated the occurrence of unique properties that are hard to realize in other systems. For example, Liu and co-workers employed thermal-responsive DBCs to construct dynamic nanostructures that possessed temperature-triggered morphology alteration properties (12, 13). Another example is the work by Wang and co-workers, where they constructed a DBC-based nanostructure that could undergo phase transitions during assembly (14). With all these unique properties, amphiphilic DBCs have been widely used in various applications, such as diagnostics, programmable nanoreactors, and, especially, drug delivery vehicle construction (15-18).

2.2.2 DBC nanostructures as drug delivery agents

When used for drug delivery, similar to other amphiphilic molecules, DBC nanostructures also exhibit low toxicity and high reproducibility in payload containment. Thus, DBC nanostructures have been considered to be a potent candidate for next-generation targeted therapy (19). After the covid pandemic in recent years and the wide usage of mRNA vaccine, significant attention has been attracted to using DBCs to make micelle-like structures for mRNA delivery (20, 21). Among these researches, some researchers have suggested that certain DBCs, which were not directly being used for the micelle structure construction, may find certain potentials in untrodden routes.

Cholesterol-conjugated DNA strand (chol-DNA) is certainly one example of these DBCs. Previously, chol-DNA was mainly used as the anchor in the process of dynamic motion and target detection, especially when the process involved cell membranes (22-25). In some other research, chol-DNA was also found to form micellular structures and single crystals with the help of other modifications (26-29). It is definite that chol-DNA has a promising potential in constructing well-performing micellular delivery agents. However, the formation of micellular structures with sole chol-DNA DBC is still unseen due to the rather small size of cholesterol being unable to form a stable hydrophobic core.

2.2.3 Hypothesis and goal of this project

In this project, we hypothesized that the chol-DNA DBC itself can form micellular structures under certain reaction conditions. Through extensive study, we discovered that under acidic conditions, chol-DNA with certain DNA sequences could form spherical micelles and nanorods. The factors that influence the morphology of the nanostructure include solution pH, salt concentration, DNA sequence, and the length of connecting spacers. Further study revealed that the assembly process of such micellular structures was a hierarchical process. We believe that this novel assembly principle of chol-DNA can provide new design principles for future

DBC assembly, and will be proven useful for the construction of new DBC micellular nanostructures for biomedical applications at a wider range of conditions.

This work was published on the journal of Bioconjugate Chemistry (30).

2.3 Results and discussion

2.3.1 General design of chol-DNA DBCs and characterization of micellular nanostructures

A typical chol-DNA DBC consists of 3 parts: Cholesterol, internal linker, and DNA strand (Figure 2-1). Figure 2-1a shows the structure of cholesterol molecules, and figure 2-1b and 2-1c show the structure of chol-DNA DBC with or without extra internal linkers. In this project, a specific GA-rich DNA sequence was used as the hydrophilic part, and all sequences used in this project can be found in Table 2-1.

Figure 2-2 shows the animated illustration of a typical chol-DNA DBC without extra internal linkers. By annealing the chol-DNA DBC with a certain protocol, we found that chol-DNA could form micelles and nanorods under acidic conditions (Figure 2-2D). Based on the constitution of DBC and the fact that the assembly took place in aqueous solution, we believe that the assembled structures should have a hydrophobic core of cholesterol in the center, and a hydrophilic shell of DNA outside the core. According to the reaction condition, assembly protocol, and the design of chol-DNA, the assembly product may vary among spherical micelles, short nanorods, and long nanorods. Thus, in the next step, we carried out comprehensive studies to investigate the factors influencing the morphology of assembled micellular structures.

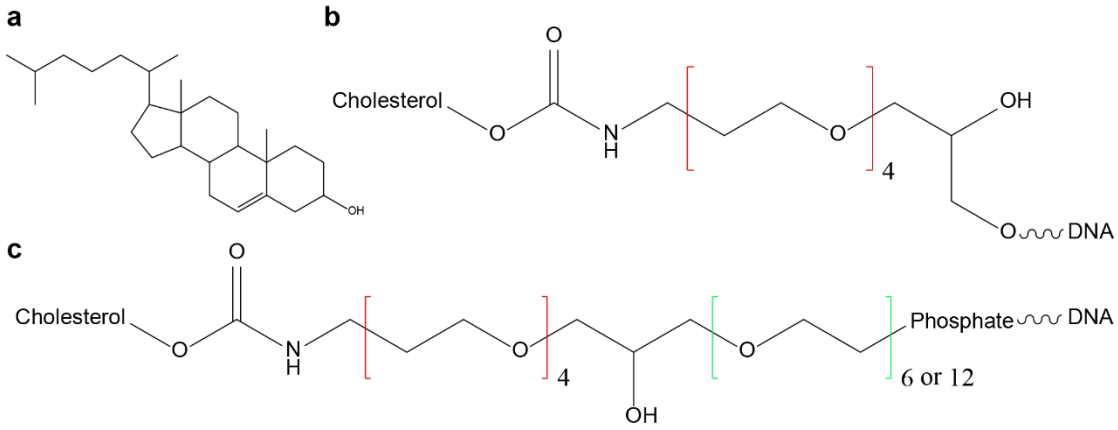

Figure 2-1. Composition of DNA-cholesterol block copolymer. (a) The molecular structure of cholesterol. (b) The structure of DNA-cholesterol without internal spacer. (c) The structure of DNA-cholesterol with internal spacer. TEG linker is indicated between red square brackets, and hexa-ethyleneglycol internal spacer is indicated between green square brackets.

Table 2-1. All DBCs and DNA strands used in this paper.

Name	Sequence (5' to 3')
18B	GGT AGT AAT AGG AGA ATG-TEG linker-cholesterol
12B	AAT AGG AGA ATG-TEG linker-cholesterol
24B	AGT GAG GGT AGT AAT AGG AGA ATG-TEG linker-cholesterol
PolyT	TTT TTT TTT TTT TTT TTT-TEG linker-cholesterol
18B1S	GGT AGT AAT AGG AGA ATG-Internal spacer-TEG linker-cholesterol
18B2S	GGT AGT AAT AGG AGA ATG-Internal spacer-Internal spacer-TEG linker-cholesterol
Complementary strand for 18B's DNA part	CAT TCT CCT ATT ACT ACC
18B's DNA part	GGT AGT AAT AGG AGA ATG
12B's DNA part	AAT AGG AGA ATG
24B's DNA part	AGT GAG GGT AGT AAT AGG AGA ATG
PolyT's DNA part	TTT TTT TTT TTT TTT TTT

Note: TEG linker = triethylene glycol linker. Internal spacer = hexa-ethyleneglycol spacer.

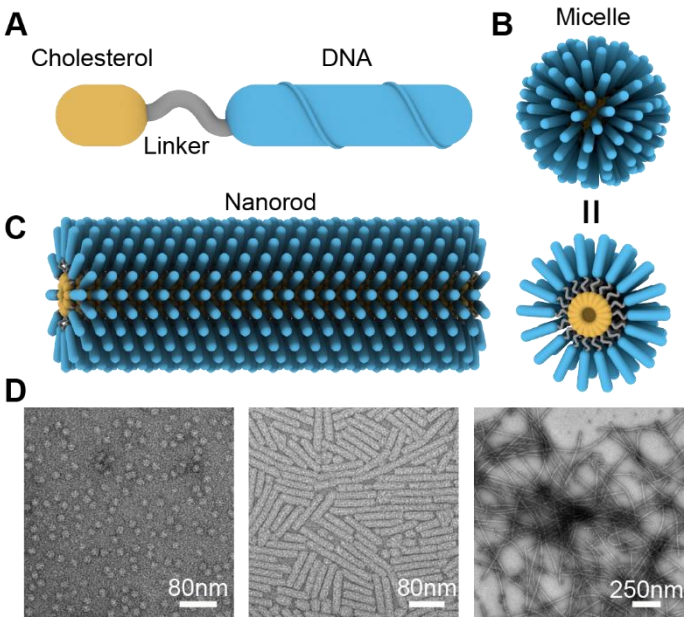

Figure 2-2. Micelles and nanorods self-assembled from chol-DNA. (A) Design of a chol-DNA DBC. (B) Schematic of spherical micelles formed by Cholesterol-DNA. (C) Schematic of a nanorod assembled from Cholesterol-DNA. (D) Representative TEM images of different types of products, including spherical micelles, short nanorods, and long nanorods.

2.3.2 Factors influencing the morphology of assembled structures

The initial design of chol-DNA DBS consists of a single cholesterol molecule, a triethylene glycol linker (TEG), and an 18-base GA-rich DNA sequence (18B). For this chol-DNA DBC, micelle-like structures were assembled at pH 3.6 with 50mM Na^+ and 1mM Mg^{2+} in the solution. Based on this initial observation, we started our investigation with the salt concentration at the same pH.

Two ions were mainly tested during the investigation: Sodium cation and magnesium cation. Sodium cation concentrations were chosen according to the concentration of cations in typical 1x PBS buffer. Magnesium cation was chosen because it plays a critical role in DNA nanostructure assembly by forming divalent bridge to mitigate the repulsion of negative charges on the DNA backbone (31, 32). It is also more widely used in actual structural DNA nanotechnology research compared to other divalent metal ions. Four varied groups of Na^+ (from 0-200 mM) and Mg^{2+} (from 0-10mM) concentrations were tested, and representative TEM images for assembled structures under corresponding conditions are presented in figure 2-3. Compared to Na^+, Mg^{2+} seems to pose a more crucial effect on the assembly of nanorods, as all groups without Mg^{2+} only showed the formation of spherical micelles or random aggregation. As both cation's concentration increased, more well-formed structures, including both spherical micelles and nanorods, were observed under TEM. This can be interpreted as these cations are necessary for the assembly of the relatively compact DNA strand shells, which is a similar situation in other DNA nanostructures. However, when both salt concentrations became too high, the number of well-formed structures under TEM drastically decreased. This can be interpreted as the high salt concentration posed the disruption of electrostatics balance of DNA parts, which is also a similar condition in other DNA nanostructures.

We then investigated the influence of pH value of the solution. To enable the buffering at a low

pH, sodium acetate-acetic acid buffer was used and a set of different pH conditions from 3.1-5.5 was maintained during annealing. With 15mM Na^+ and 1mM Mg^{2+}, 18B assembly under different pH was tested (Figure 2-4). Under the pH lower than 4.5, nanorods were always formed, while under the pH higher than 4.5, only spherical micelles were observed. This result confirms that pH is indeed an influential factor in determining the assembly result of chol-DNA, and this can be interpreted that under different pH, the degree of protonation of DNA part is different, thus ultimately influencing the hybridization of DNA strands.

As mentioned in previous investigations, the cation and pH may mainly influence the hybridization of DNA stands and the formation of hydrophilic DNA shells. Thus, the importance of cations on the chol-DNA DBC assembly also suggests that the sequence of DNA strands may play an important role during the assembly as well. To test this hypothesis, we further designed three additional chol-DNA DBCs with different DNA sequences: 12B with a 12-base GA-rich sequence, 24B with a 24-base GA-rich sequence, and polyT with 18-base of T nucleotides. The Poly-T sequence can greatly hinder the DNA hybridization. The assembly was carried out with 15mM Na^+ and 1mM Mg^{2+} at pH=3.1-5.5 (Figure 2-5). As expected, the Poly-T chol-DNA failed to assemble into any well-formed structures, while all other DBCs generated well-formed spherical micelles at specific pH. However, even though spherical micelles were observed for 12B and 24B assembly, no nanorod assembly was observed for these two DBCs. This result suggests that to form micellular structures, a hybridization strength among DNA strands is necessary, and to form nanorods, a specific sequence of DNA strands is required.

To further confirm the importance of DNA hybridization interactions on micellular structure formation, we designed additional experiments where 18B was annealed together with its complementary DNA strand (Figure 2-6). The experiment was carried out with 15mM Na+ and 1mM Mg^{2+}. When the complementary DNA strand was added, only random aggregation was

assembled. This is because the hybridization between the DNA parts on 18B is disrupted by the complementary DNA strands, thus failing the formation of the hydrophilic DNA shell. This result successfully confirmed the critical role of DNA hybridization and the formation of hydrophilic DNA shell during micellular structure assembly.

We also investigated whether the sequence of DNA part will influence micellular structure formation. The initial 18B DNA sequence contains 78% guanine and adenine. It is considered that a high content of guanine and adenine will induce the formation of special DNA secondary structures, such as G-quadraplex (33). Thus, in comparison, we further designed two different chol-DNA DBCs with DNA sequences having 100% GA content (18B-high GA) and 56% GA content (18B-low GA), and tested their assembly under 15mM Na^+ and 1mM Mg^{2+} at pH=3.1-5.0. As shown in Figure 2-7, for 18B-high GA, it has a higher tendency to form secondary structures, thus higher tendency to hybridize. However, it only formed structures without well-defined edges, possibly due to the high hybridization tendency making the cross-talking too random. On the other hand, for 18B-low GA, the level of interaction between adjacent DNA strands should be lower, and indeed only a small number of spherical micelles were formed at pH 3.1. This result further demonstrates that the assembly of chol-DNA is dependent on the sequence of the DNA part, and the hybridization strength between DNA parts should fall into a stringent range. Besides, among all experimental setups, the assembly result of spherical micelles is more common than nanorods, indicating that the formation of nanorods may be more difficult than the formation of spherical micelles.

Finally, we confirmed the influence of cholesterol hydrophobic core during the micellular structure formation. To test this, the assembly result of 12B, 18B, 24B, and PolyT without cholesterol and internal linkers was tested (Figure 2-8). For description, these strands are labeled as DBC-DNA-only. For the initial chol-DNA DBC 18B, a pH range of 3.1-5.5 was tested, and for all other DBC, only pH=3.6 was tested. For all groups, 15mM Na^+ and 1mM

Mg^{2+} were used for testing. The TEM result showed that although no ordered micellular structure was produced for 12B-DNA-only, 18B-DNA-only, and 24B-DNA-only, they did assembled into random aggregation. On the other hand, nothing was observed for Poly-T-DNA-only under TEM. This outcome is consistent with previous results that 12B, 18B, and 24B could form well-formed micellular nanostructures but Poly-T could not. It also confirmed that the hydrophobic interactions between cholesterol should be a key driving force for micellular nanostructure formation.

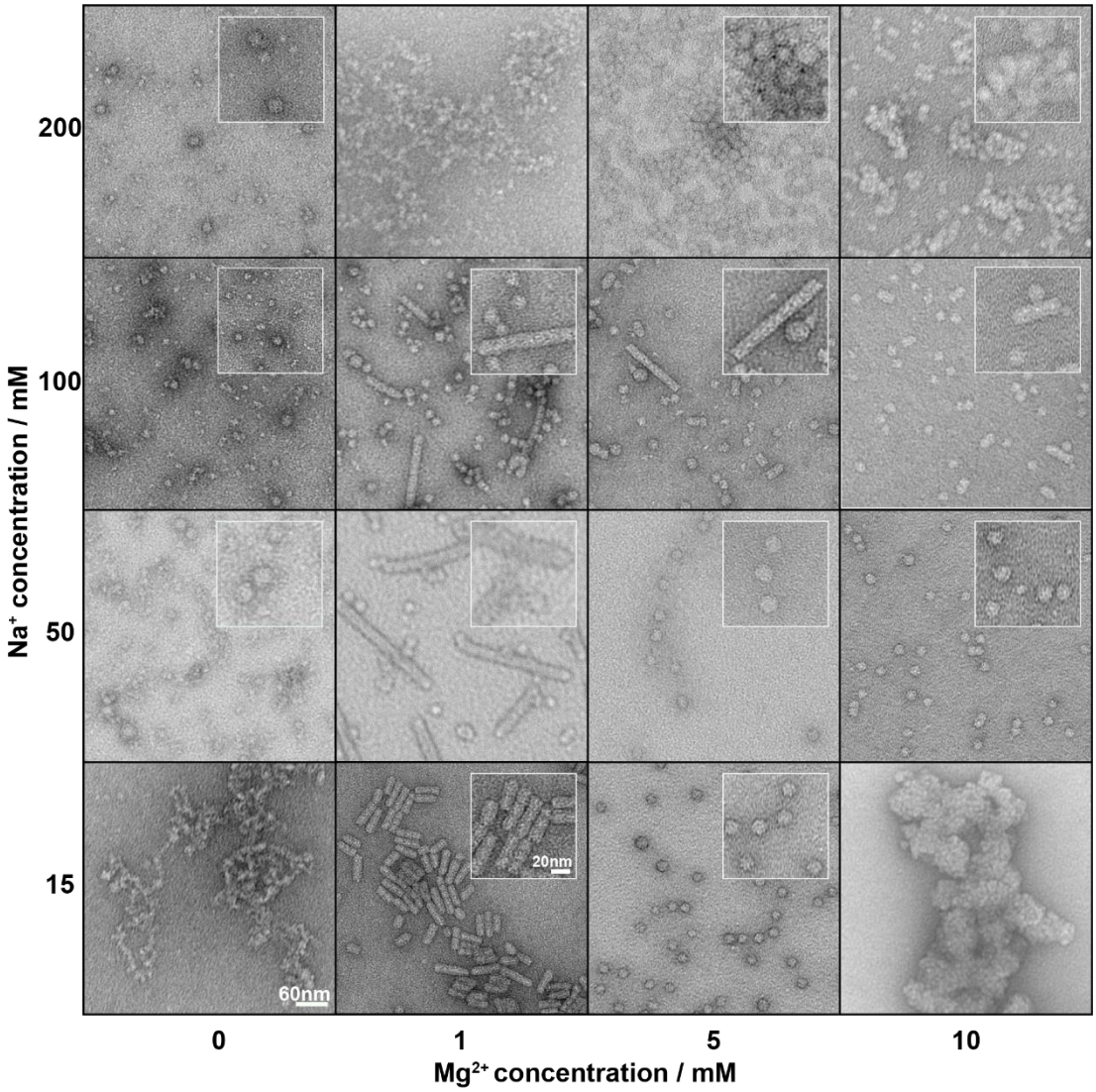

Figure 2-3. Representative TEM images of 18B chol-DNA DBC annealed with different salt concentration. The rationale for choosing Na^+ and Mg^{2+} concentration can be found in the "Materials and methods" section. Large images are captured with the magnification of 25k times under TEM. They all share the same scale bar as shown in the lower left. Small images are focused ones captured with the magnification of 50k times under TEM. They also share the same scale bar as shown in the lower middle. Groups without well-defined product do not include a focused image.

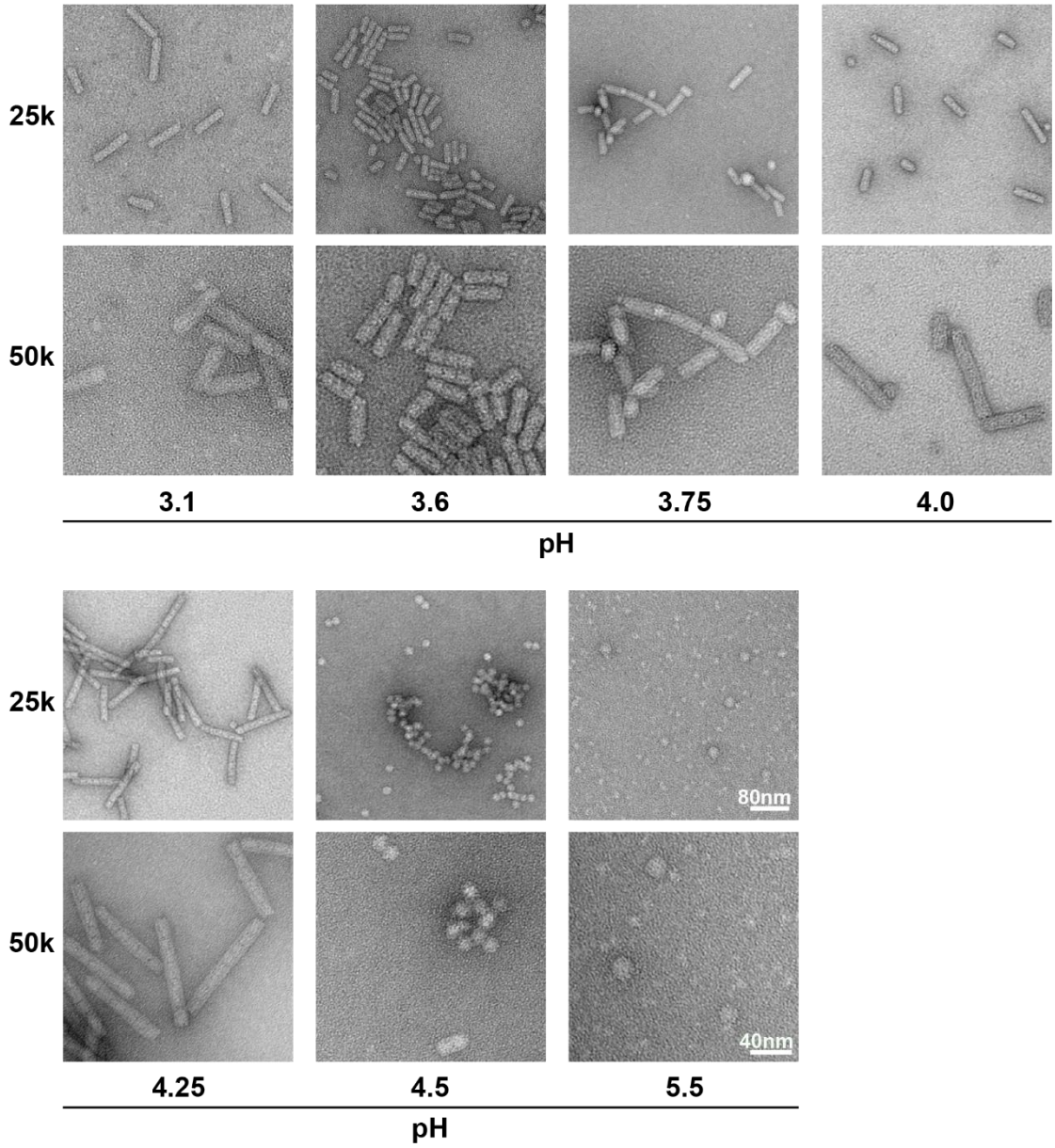

Figure 2-4. TEM images of the annealing product of 18B under different pH. These groups are all tested in the solution with 1mM Na^{+} and 1mM Mg^{2+}. The left column indicates the magnification rate of TEM setup when capturing the image. Images with the same magnification share the same scale bar.

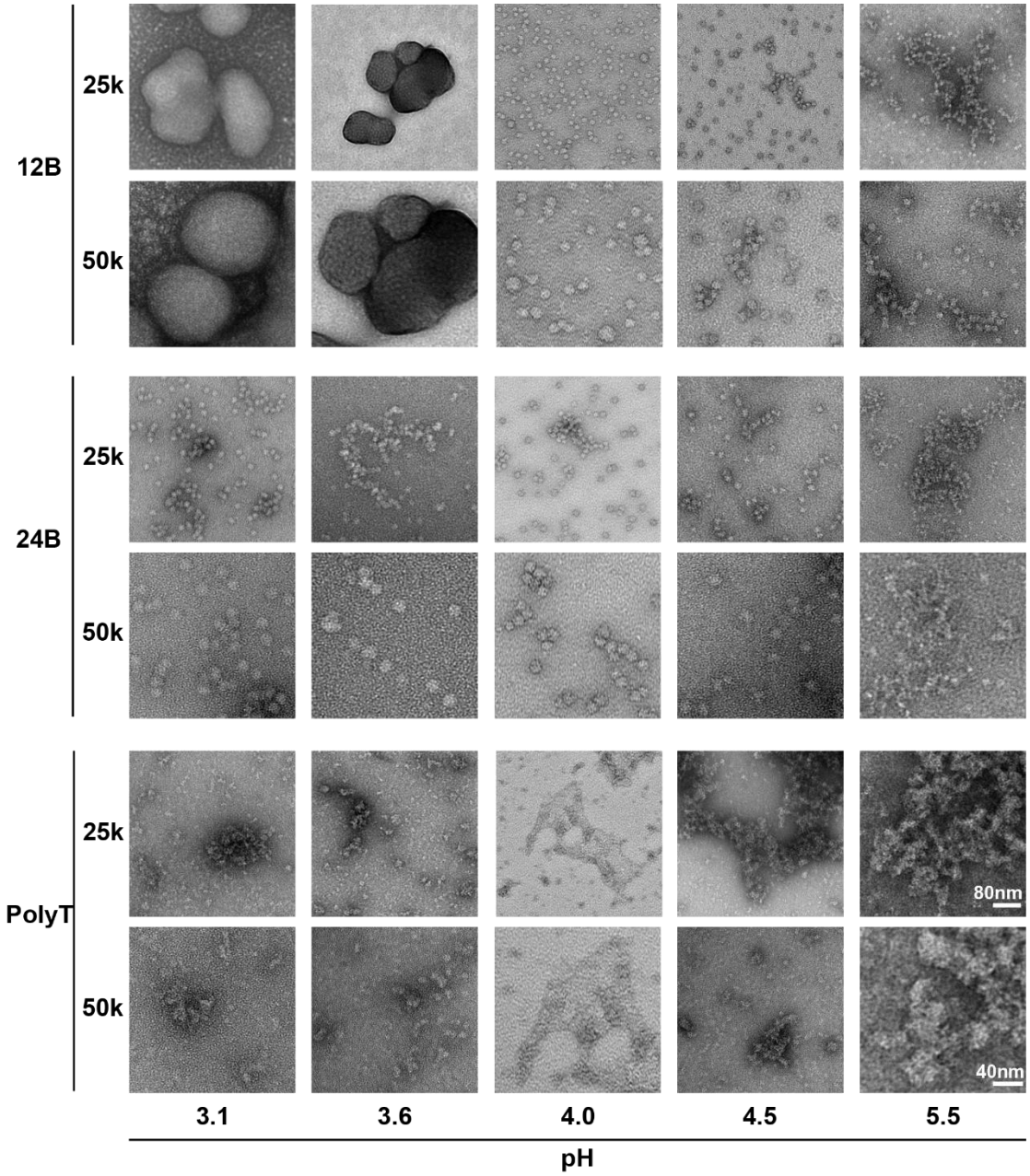

Figure 2-5. TEM images of the assembly products of 12B, 24B and PolyT under different pH. These groups are all tested in the solution with 15mM Na^{+} and 1mM Mg^{2+}. “25k” and “50k” indicate the magnification rates of TEM setup when capturing the image. Images with the same magnification share the same scale bar.

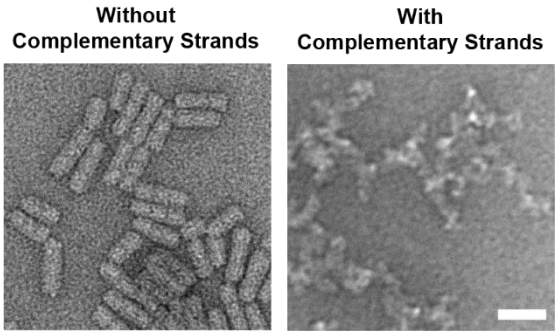

Figure 2-6. TEM images of the assembly result of 18B chol-DNA annealed in the presence of the complementary strand of its DNA part. All figures share the same scale bar. The scale bar is 40 nm.

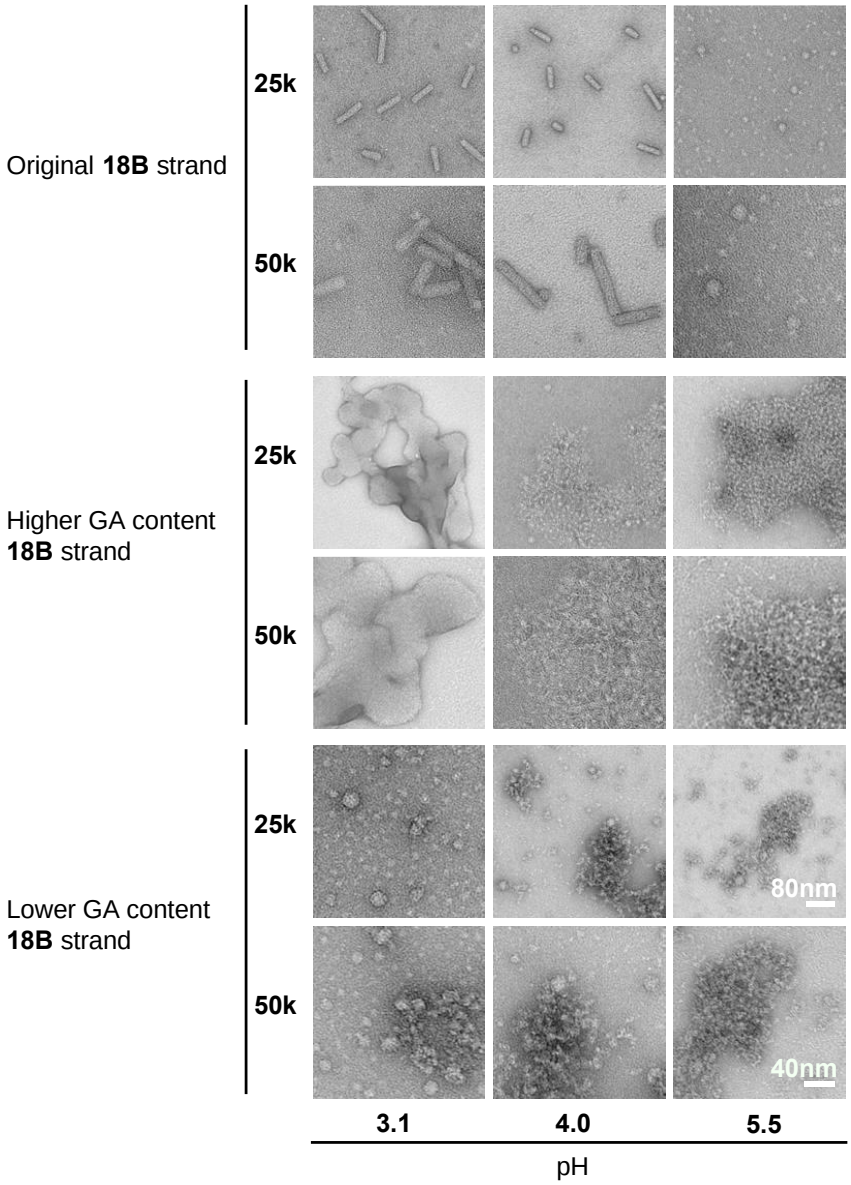

Figure 2-7. TEM images of the assembly products of 18B with 100% GA and 18B with 56% GA, in comparison to the original 18B with 78% GA. The samples are all assembled in the buffer with 15mM Na^{+} and 1mM Mg^{2+}. "25k" and "50k" indicate the magnification of TEM setup when capturing the images. Images with the same magnification share the same scale bar.

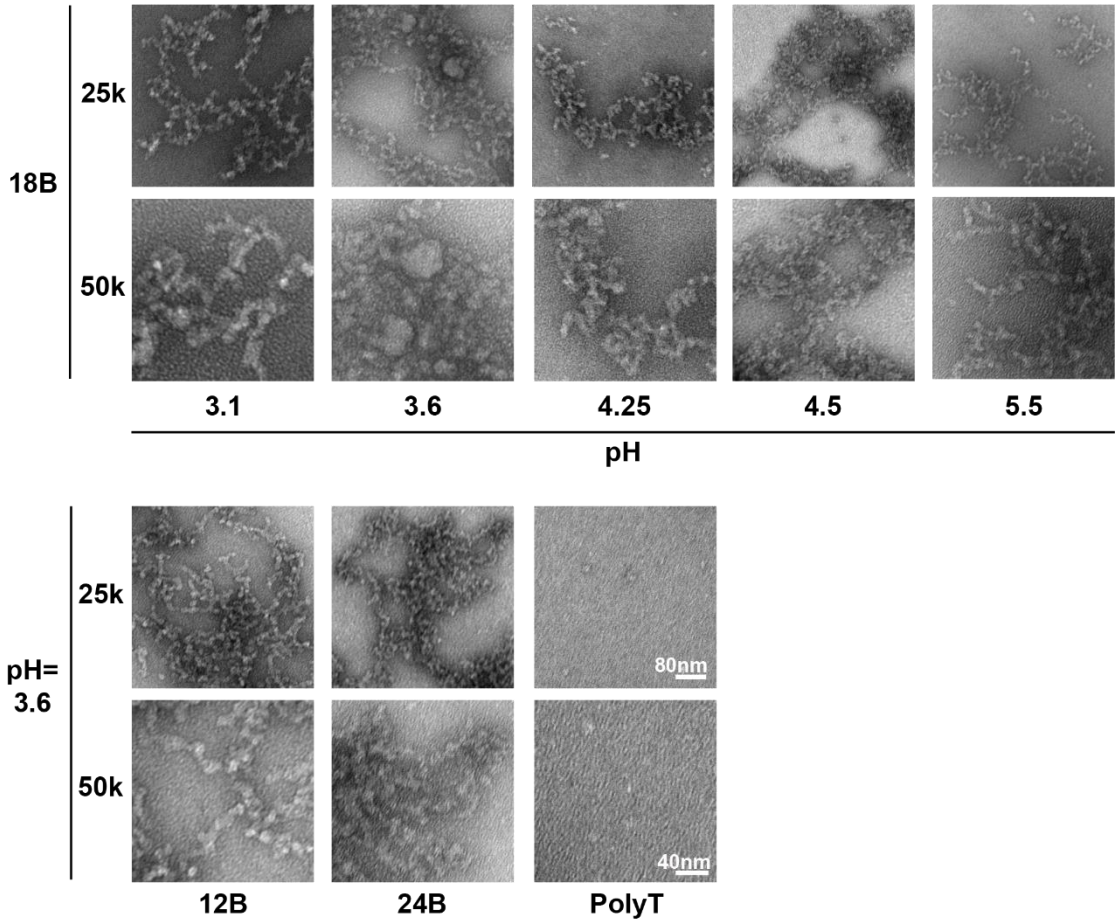

Figure 2-8. TEM images of the assemblies of sole DNA strands. The upper five groups showed assembly result of 18B-DNA-only at different pH, with 15mM Na^{+} and 1mM Mg^{2+}. The lower three groups compare 12B-DNA-only, 24B-DNA-only and PolyT-DNA-only, annealed at pH=3.6, with 10mM Na+ and 1mM Mg2+. “25k” and “50k” indicate the magnification of the image. Images with the same magnification share the same scale bar.

2.3.3 Mechanism of the transition from spherical micelles to nanorods

In all TEM images in previous sections, we constantly noticed an interesting feature on nanorods that they contained uniform units separated by small but visible gaps (Figure 2-9a). We came up with a hypothesis that the nanorods were hierarchically assembled from performed spherical micelles, and the gap was the result of incomplete merge of spherical micelles.

To justify this hypothesis, we designed two more chol-DNA DBCs. They all have the same DNA part as 18B, but they have longer internal linkers: 18B1S has one more hexa-ethyleneglycol internal linker, and 18B2S has two more. We tested their assembly with 15mM Na^+ and 1mM Mg^{2+} under pH=3.1-5.5 (Figure 2-10, 2-11), and they all assembled into well-formed micellular structures within appropriate pH range. The 18B1S nanorods could grow to several micrometers in length, and 18B2S nanorods could grow even longer (Figure 2-12). To compare with 18B nanorods, we took the assembly at pH=3.6 out for all three designs. It is obvious that the periodic gaps on 18B1S and 18B2S nanorods became more pronounced (Figure 2-9b, 2-9c). Besides, we measured the width of the nanorods and both 18B1S and 18B2S nanorods showed higher average width than 18B nanorods (Figure 2-9d). We interpret these differences to be caused by the longer internal linker, and this difference infers the transfer mechanism we hypothesized. Because the 18B1S nanorods had a clear gap and clean background under TEM, we selected this design for further investigations unless specified.

First, to rule out the possibility that the nanorods were formed due to the drying process when preparing samples for TEM imaging, we also imaged the assemblies in liquid-phase atomic force microscopy (AFM). 18B1S nanorods assembled with 15mM Na^+ and 1mM Mg^{2+} under pH=4.25, and 18B2S nanorods assembled with 15mM Na^{2+} and 1mM Mg^{2+} under pH=3.75 were imaged, and they all showed a complete nanorod morphology under AFM (Figure 2-13). This result confirmed that the nanorods were formed in the solution. Having this result as the

prerequisite, we further carried out a time-course study on the growth process of 18B1S nanorods. 18B1S chol-DNA was annealed with 15mM Na^+ and 1mM Mg^{2+} under pH=4.25, and the sample was imaged using TEM at different time points during annealing (Figure 2-14). Spherical micelles started to form at 5 min, and the merging of the spherical micelles could be noticed from around 10 min. After 30 min, well-formed nanorods started to appear in the images and gradually became dominant over annealing. Besides, from the appearance of the nanorods, the gaps were always clearly visible until the final stage. From this time-course investigation, the hierarchical assembly pathway of such chol-DNA DBC is rather clear: The DBCs first form spherical micelles, and then the micelles further merge into nanorods.

For the black gaps under TEM images, at current stage, we are confident in our initial hypothesis that it is caused by the merging of spherical micelles. However, we further hypothesize that the gaps might be a transitional state and would eventually disappear if given more time. Thus, we incubated the 18B1S nanorods under room temperature after annealing and monitored the sample's morphology using TEM on different days (Figure 2-15). However, even after 15 days, the gaps were still visible on nanorods, and no obvious morphology change could be observed on nanorods. Then we further modified our hypothesis to interpret the occurrence of black gaps (Figure 2-16). The nanorods with gaps were hierarchically assembled from spherical micelles and were proven to be rather stable under room temperature. However, the black gap under TEM was the indication that the merge of the spherical micelles was not complete enough. Compared to other amphiphilic DBCs with larger hydrophobic molecules conjugated, our chol-DNA DBC's hydrophobic molecule, which is cholesterol, is rather small in size. Therefore, the formed hydrophobic core in the middle of spherical micelles is much smaller than the outer hydrophilic DNA shell. In this case, during the merging process, the large DNA shell may hinder the interactions among centered cholesterols, resulting in a large energy penalty to form perfectly merged large micelles. In contrast, the formation of the

nanorod with gaps, which indicates that the hydrophobic cores are not completely merged with each other, maybe a response to reduce such energy penalty. We are still working on the investigation on this hypothesis.

Besides aforementioned experiments, we also tested the critical micelle concentration for 18B1S by imaging the assembled structures with different starting DBC concentrations using TEM (Figure 2-17). The spherical micelles started to appear at 1uM concentration, and the nanorods started to appear at 5uM concentration.

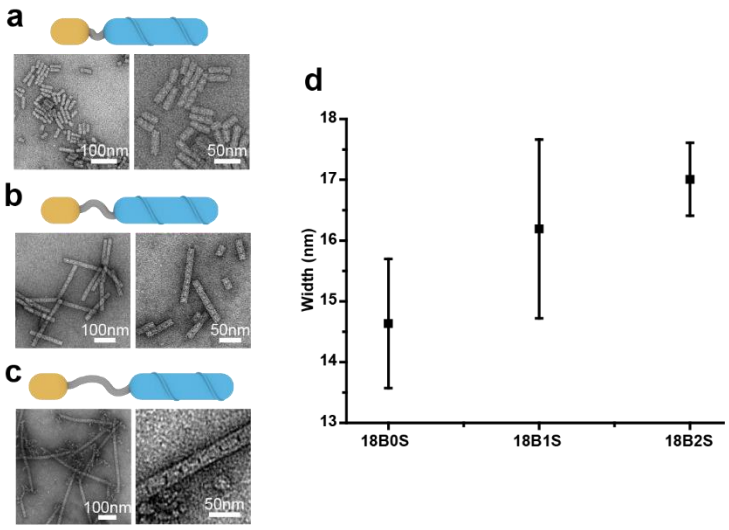

Figure 2-9. Assembly of 18B with longer internal linkers. All experiments are carried out with 15mM Na^{+} and 1mM Mg^{2+} under pH=3.6. (a) Representative TEM images of 18B nanorods. (b) Representative TEM images of 18B1S nanorods. (c) Representative TEM images of 18B2S nanorods. (d) Measurement of nanorod widths. 20 data points were collected for each group and the average value and standard deviation were calculated and illustrated on the plot. With more internal spacers incorporated in the Cholesterol-DNA, the average width of nanorods grows larger with a nearly linear pattern. This result is consistent with our proposed assembly mechanism that cholesterol sits inside as the hydrophobic core while DNA parts point outwards.

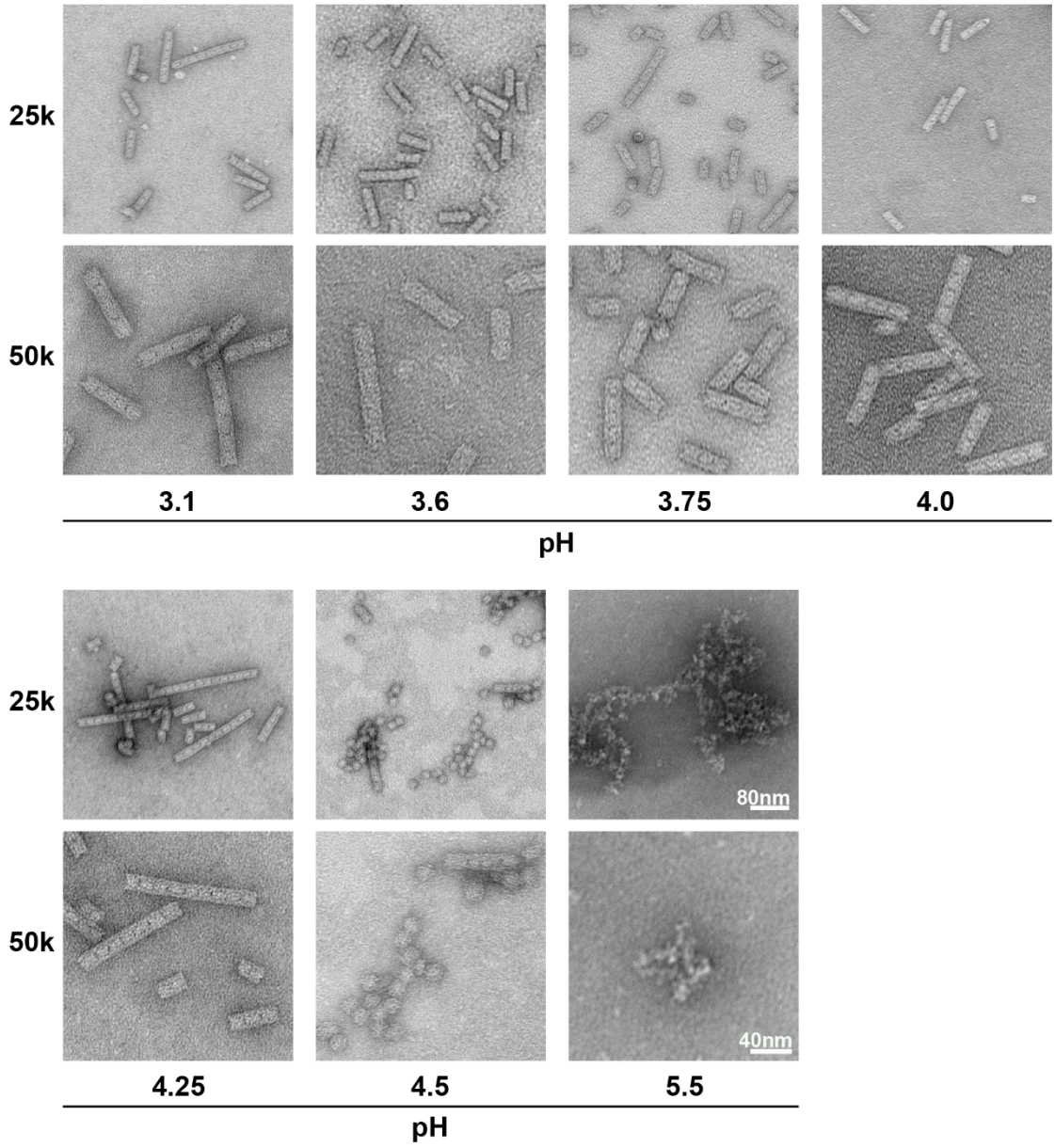

Figure 2-10. TEM images of the product of 18B1S under different pH. These groups are all tested in the solution with 15mM Na^{+} and 1mM Mg^{2+}. The left column indicates the magnification of TEM setup when capturing the images. Images with the same magnification share the same scale bar.

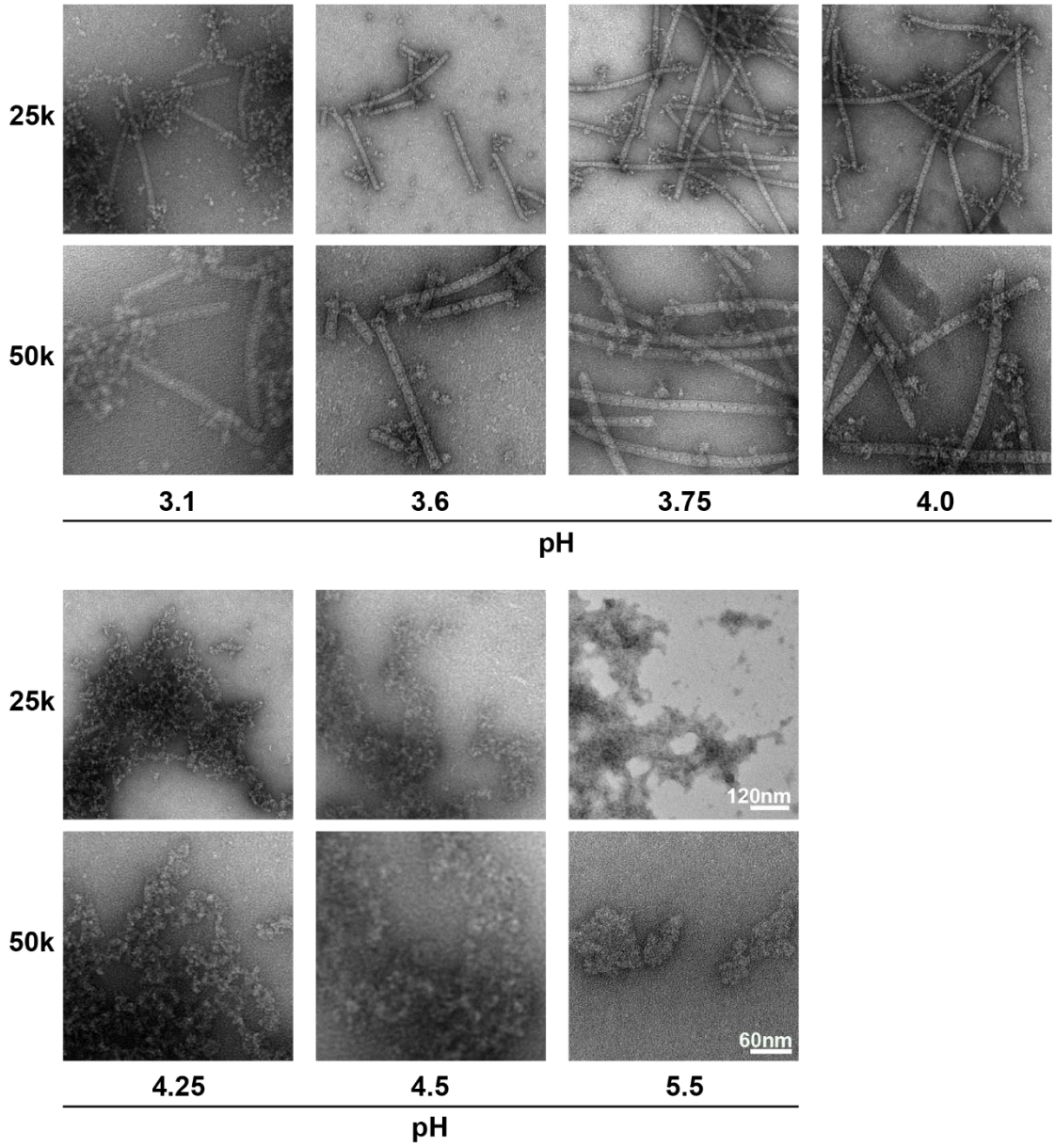

Figure 2-11. TEM images of the product of 18B2S under different pH. These groups are all tested in the solution with Na^{+} and 1mM Mg^{2+}. The left column indicates the magnification of TEM setup when capturing the image. Images with the same magnification share the same scale bar. Note that for these groups, the nanorods are too long to be completely included in this grid.

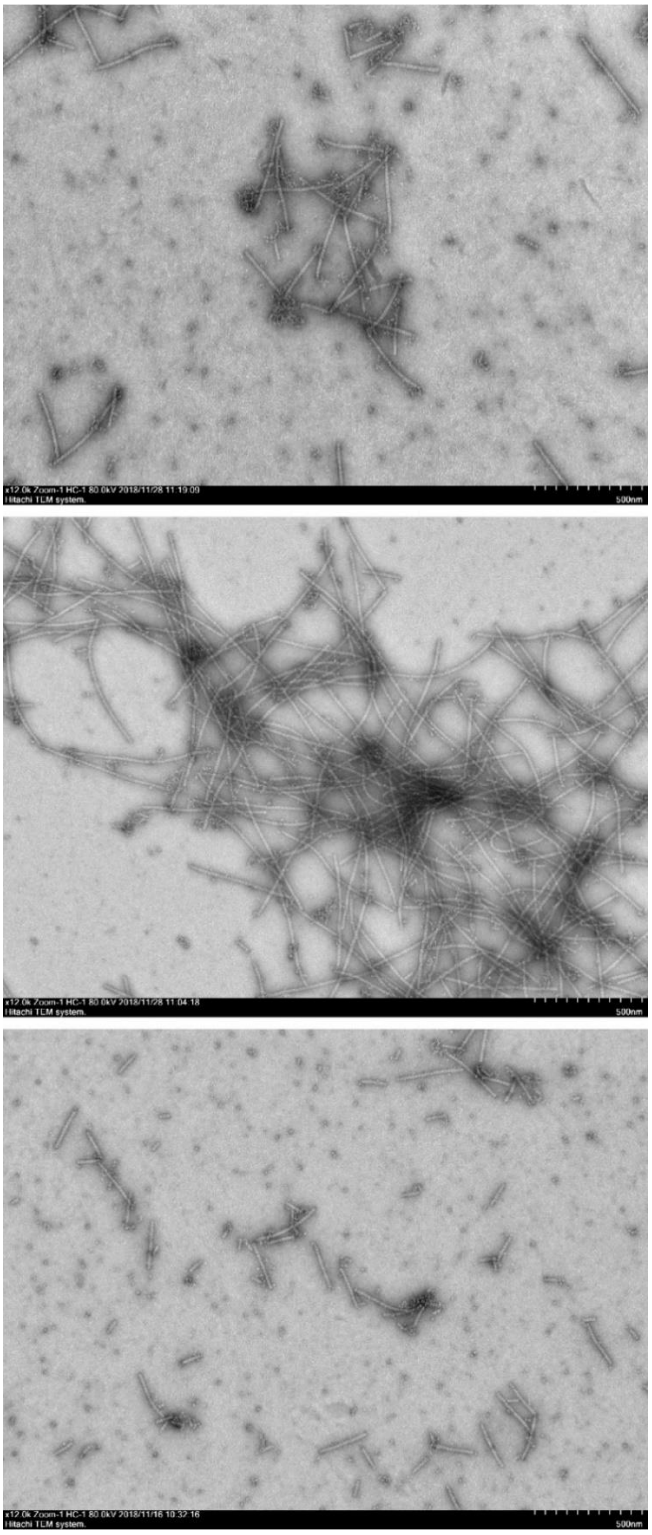

Figure 2-12. TEM images showing the full size of 18B2S nanorods. The upper image shows the assembly under pH=3.6. The middle image shows the assembly under pH=3.75. The lower image shows the assembly under pH=4.25. These images are directly captured under TEM. Scale bars are presented at the lower right corner of each image.

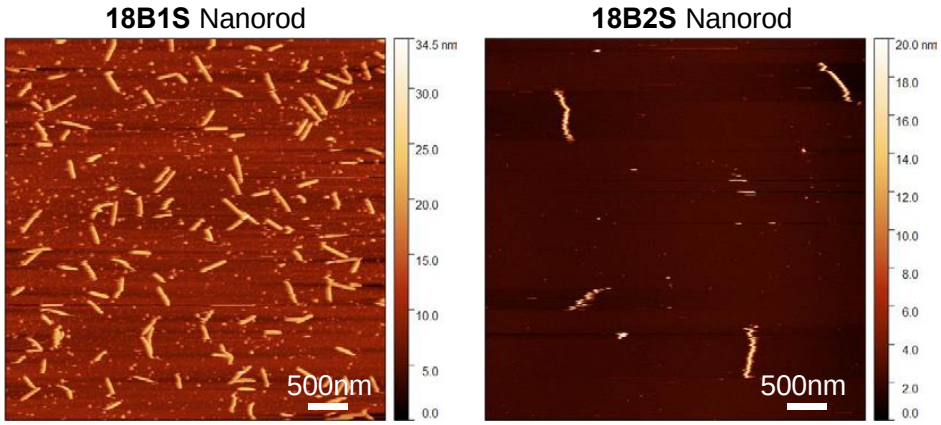

Figure 2-13. Liquid-phase AFM images of 18B1S nanorod (pH=4.25, 15mM Na+ and 1mM Mg2+) and 18B2S nanorod (pH=3.75, 15mM Na+ and 1mM Mg2+).

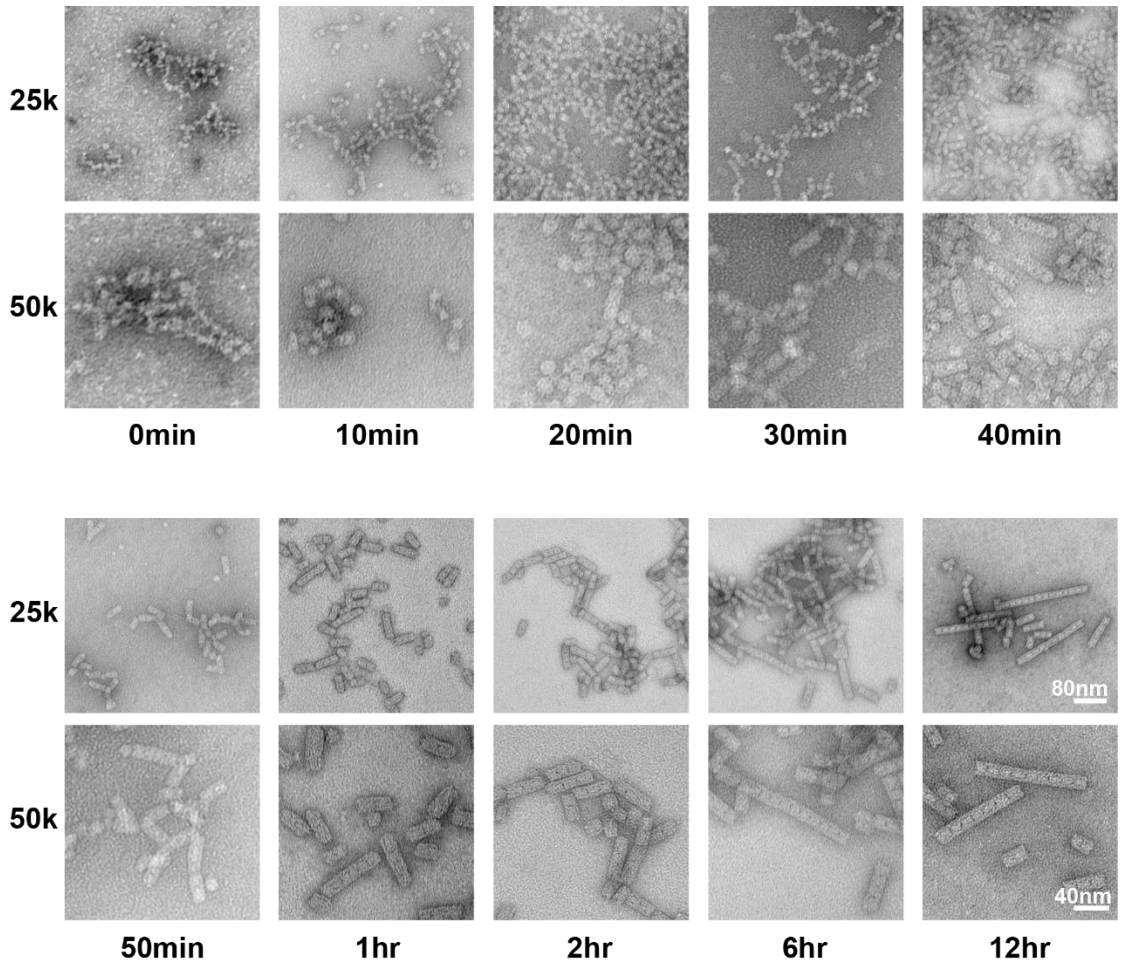

Figure 2-14. TEM images of the assembly of 18B1S collected at different annealing time points. These groups are all tested in the solution with pH=4.25, 15mM Na^{+} and 1mM Mg^{2+}. The left column indicates the magnification rate of TEM setup when capturing the image. Images with the same magnification share the same scale bar.

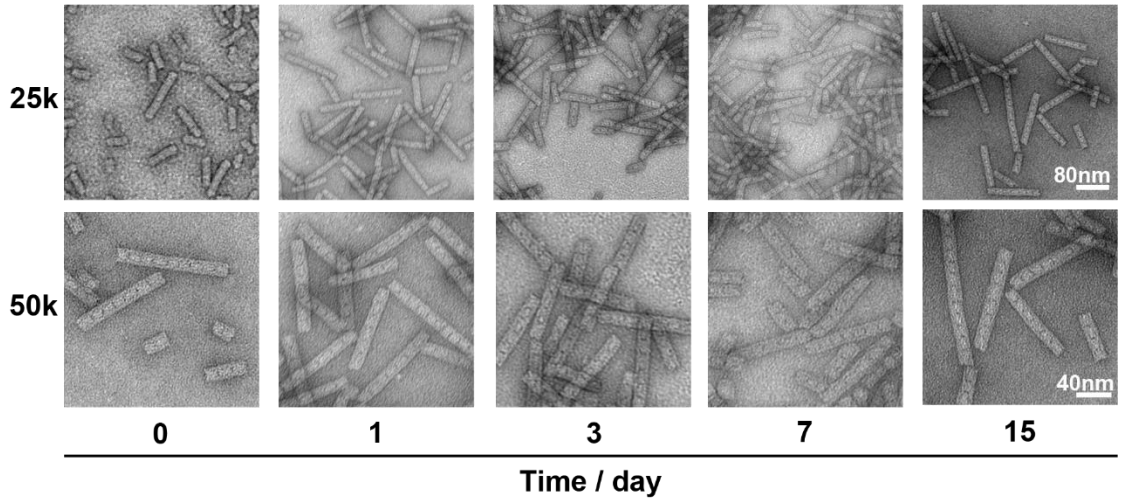

Figure 2-15. TEM images of preassembled 18B1S nanorods placed under room temperature for long periods of time. These groups are all tested in the solution with pH=4.25, 15mM Na^{+} and 1mM Mg^{2+}. The left column indicates the magnification rate of TEM setup when capturing the image. Images with the same magnification share the same scale bar. After 15 days, the black gaps were still obvious on nanorods.

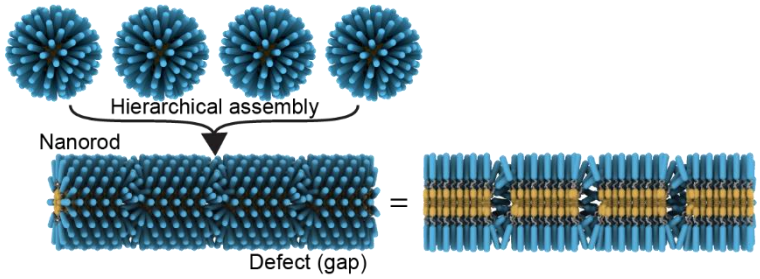

Figure 2-16. Proposed hierarchical assembly of micelles leads to the formation of the nanorods and the visible periodic gaps in the nanorods.

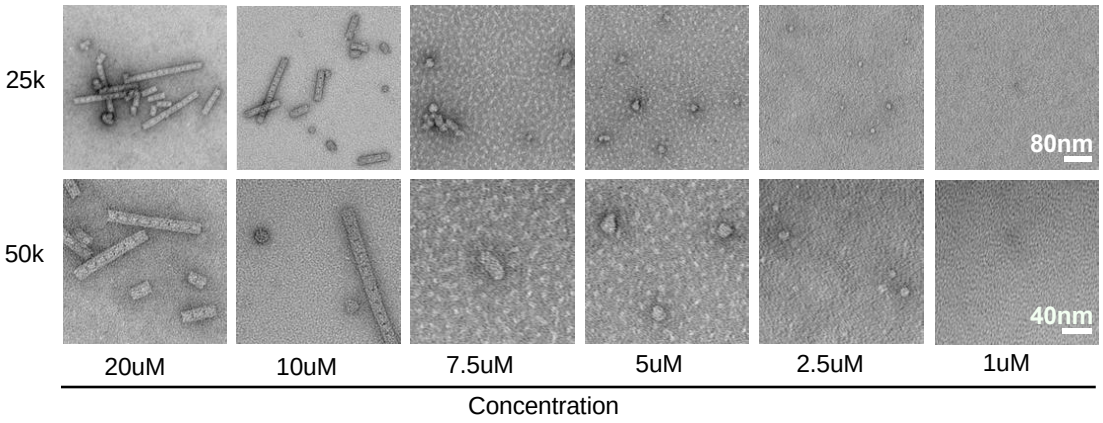

Figure 2-17. Assembly of 18B1S at different strand concentrations. For all groups, the reaction solution was incubated on the TEM grid overnight to ensure the complete adhesion. When strand concentration lowered to 1uM, no well-defined structures could be observed under TEM. All groups were assembled in the solution under pH=4.25 with 15 mM Na^{+} and 1mM Mg^{2+}. "25k" and "50k" indicate the magnification of the images. Images with the same magnification share the same scale bar.

2.4 Conclusion

In this project, we discovered that under acidic conditions, sole cholesterol-DNA block copolymer could form micellular structures, including spherical micelles and nanorods. The morphology of the formed micellular nanostructures was tuned by salt concentration, pH, and DNA sequence design. One main observation of the nanorod structures was the clearly visible black gaps. Further investigation confirmed that such black gaps were formed during the incomplete merging of spherical micelles into nanorods through a hierarchical pathway. We hypothesized that such incomplete merging is caused by the large difference in the 777size of the hydrophobic core and hydrophilic shell; However, this hypothesis still needs further confirmation.

Using amphiphilic DBCs to construct nanostructures as drug delivery vehicles is a hot topic in recent research (20). A novel supplement to the toolbox of amphiphilic DBC nanostructure is largely desired nowadays. We believe that our work not only further proves the versatility of amphiphilic DBCs, but also provides insights on new design principles and assembly mechanisms for future investigations. For the follow-up study of this work, we will try to confirm the hypothesis about the incomplete merging of spherical micelles into nanorods. Besides, we will try other hydrophobic modifications on DNA strands to check if such novel assembly pathway can be applied to a wider range of DBC constitutions and reaction conditions.

2.5 Material and Methods

Cholesterol-DNA block copolymer and DNA strand preparation. All the DNA block copolymers (DBC) and DNA strands were directly purchased from Integrated DNA Technologies (IDT). For Cholesterol-DNA, cholesterol was conjugated to the 3’ end of DNA strand, and a triethylene glycol (TEG) linker was required between these 2 parts. The internal hexa-ethyleneglycol spacer was added between DNA part and TEG linker, and multiple sets of

internal spacers were able to be incorporated. The synthesis of Cholesterol-DNA required High Performance Liquid Chromatography (HPLC) purification, thus the influence of impurity could be excluded during assemblies. For DNA strands, they were ordered with the "DNA oligo" service and provided as single strands. Only standard desalting was ordered for single strand DNA. All DBCs and DNA strands were dissolved in Deionized water (DI water) with the final concentration of 100 μM according to IDT's instruction. The DBCs and DNA strands' concentration was all 20 μM in reaction solution unless specifically indicated.

DNA sequence design. The initially tested DBC 18B has a DNA part with randomly assigned 18 bases. When designing this sequence, all hairpin, self- and hetero-dimer structures under physiological conditions were avoided which was confirmed using OligoAnalyzer on IDT's website. 12B's DNA part was designed by deleting 6 bases from 18B's DNA part's 5' end, and 24B's DNA part was designed by adding 6 bases to 18B's DNA part's 5' end. Still, all potential secondary structures under physiological conditions were avoided for these two strands. PolyT was designed by switching all bases of 18B's DNA part to thymine. It was used as a control group in this paper because it would not have any interactions between DNA strands. The sole DNA parts of all DBCs and the complementary strand of 18B's DNA part were also designed and prepared.

Annealing process. Many amphiphilic DBCs, including Cholesterol-DNA, need to undergo an annealing process for successful assembly. The annealing process for most trials in this paper was:

Step 1: Stay at 37 °C for 30 minutes;

Step 2: From 37 to 29 °C, decrease 0.1 °C for every 10 minutes;

Step 3: Stay at 29 °C forever.

This annealing process was adapted from previous research (11-13). We tested different initial annealing temperature and discovered that 37 °C was the most appropriate one for our system. We also tested the influence of the time of staying at the final 29 °C stage and found no noticeable difference between all groups. Unless specifically indicated, this annealing process was used by all trials in this paper.

Tuning the salt concentration and pH. For salt concentration, sodium ion was chosen to tune the ion strength in the buffer for the ease of experiment. The 4 levels of sodium ion concentration were referred to the buffer constitution of phosphate-buffered saline (PBS). To be detailed, Low (Comparable to 0.1× PBS) had 15 mM Na^+, Medium (Comparable to 1/3 1× PBS) had 50 mM Na^+, High (Comparable to 2/3× PBS) had 100 mM Na^+, and Very high (Comparable to 4/3× PBS) had 200 mM Na^+. For both salt concentration and pH control, NaAc-HAc buffers with different Na+ concentration and pH were prepared. As for magnesium concentration, the 4 levels chosen were referred to the general practice of DNA nanostructure assembly. $MgCl_2$ solution with different concentration was prepared for controlling Mg^{2+} concentration in the reaction buffer. The reaction buffer constitution was tuned by mixing NaAc-HAc buffer, $MgCl_2$ buffer and Cholesterol-DNA solution with a certain ratio that would produce the desired condition.

Sodium Acetate was purchased from LabChem Inc. Glacial acetic acid was purchased from Macron Fine Chemicals. Magnesium chloride was purchased from EMD Millipore Corporation.

Transmission electron microscopy (TEM) imaging. For the sample preparation for TEM imaging, 3 μL sample was deposited on the surface charged carbon film coated copper EM grids for 30 seconds, then a filter paper was used to remove the excess liquid on the grid. 8 μL 1% uranyl formate (UF) solution was used for negative staining, and excess liquid was also

removed with a filter paper after 20 seconds. The samples were imaged using a Hitachi HT-7700 120 kV W (Tungsten) TEM with AMT CCD camera. Note that the number of nanostructures shown on the images does not represent the actual yield of them, and the brightness of the figures solely depend on the staining and imaging technique.

To prepare the 1% UF solution, 10mg UF powder was dissolved in 1 mL DI water and heated to the point when no changes further appeared. Then 1 μL of 5 M NaOH was added to the solution and mixed well. The solution was further filtered using a 0.2 μm syringe filter with cellulose acetate membrane and the filtrate was collected. Copper EM grids were charged using Pelco easiGlow Glow Discharge Cleaning System. UF powder was purchased from Electron Microscopy Sciences. 5 M NaOH was purchased from Fisher Scientific. EM grids were purchased from Electron Microscopy Sciences, and the model of grids was CF400-CU. 0.2 μm syringe filter was purchased from VWR International.

Atomic force microscopy (AFM) imaging. Topographic AFM images were captured by peak force tapping mode (PFT) experiments on a Multimode VIII system (Bruker Corporation, Santa, Barbara, CA) in liquid. The samples were prepared by deposition of a 2 μL sample onto freshly cleaved mica. And then the liquid cell was filled with around 80 μL 1× buffer with. Commercial silicon nitride cantilevers with integrated sharpened tips (Bruker, SNL-10) were used.

Testing the stability of nanorods. We used 18B1S in the buffer with pH=4.25, low salt concentration and 1 mM Mg^{2+} to do the annealing, then placed the product solution under room temperature for different time to see whether the black gaps would disappear. Samples were collected on day 0, 1, 3, 7 and 15, and imaged under TEM.

Polyacrylamide gel electrophoresis (PAGE). Nondenaturing polyacrylamide gel was prepared according to the standard protocol provided by Thermo Scientific. A 20% native polyacrylamide gel was prepared with 1X TBE and 10mM Mg^{2+} for the separation of small

DNA fragments. 100ng sample was loaded in each well. 6 μL DNA ladder was loaded for reference. The electrophoresis was carried out with 120V for 180 minutes, and stained with 1× SYBR gold for 10 minutes, followed by washing with DI water. The gel was imaged using Bio-Rad Gel Doc EZ Imager.

The polyacrylamide solution, ammonium persulfate, TEMED and electrophoresis instruments were purchased from Bio-Rad Laboratories. The DNA ladder used was GeneRuler Ultra Low Range DNA Ladder purchased from Thermo Scientific. The 1× TBE was prepared by mixing 27g tris, 13.75g boric acid, and 1.85g EDTA in 500mL DI water and diluted to the desired concentration. Tris was purchased from Sigma-Aldrich Co. Boric acid was purchased from Spectrum chemical MFG. Corp. EDTA was purchased from Avantor Performance Materials. The concentration of Mg^{2+} was controlled using 1M $MgCl_2$ solution.

Sample preparation for PAGE analysis. For the experimental group, 20 μM 18B's DNA part was annealed in the solution with pH=3.1, low salt concentration and 1mM Mg^{2+}. This was the lowest pH condition we employed in this paper. After annealing, the solution was diluted, adjusted to neutral pH with 5M NaOH, and mixed with equal amount of its complementary strand. The mixture was vortexed for 30 minutes under room temperature to ensure the complete hybridization. For the control group, 20 μM of 18B's DNA part was directly diluted into the same concentration and mixed with equal amount of its complementary strand without annealing. The concentration of double strands was measured using Thermo Scientific Nanodrop 2000 Spectrophotometer.

Annealing 18B with the complementary strand of its DNA part. 20 μM 18B and its DNA part's complementary strand were mixed together to do the normal annealing in the solution with pH=3.6, low salt concentration and 1mM Mg2+. The assembly product of 20 μM 18B annealed under same condition without the complementary strand was chosen as the control

group.

Collecting samples of 18B1S at different annealing point. 18B1S was used to do the normal annealing in the solution with pH=4.25, low salt concentration and 1mM Mg^{2+} because this group produced nanorods with clear black gaps under TEM. Samples at 0, 5, 10, 20, 30, 40, 240, 440, 640 and 840 minutes after annealing starts were collected and imaged under TEM. 0 to 40-minute groups were samples at 37°C. The 240-minute sample was collected at 35°C. The 440-minute sample was collected at 33°C. The 640-minute sample was collected at 31°C. The 840-minute sample was collected at 29°C.

Using 18B1S to undergo annealing process with different total time. For all groups in this trial, 20 μM 18B1S and the solution with pH=4.25, low salt concentration and 1mM Mg^{2+} were used. The basic steps of the annealing process used by each group were the same as the original one aforementioned; However, the time length of each step was different, so the total annealing time varies: 0, 10, 20, 30, 40, 50, 60, 120, 360, and 720 minutes. The samples were collected after the annealing process was done and imaged under TEM.

Measuring the size of nanostructures using ImageJ. The width of the nanorods was analyzed using ImageJ and plotted to exhibit the trend. Three experimental groups were used for comparison: 18B, 18B1S, and 18B2S annealed in the solution with pH=3.6, low salt concentration and 1mM Mg^{2+}. 20 data points were selected for each group and their average width was calculated and plotted. Standard deviation of each group was also calculated and plotted as error bars.

Measuring the CMC of DNA-cholesterol DBC. 18B1S was assembled at concentrations of 10μM, 7.5μM, 5μM, 2.5μM, 1μM, 0.5μM and 0.1uM. Then the reaction solution was incubated on the TEM grid overnight to ensure the complete adhesion. The assembly of all groups was checked using TEM imaging. The strand concentration was considered below CMC

if no well-defined structure could be found.

2.6 Reference

1. Ke Y, Castro C, Choi JH. Structural DNA Nanotechnology: Artificial Nanostructures for Biomedical Research. Annu Rev Biomed Eng. 2018;20:375-401.

2. Mai Y, Eisenberg A. Self-assembly of block copolymers. Chem Soc Rev. 2012;41(18):5969-85.

3. Bousmail D, Chidchob P, Sleiman HF. Cyanine-Mediated DNA Nanofiber Growth with Controlled Dimensionality. J Am Chem Soc. 2018;140(30):9518-30.

4. Qi H, Ghodousi M, Du Y, Grun C, Bae H, Yin P, et al. DNA-directed self-assembly of shape-controlled hydrogels. Nat Commun. 2013;4:2275.

5. Jiang T, Meyer TA, Modlin C, Zuo X, Conticello VP, Ke Y. Structurally Ordered Nanowire Formation from Co-Assembly of DNA Origami and Collagen-Mimetic Peptides. J Am Chem Soc. 2017;139(40):14025-8.

6. Wilks TR, Bath J, de Vries JW, Raymond JE, Herrmann A, Turberfield AJ, et al. "Giant surfactants" created by the fast and efficient functionalization of a DNA tetrahedron with a temperature-responsive polymer. ACS Nano. 2013;7(10):8561-72.

7. Chien MP, Thompson MP, Gianneschi NC. DNA-nanoparticle micelles as supramolecular fluorogenic substrates enabling catalytic signal amplification and detection by DNAzyme probes. Chem Commun (Camb). 2011;47(1):167-9.

8. Wang Y, Wu C, Chen T, Sun H, Cansiz S, Zhang L, et al. DNA micelle flares: a study of the basic properties that contribute to enhanced stability and binding affinity in complex biological systems. Chem Sci. 2016;7(9):6041-9.

9. Lu Y, Yue Z, Xie J, Wang W, Zhu H, Zhang E, et al. Micelles with ultralow critical micelle concentration as carriers for drug delivery. Nat Biomed Eng. 2018;2(5):318-25.

10. Zhou C, Zhang Y, Dong Y, Wu F, Wang D, Xin L, et al. Precisely Controlled 2D Free-

Floating Nanosheets of Amphiphilic Molecules through Frame-Guided Assembly. Adv Mater. 2016;28(44):9819-23.

11. Dong Y, Sun Y, Wang L, Wang D, Zhou T, Yang Z, et al. Frame-guided assembly of vesicles with programmed geometry and dimensions. Angew Chem Int Ed Engl. 2014;53(10):2607-10.

12. Zhao Z, Chen C, Dong Y, Yang Z, Fan QH, Liu D. Thermally triggered frame-guided assembly. Angew Chem Int Ed Engl. 2014;53(49):13468-70.

13. Wu F, Zhao Z, Chen C, Cao T, Li C, Shao Y, et al. Self-Collapsing of Single Molecular Poly-Propylene Oxide (PPO) in a 3D DNA Network. Small. 2018;14(10).

14. Wang L, Feng Y, Yang Z, He YM, Fan QH, Liu D. Reversibly controlled morphology transformation of an amphiphilic DNA-dendron hybrid. Chem Commun (Camb). 2012;48(31):3715-7.

15. Yang CJ, Pinto M, Schanze K, Tan W. Direct synthesis of an oligonucleotide-poly(phenylene ethynylene) conjugate with a precise one-to-one molecular ratio. Angew Chem Int Ed Engl. 2005;44(17):2572-6.

16. Trinh T, Chidchob P, Bazzi HS, Sleiman HF. DNA micelles as nanoreactors: efficient DNA functionalization with hydrophobic organic molecules. Chem Commun (Camb). 2016;52(72):10914-7.

17. Tan X, Li BB, Lu X, Jia F, Santori C, Menon P, et al. Light-triggered, self-immolative nucleic Acid-drug nanostructures. J Am Chem Soc. 2015;137(19):6112-5.

18. Chan MS, Tam DY, Dai Z, Liu LS, Ho JW, Chan ML, et al. Mitochondrial Delivery of Therapeutic Agents by Amphiphilic DNA Nanocarriers. Small. 2016;12(6):770-81.

19. Pack DW, Hoffman AS, Pun S, Stayton PS. Design and development of polymers for gene delivery. Nat Rev Drug Discov. 2005;4(7):581-93.

20. Banga RJ, Chernyak N, Narayan SP, Nguyen ST, Mirkin CA. Liposomal spherical

nucleic acids. J Am Chem Soc. 2014;136(28):9866-9.

21. Hou X, Zaks T, Langer R, Dong Y. Lipid nanoparticles for mRNA delivery. Nat Rev Mater. 2021;6(12):1078-94.

22. Stengel G, Simonsson L, Campbell RA, Hook F. Determinants for membrane fusion induced by cholesterol-modified DNA zippers. J Phys Chem B. 2008;112(28):8264-74.

23. Kocabey S, Kempter S, List J, Xing Y, Bae W, Schiffels D, et al. Membrane-assisted growth of DNA origami nanostructure arrays. ACS Nano. 2015;9(4):3530-9.

24. Johnson-Buck A, Jiang S, Yan H, Walter NG. DNA-cholesterol barges as programmable membrane-exploring agents. ACS Nano. 2014;8(6):5641-9.

25. Gunnarsson A, Jonsson P, Marie R, Tegenfeldt JO, Hook F. Single-molecule detection and mismatch discrimination of unlabeled DNA targets. Nano Lett. 2008;8(1):183-8.

26. Magnusson JP, Fernandez-Trillo F, Sicilia G, Spain SG, Alexander C. Programmed assembly of polymer-DNA conjugate nanoparticles with optical readout and sequence-specific activation of biorecognition. Nanoscale. 2014;6(4):2368-74.

27. Banchelli M, Gambinossi F, Durand A, Caminati G, Brown T, Berti D, et al. Modulation of density and orientation of amphiphilic DNA on phospholipid membranes. II. Vesicles. J Phys Chem B. 2010;114(21):7348-58.

28. Choi KM, Kwon IC, Ahn HJ. Self-assembled amphiphilic DNA-cholesterol/DNA-peptide hybrid duplexes with liposome-like structure for doxorubicin delivery. Biomaterials. 2013;34(16):4183-90.

29. Brady RA, Brooks NJ, Fodera V, Cicuta P, Di Michele L. Amphiphilic-DNA Platform for the Design of Crystalline Frameworks with Programmable Structure and Functionality. J Am Chem Soc. 2018;140(45):15384-92.

30. Zhang Y, Peng R, Xu F, Ke Y. Hierarchical Self-Assembly of Cholesterol-DNA Nanorods. Bioconjug Chem. 2019;30(7):1845-9.

31. Hu Y, Chen Z, Hou Z, Li M, Ma B, Luo X, et al. Influence of Magnesium Ions on the Preparation and Storage of DNA Tetrahedrons in Micromolar Ranges. Molecules. 2019;24(11).

32. Hong F, Zhang F, Liu Y, Yan H. DNA Origami: Scaffolds for Creating Higher Order Structures. Chem Rev. 2017;117(20):12584-640.

33. Varshney D, Spiegel J, Zyner K, Tannahill D, Balasubramanian S. The regulation and functions of DNA and RNA G-quadruplexes. Nat Rev Mol Cell Biol. 2020;21(8):459-74.

Chapter 3. Building Large DNA Bundles via Controlled Hierarchical Assembly of DNA Tubes

3.1 Abstract

One of the major merits of structural DNA nanotechnology is the capability of building designer nanoscale artificial structures. During the last decades, various nanoscale artificial structures have been fabricated with unprecedented blooming of numbers. However, a simple but versatile constructing method to assemble large-scale DNA structures, for example, from nanoscale to microscale, is still remained challenging. In this project, we designed a molecular assembly system in which simple DNA DX tiles can assemble into nanotube structures, then nanotubes can further assemble into large one-dimensional bundle structures. Such an assembly pathway is a hierarchical assembly process, where different sequences, including sticky ends and cohesive linkers, are incorporated into DX tile structures to induce the 2-step formation of nanotubes and bundles. The resulting DNA bundles, with length of >10 micrometers and width of hundreds of nanometers, were produced and imaged with various analytical instruments. The assembly of the bundle was also revealed to be co-determined by various features, like cationic strength in the assembly buffer and the linker design on the DX tiles. Furthermore, based on the system, multi-component DNA bundles with varied spatial and compositional features were assembled, illustrating this system's high programmability and versatility. Finally, dynamic capability was also implemented into the system, demonstrated by the reversible reconfigurations of the assembly morphology through toehold-mediated strand displacement reactions. We believe that this assembly strategy can provide a new option for large-scale DNA structure rational design with designated features and properties. Besides, such strategy may find potential applications in a variety of fields in nanotechnology and material science, including the development of next-generation micron-sized materials, vectors, sensors, and machines.

3.2 Background

3.2.1 Bundle fiber structures in nature

Bundle fiber structures, which are commonly presented in natural organisms, can involve in numerous biological functions and processes, including cell migration, cell division, molecular transportation, etc (1). Besides, they also play important roles in various pathological processes, including cancer cell apoptosis, tumor progression and tumor metastasis (2, 3). Among all the examples of natural bundle fiber structures, they are typically assembled from lower-order small monomers through hierarchically prescribed assembly pathway (4, 5). One most famous examples of this assembly pathway is the assembly of muscle fibers, where a bunch of different types of muscle cells are involved in the assembly of the whole bundler structure (6). Up to now, extensive efforts have been made to build artificial bundled fiber structures that can mimic their canonical opponents' both functional and structural perspectives. Serving as robust biomimetic models, they are believed to deliver potential applications in biology and biomedical applications, such as physiological research and cell programming (7-9).

3.2.2 The effort of using DNA nanotechnology in building bundle fiber structures

One of the most dominating applications of DNA nanotechnology lies in structural DNA nanotechnology. Structural DNA nanotechnology represents the method of using DNA as the basic building blocks to realize precise fabrication of nanoscale designer structures with prescribed properties through self-assembly pathways. Nowadays, structural DNA nanotechnology is one of the most robust and versatile molecular assembly strategies in nanotechnology (10, 11). On the other hand, as this strategy continues to develop, DNA nanostructures have been increasingly participating in the construction of higher-scale structures and more complex systems. Previous research has focused on the conjugation between DNA nanostructures and other molecules, such as inorganic particles, organic

polymers, and biological molecules (11, 12). However, creating macro-structures only using DNA is also intriguing. The homogenous constitution of these DNA macro-structures can avoid the sophisticated interactions between DNA and other molecules, enabling a more straightforward control on product's size, shape, and function (13). Thus, they are widely employed in the construction of meta-materials such as micro-electronics and artificial organelles, and new applications of these materials keep emerging in recent years (14-19).

A regular strategy for constructing DNA macro-structures is to involve modular designs. For instance, Yin and coworkers constructed a set of gigadalton-sized 3D nanostructures using DNA bricks, of which the assembly model closely resembles to Lego blocks (20). Another example from Yan's group is to use six-helix bundle DNA origami as the mimic of single-strand DNA to construct architectures on a submicrometer-to-micrometer scale (21). These successful results are truly elegant and stunning, vividly reflecting the robustness of this strategy. However, a module with a simple constitution while retaining the potential to construct complex DNA macro-structures is still in demand. This module is expected to avoid several difficulties in previous methods, including the complexity of designing orthogonal interaction patterns within and among modules, and the labor-extensive situation while handling a massive number of DNA strands. Considering these demands and expectations, researchers have switched their attention to some heavily investigated simpler DNA nanostructures, and one example of them is the DNA double-crossover (DX) tile structure.

3.2.3 DNA DX tile structure

DX tile structure is one of the first DNA nanostructures being constructed (22). It is assembled by a set of DNA single strands with delicately designed binding patterns. DNA DX tile structures have certain advantages over other DNA nanostructures, such as the simplicity of design and the scalability to large structures. Therefore, although DX tile structures were first

developed two decades ago, they are still extensively used in DNA nanotechnology nowadays (23-28). One of the major applications of the DX tile structure is constructing DNA DX nanotubes. Numerous nanotubes with different length and diameter were assembled, fulfilling various needs including drug delivery, nanomachine, and nanofabrication (29-31). One new application for DX tile nanotube, which recently attracted much interest, is to work as a basic module to further assemble into macro-structures. For example, Schulman group designed rigid DNA nano-junctions to connect nanotubes into micron-scale framework architectures (23). Another more recent example is that Burns utilized the bridging effect of high concentration Mg^{2+} on adjacent phosphate anions between two nanotubes to condense flexible nanotubes into rigid nanofibers (32).

All these previous works inspire us that DNA DX nanotubes can become a potent candidate for constructing solely DNA-based macro-structure. However, certain problems are still pending to be resolved, such as the poor assembly pattern control between nanotubes and the confined application caused by the specific assembly condition. For example, in the before-mentioned work by Burns, where sole cation-driven process of nanofiber assembly was employed, compared to DNA-sequence-driven assembly, such over-simplified process lacks control over bundle formation, including DNA tube's registration and density, bundle width, bundle surface programmability, and dynamic capability (32). Furthermore, this cation-bridged DNA bundle assembly requires high cationic strength (~ 40-50mM of Mg^{2+}), which is too high compared to physiological conditions and can limit its subsequent biomedical applications. Thus, a more robust and advanced strategy of using DNA nanotubes to further assemble into higher-order bundled fibers is still highly wanted.

3.2.4 Hypothesis and goal of this project

Considering the optimization of nanotube systems, herein we designed a system where DX

tiles first assemble into nanotubes, then nanotubes further assemble into micrometer-scale rigid DNA bundles. DX tile is flanked with a cohesive linker to introduce programmable binding process from DNA nanotubes to large DNA bundles cooperated with a moderate range of cationic strength. More importantly, such cohesive linker provides a chaperoning force to better control the major assembly parameters including width, compactness, constitution, and reconfigurability. Comprehensive studies were carried out to unveil the design principle of the cohesive linkers towards higher tunability on DNA bundle assembly. We envision that this project can provide strategies for future rational design on constructing macro-sized biomimetic functional materials, and the DNA bundle structure fabricated in this project can potentially find various applications in materials science, synthetic biology, and biomedical research.

This project was published on ACS Nano (33).

3.3 Results and discussion

3.3.1 General design and characterization of DNA bundles

The overall scheme of DNA bundle assembly is shown in Figure 3-1a. The assembly starts from the formation of DNA double-crossover tile (DX tile), which consists of 5 single-strand DNA labeled S1 to S5. The backbone of this DX tile (Grey) is 37bp long, and 5-nucleotide sticky ends on S2 and S4 strands (Labeled in cyan and purple) are flanking on both sides (Figure 3-1a). These sticky ends are capable of inducing the assembly of DX tiles into DNA nanotubes. In this project, to further promote the assembly of DNA nanotubes into DNA bundles, a 7-nucleotide linker sequence was introduced to this DX tile (Green strand). These linkers are designed to protrude on the outer surface of nanotubes after assembly. Hybridization between DNA linkers enables binding between DNA tubes that induces growth both along and perpendicular to the longitudinal direction of DNA tubes, leading to the formation of long and

wide DNA bundles. During the assembly, as indicated in previous literatures, certain divalent ions (i.e., Mg2+) can also participate in such process to help the hybridization of DNA nanotubes (32).

In this project, multiple DX tiles are designed to fulfill various needs in the investigation process. Besides, to investigate the influence of the newly introduced linker sequence, a large set of linkers are designed and used in this project. All sequences of these DX tiles and linkers, their labeling, and a brief description of the usage of linker sequences are shown in Figure 3-2 and Table 3-1. Please refer to this information during the result discussion in the following paragraphs.

The assembly of DX tiles, nanotubes, and DNA bundles were first characterized by routine agarose gel electrophoresis analysis (Figure 3-1b). In this experiment, DX tiles were assembled using Tile C, in which the sticky ends are non-cohesive and can not further induce the nanotube formation (Figure 3-1c). DNA nanotubes were assembled using Tile A with cohesive sticky ends but without flanking linkers (Figure 3-1d). DNA bundles were assembled using Tile A with both cohesive sticky ends and flanking linkers, and the linker sequence was 5'-CGCGTTT-3'. The DX tiles underwent the self-assembly process with a slow annealing protocol in an aqueous buffer containing 1x TE and 20mM $MgCl_2$ (See Materials and Methods part for further reference). On the agarose gel analysis image, all assemblies showed anticipated migration: DX tiles showed the fastest mobility on the gel, because of its lowest molecular weight and size. However, both nanotubes and DNA bundles were retained in the wells, suggesting the successful formation of large structures.

To further unambiguously visualize these structures, atomic force microscopy (AFM), confocal laser scanning microscopy (CLSM), and transmission electron microscopy (TEM) were used for high-resolution imaging. AFM was used to image the morphology of DX tiles, and the

nanoscale rectangular structures of DX tiles were revealed with the correct dimensions. Some loose connections of DX tiles into clusters were also observed, suggesting the assembly pathway of DX tiles into DNA nanotubes (Figure 3-1c). Furthermore, both CLSM and TEM were used to image nanotubes and DNA bundles (Figure 3-1d, 3-1f). Micrometer-long DNA tubes with an average width of 14-15 nm (7-8 tiles along the tube circumference) were observed if no linker was incorporated, which matches well with previous reports using similar DX tile designs to assemble DNA nanotubes (34). However, when the cohesive linker of 5'-CGCGTTT-3' was incorporated, the binding and bundling between DNA nanotubes were induced and long and wide DNA bundle structures were grown. The DNA bundles are ultra-stiff, with a length of ~50um and a width of ~ 150nm. We also further imaged more DNA bundles and found that the size distribution of DNA bundles may be large, which enables the formation of ultra-wide and long DNA bundles (Figure 3-3). All these figures confirmed the successful assembly of the three states of DNA structures in such system.

As mentioned before, a specific linker sequence was used in this experiment to induce the formation of DNA bundles. Indeed, the linker sequence is one of the major influential features in our system. To compare with the 5'-CGCGTTT-3' sequence which can induce DNA bundle formation, we further tested the assembly of DX tiles with 5'-TTTTTTT-3' linker sequence. This sequence is widely used in DNA nanotechnology to prevent the hybridization of DNA sequences. As shown in the agarose gel analysis image, such DX tile still assembled into higher-order structures, indicating that the sticky ends were still functioning. However, TEM and CLSM images revealed the morphology of the assembly to be DNA nanotubes, and no further assembled DNA bundles were found in the images (Figure 3-1e). This result confirms the importance of the linker in the DNA bundle assembly process, and points out the further investigation direction of this project. It is also necessary to point out that besides the linker, other factors can also influence the assembly of DNA bundles, including annealing temperature

and salt content in the buffer. Thus, in the next step, these factors will also be comprehensively investigated.

In addition to the DX tiles, nanotubes, and DNA bundle morphology, in TEM images, clear, thin white stripes could also be observed to occur periodically on the DNA bundles (Figure 3-1f). The white stripes crossed the bundles perpendicularly throughout the whole structure, and the intervals of the white stripes were measured to be ~15nm. The width of this interval corresponds well to the size of a single DX tile (42bp long), thus, the cause of these white stripes was hypothesized to be the linkers aligned on the surface of the DNA bundle. More investigations on these white stripes will be covered in the following parts of this thesis.

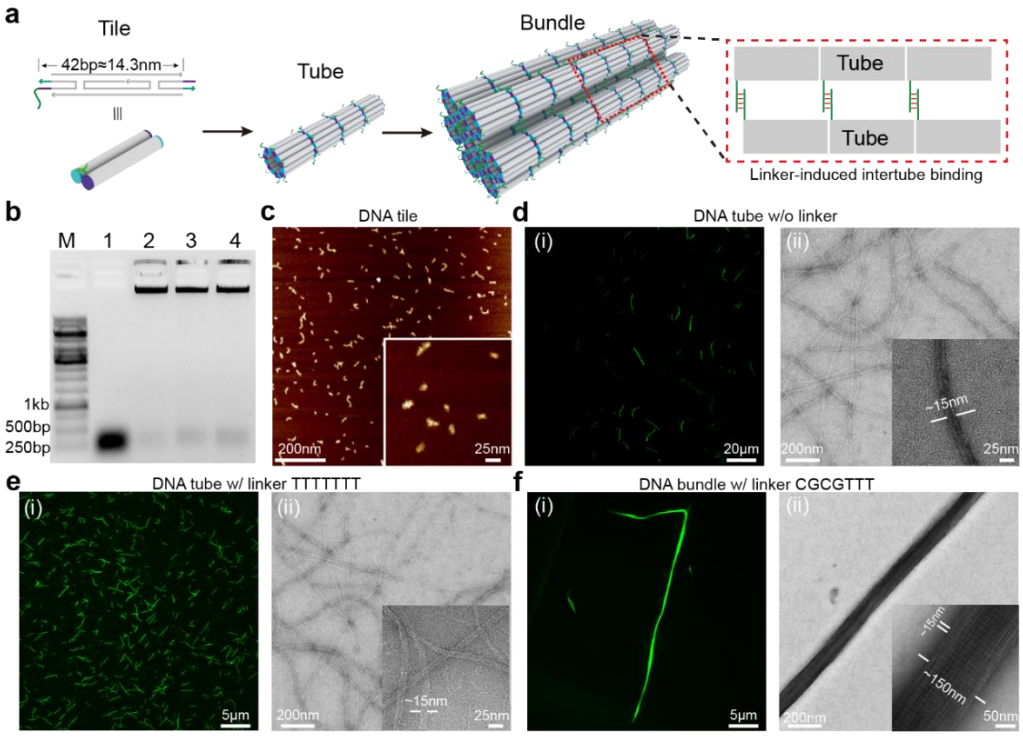

Figure 3-1. General design and characterization of DNA bundles. For all results, structures were assembled from Tile A unless indicated. (a) The proposed hierarchical assembly pathway of DNA bundles from DNA tiles and DNA tubes. DNA DX tiles first assemble into narrow tubes via sticky-end cohesions (cyan and purple strands), then further assemble into ultra-stiff, long and wide DNA bundles through DNA linkers (green strands) that protruding from the exterior surface of the tubes. (b) Agarose gel electrophoresis analysis of DNA tiles, tubes, and bundles. M: DNA Marker. Lane 1: DNA tiles assembled from Tile C. Lane 2: DNA tubes assembled from tiles without linkers. Lane 3: DNA tubes assembled from tiles with linker of TTTTTTT (7T). Lane 4: DNA bundles assembled from tiles with linker of CGCGTTT. (c) Atomic microscopy images of DNA tiles. (d) Confocal laser scanning microscopy (CLSM) (i) and TEM (ii) images of DNA tubes with no linkers. (e) CLSM (i) and TEM (ii) images of DNA tubes with linker of 7T. (f) CLSM (i) and TEM images (ii) of DNA bundles. The periodic white stripes with interval of ~15 nm observed on TEM images of DNA bundles (ii, inset) represent the existence of highly oriented DNA linkers after inter-tube binding.

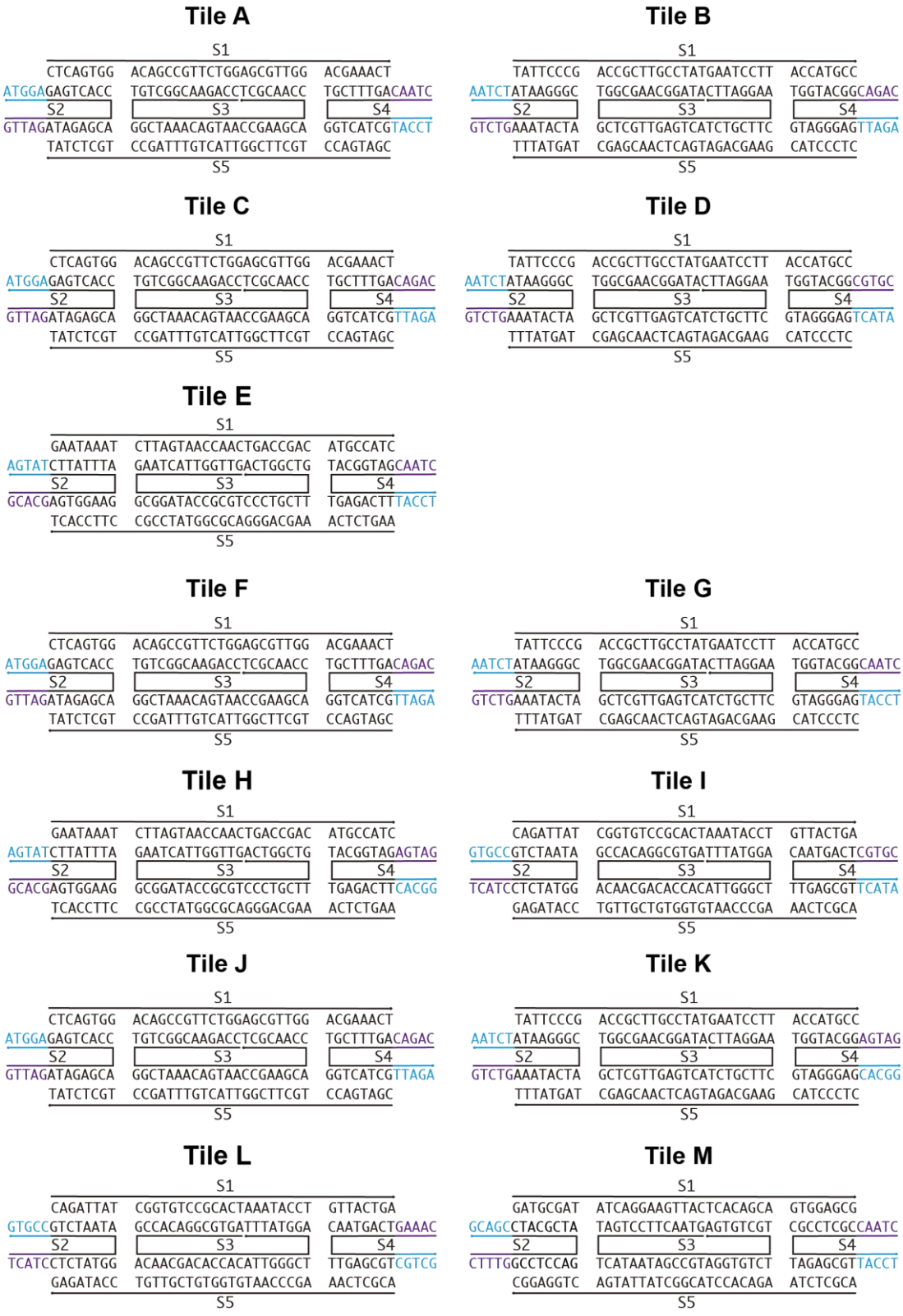

Figure 3-2. Designs and sequence of all DNA tiles used in this project. Linker sequences are extended from the 5' end of S2 strand unless specified.

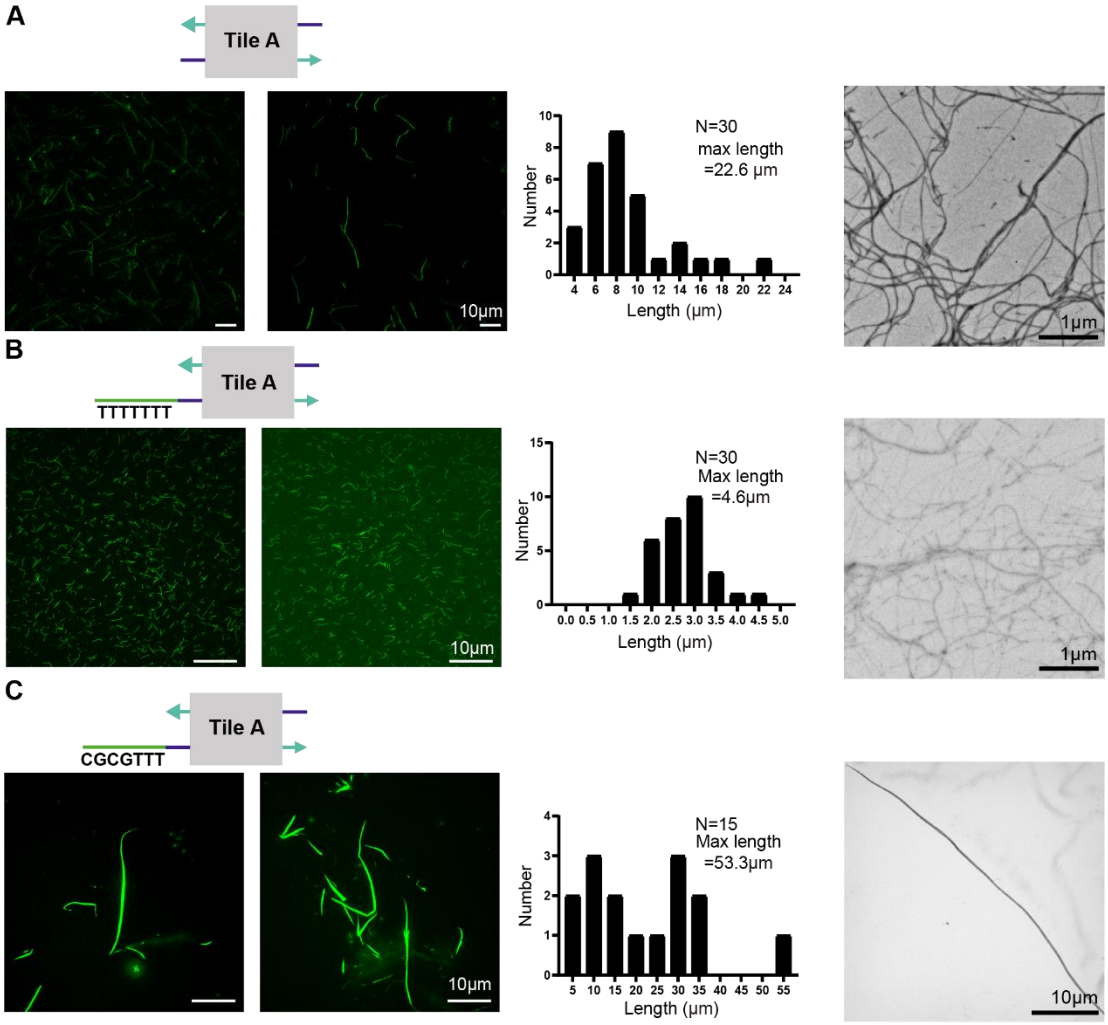

Figure 3-3. Representative extra CLSM and TEM images for DNA tubes and DNA bundles. (a) DNA tubes assembled from Tile A with no linker. (b) DNA tubes assembled from Tile A with a non-cohesive linker of TTTTTTT. (c) DNA bundles assembled from Tile A with a cohesive linker of CGCGTTT. In these figures, some ultra-long and wide DNA bundles could be observed.

Table 3-1. Sequences for DNA strands

Tile	Strand Name	Strand Sequence
A	S1	CTCAGTGGACAGCCGTTCTGGAGCGTTGGACGAAACT
	S2	GTTAGATAGAGCACCACTGAGAGGTA
	S3	CCAGAACGGCTGTGGCTAAACAGTAACCGAAGCACCA ACGCT
	S4 to tile A	CTAACAGTTTCGTGGTCATCGTACCT
	S5	CGATGACCTGCTTCGGTTACTGTTTAGCCTGCTCTAT
	S2 polyT linker	TTTTTTT GTTAGATAGAGCACCACTGAGAGGTA
	S2 CGTTT linker	CGTTT GTTAGATAGAGCACCACTGAGAGGTA
	S2 CGCGTTT linker	CGCGTTT GTTAGATAGAGCACCACTGAGAGGTA
	S2CGCGCGTTT linker	CGCGCGTTT GTTAGATAGAGCACCACTGAGAGGTA
	S2 Varied T linker	CGCGTn GTTAGATAGAGCACCACTGAGAGGTA
	S2 ATCTGCA linker	ATCTGCA GTTAGATAGAGCACCACTGAGAGGTA
	S2 CGCAGCA linker	CGCAGCA GTTAGATAGAGCACCACTGAGAGGTA
	S2 TCGTCGT linker	TCGTCGT GTTAGATAGAGCACCACTGAGAGGTA
	S2 TTTCGCG linker	TTTCGCG GTTAGATAGAGCACCACTGAGAGGTA
	S2 GCTAACT linker	GCTAACT GTTAGATAGAGCACCACTGAGAGGTA
	S2 ATCTACA linker	ATCTACA GTTAGATAGAGCACCACTGAGAGGTA
	S2 TGGTATT linker	TGGTATT GTTAGATAGAGCACCACTGAGAGGTA
	S2 TTTTTCG linker	TTTTTCG GTTAGATAGAGCACCACTGAGAGGTA
	S2 CGTTTTT linker	CGTTTTT GTTAGATAGAGCACCACTGAGAGGTA
	S2 ACGTACGT linker	ACGTACGT GTTAGATAGAGCACCACTGAGAGGTA
	S2 CGCGCGT linker	CGCGCGT GTTAGATAGAGCACCACTGAGAGGTA
	S2 CCGACGAT linker	CCGACGAT GTTAGATAGAGCACCACTGAGAGGTA
	S2 inner linker	GTCTGAAATACTACGGGAATATCTAA TTTGCGC
	S3 CGCGTTT linker	CGCGTTT CCAGAACGGCTGTGGCTAAACAGTAACCGAAGCACCA ACGCT
	S4 to tile B	CAGACAGTTTCGTGGTCATCGTTAGA
B	S1	TATTCCCGACCGCTTGCCTATGAATCCTTACCATGCC
	S2	GTCTGAAATACTACGGGAATATCTAA
	S3	ATAGGCAAGCGGTGCTCGTTGAGTCATCTGCTTCAAGG ATTC
	S4 to tile B	CAGACGGCATGGTGTAGGGAGTTAGA
	S5	CTCCCTACGAAGCAGATGACTCAACGAGCTAGTATTT
	S2 polyA linker	AAAAAAA GTCTGAAATACTACGGGAATATCTAA
	S4 to tile C	CGTGCGGCATGGTGTAGGGAGTCATA
C	S1	CTCAGTGGACAGCCGTTCTGGAGCGTTGGACGAAACT
	S2	GTTAGATAGAGCACCACTGAGAGGTA
	S3	CCAGAACGGCTGTGGCTAAACAGTAACCGAAGCACCA ACGCT
	S4 to tile C	CTAACAGTTTCGTGGTCATCGTACCT
	S5	CGATGACCTGCTTCGGTTACTGTTTAGCCTGCTCTAT

	S4 to tile D	CAGACAGTTTCGTGGTCATCGTTAGA
	S2 CCGACGAT linker	CCGACGAT GTTAGATAGAGCACCACTGAGAGGTA
D	S1	TATTCCCGACCGCTTGCCTATGAATCCTTACCATGCC
	S2	GTCTGAAATACTACGGGAATATCTAA
	S3	ATAGGCAAGCGGTGCTCGTTGAGTCATCTGCTTCAAGG ATTC
	S4 to tile D	CAGACGGCATGGTGTAGGGAGTTAGA
	S5	CTCCCTACGAAGCAGATGACTCAACGAGCTAGTATTT
	S2 ATCTGCAA linker	ATCTGCAA GTCTGAAATACTACGGGAATATCTAA
	S4 to tile E	CGTGCGGCATGGTGTAGGGAGTCATA
E	S1	GAATAAATCTTAGTAACCAACTGACCGACATGCCATC
	S2	GCACGAGTGGAAGATTTATTCTATGA
	S3	GTTGGTTACTAAGGCGGATACCGCGTCCCTGCTTGTCG GTCA
	S4 to tile E	CTAACGATGGCATTGAGACTTTACCT
	S5	AAGTCTCAAAGCAGGGACGCGGTATCCGCCTTCCACT
	S2 ACATGATC linker	ACATGATC GCACGAGTGGAAGATTTATTCTATGA
	S4 to tile C	CTAACGATGGCATTGAGACTTTACCT
F	S1	CTCAGTGGACAGCCGTTCTGGAGCGTTGGACGAAACT
	S2	GTTAGATAGAGCACCACTGAGAGGTA
	S3	CCAGAACGGCTGTGGCTAAACAGTAACCGAAGCACCA ACGCT
	S4 to tile F	CTAACAGTTTCGTGGTCATCGTACCT
	S5	CGATGACCTGCTTCGGTTACTGTTTAGCCTGCTCTAT
	S4 to tile G	CAGACAGTTTCGTGGTCATCGTTAGA
	S2 ATCTGCA linker	ATCTGCA GTTAGATAGAGCACCACTGAGAGGTA
G	S1	TATTCCCGACCGCTTGCCTATGAATCCTTACCATGCC
	S2	GTCTGAAATACTACGGGAATATCTAA
	S3	ATAGGCAAGCGGTGCTCGTTGAGTCATCTGCTTCAAGG ATTC
	S4 to tile G	CAGACGGCATGGTGTAGGGAGTTAGA
	S5	CTCCCTACGAAGCAGATGACTCAACGAGCTAGTATTT
	S4 to tile F	CTAACGGCATGGTGTAGGGAGTACCT
	S2 GTCAACT linker	GTCAACT GTCTGAAATACTACGGGAATATCTAA
H	S1	GAATAAATCTTAGTAACCAACTGACCGACATGCCATC
	S2	GCACGAGTGGAAGATTTATTCTATGA
	S3	GTTGGTTACTAAGGCGGATACCGCGTCCCTGCTTGTCG GTCA
	S4 to tile H	CTAACGATGGCATTGAGACTTTACCT
	S5	AAGTCTCAAAGCAGGGACGCGGTATCCGCCTTCCACT
	S2 AATACCA linker	AATACCA GCACGAGTGGAAGATTTATTCTATGA
	S4 to tile I	GATGAGATGGCATTGAGACTTCACGG
I	S1	CAGATTATCGGTGTCCGCACTAAATACCTGTTACTGA
	S2	TCATCCTCTATGGATAATCTGCCGTG
	S3	AGTGCGGACACCGACAACGACACCACATTGGGCTAGG TATTT

	S4 to tile I	GATGATCAGTAACTTGAGCGTCACGG
	S5	ACGCTCAAAGCCCAATGTGGTGTCGTTGTCCATAGAG
	S2 AGTTGAC linker	AGTTGAC TCATCCTCTATGG ATAATCTGCCGTG
	S4 to tile H	CGTGCTCAGTAACTTGAGCGTTCATA
J	S1	CTCAGTGGACAGCCGTTCTGGAGCGTTGGACGAAACT
	S2	GTTAGATAGAGCACCACTGAGAGGTA
	S3	CCAGAACGGCTGTGGCTAAACAGTAACCGAAGCACCA ACGCT
	S4 to tile J	CTAACAGTTTCGTGGTCATCGTACCT
	S5	CGATGACCTGCTTCGGTTACTGTTTAGCCTGCTCTAT
	S4 to tile K	CAGACAGTTTCGTGGTCATCGTTAGA
	S2 CGCGTTT linker	CGCGTTT GTTAGATAGAGCACCACTGAGAGGTA
K	S1	TATTCCCGACCGCTTGCCTATGAATCCTTACCATGCC
	S2	GTCTGAAATACTACGGGAATATCTAA
	S3	ATAGGCAAGCGGTGCTCGTTGAGTCATCTGCTTCAAGG ATTC
	S4 to tile K	CAGACGGCATGGTGTAGGGAGTTAGA
	S5	CTCCCTACGAAGCAGATGACTCAACGAGCTAGTATTT
	S4 to tile L	GATGAGGCATGGTGTAGGGAGCACGG
	S2 GNP handle	GTCAACTCGTA GTTAGATAGAGCACCACTGAGAGGTA
	S2 STV handle	5'Biotin-TTTT GTTAGATAGAGCACCACTGAGAGGTA
L	S1	CAGATTATCGGTGTCCGCACTAAATACCTGTTACTGA
	S2	TCATCCTCTATGGATAATCTGCCGTG
	S3	AGTGCGGACACCGACAACGACACCACATTGGGCTAGG TATTT
	S4 to tile L	GATGATCAGTAACTTGAGCGTCACGG
	S5	ACGCTCAAAGCCCAATGTGGTGTCGTTGTCCATAGAG
	S4 to tile M	CAAAGTCAGTAACTTGAGCGTCGTCG
	S2 CGTTTCG linker	CGTTTCG TCATCCTCTATGGATAATCTGCCGTG
M	S1	GATGCGATATCAGGAAGTTACTCACAGCAGTGGAGCG
	S2	CTTTGGCCTCCAGATCGCATCCGACG
	S3	GTAACTTCCTGATTCATAATAGCCGTAGGTGTCTTGCT GTGA
	S4 to tile M	CAAAGCGCTCCACTAGAGCGTCGTCG
	S5	ACGCTCTAAGACACCTACGGCTATTATGACTGGAGGC
	S4 to tile J	CTAACCGCTCCACTAGAGCGTTACCT
	S2 GNP handle	ATCTACAGGCACTTTGGCCTCCAGATCGCATCCGACG
	S2 STV handle	5'Biotin-TTTTCTTTGGCCTCCAGATCGCATCCGACG

3.3.2 Inserted cohesive linker's influence on DNA bundle assembly

First, we investigated the influence of the inserted linker's influence on DNA nanotube and bundle assembly. Several factors were tested, including insertion position, binding strength of cohesive linkers, and the poly-T spacer length of linkers.

The influence of the insertion position of cohesive linkers was first investigated. Based on previous papers' results, sequences inserted to the DX tiles can protrude out to different directions after the formation of nanotubes depending on their insertion position. On several specific positions, the linkers can protrude to either outer or inner surface of the nanotube perpendicularly, while other positions, at which the linkers will point more parallel to the nanotube surface, will cause the nanotube less stable (25). Thus, we tested the insertion of 5'-CGCGTTT-3' linker on both 5' end and 3' end of S2 strand of Tile A. The linker will protrude out on the outer surface of nanotubes if inserted on the 5' end of S2 strand, while inner surface if inserted on the 3' end. The assembly was carried out using normal annealing protocol. As shown in figure 4a, compared to the result in figure 1f which has all linkers on the outer surface, when linkers are presented on the inner surface of nanotubes, only nanotubes could be observed after assembly and no DNA bundles could be observed. This can be interpreted that if the linkers are pointing inwards, their accessibility is largely decreased, thus preventing the further bundling of nanotubes. This result confirms the design principle of our system that the inserted cohesive linkers should be presented on the outwards of the nanotube in order to induce the bundling process of nanotubes to further assemble into DNA bundles.

Insertion of cohesive linkers on different strands was also tested. Considering the insertion positions that will cause the linkers to point outwards, there are many positions that will meet this criterion. Thus, we further investigated the insertion on S3 strand that will also cause the linker to point outwards, and imaged the assembly product using TEM. As shown in figure 3-

4b, compared to the result in figure 3-1f, the assembly of S3 insertion showed minimal differences in morphology. Thus, we concluded that as long as linkers are on the outer surface of nanotubes, their position only induced subtle influence on assembly. For future experiments in this project, we will insert the cohesive linkers on the 5' end of S2 strands unless specified otherwise.

The factors about the linker designs were then investigated. First, the binding strength of DNA linkers was thoroughly tested. As demonstrated in previous results, the linker of 5'-CGCGTTT-3' exhibited potent capability to induce the bundle assembly from DX tiles and DNA nanotubes. As the main binding force coming from the 2 pairs of CG, in comparison, we further designed a linker with lower binding strength (5'-CGTTT-3') and higher binding strength (5'-CGCGCGTTT-3'). The binding strength of these two linkers was tuned by varying the pairs of CG while keeping the length of the poly-T linker the same. Under the same annealing protocol, the linker of 5'-CGTTT-3' failed to induce the bundling of nanotubes, while in contrast, the specific assembly of DX tiles with the linker of 5'-CGCGCGTTT-3' was interrupted and only random aggregations could be observed under TEM (Figure 3-5a). This result infers that an appropriate binding strength is critical to result in the successful assembly of DNA bundles (Figure 3-5b). To confirm this hypothesis, we further designed several cohesive linkers, including both rationally and randomly designed ones, and tested their influence on DNA bundle assembly (Table 3-1). Figure 3-6 shows the assembly results of DX tile A with these further designed linkers under TEM, and they did demonstrate varied results on the assembly product. To quantitively investigate these linkers' influence, OligoAnalyzer and NUPACK were used to simulate their self-binding strength (35). The result showed that under such reaction condition, linkers with self-complementary binding ΔG between -7 to -10 kcal/mol can promote the assembly into DNA bundles, no matter how many base pairs are formed between linkers (Figure 3-7). Thus, we conclude that there is indeed an appropriate window of

binding strength of cohesive linkers for DNA bundle assembly. However, we also need to point out that as the binding ΔG can be varied when reaction condition changes, this appropriate window is not set for all conditions.

Finally, as we kept the poly-T spacer the same in previous investigations, it is natural to wonder whether the poly-T spacer length will pose influence on DNA bundle assembly. We designed a set of linker sequences, 5'-CGCGT_n-3', by keeping 2 pairs of CG and varying the number of T nucleotides. In this case, the contributing factor for binding strength is set, and only the length of the poly-T spacer is varied. The assembly of DX tiles with n=0 to 21 linkers was tested using the same assembly protocol and their assembly results were imaged using TEM (Figure 3-8a). It is revealed that DNA bundles started to form from n=2, and with n increasing, the bundles generally demonstrated an increasing width (Figure 3-8b). This may possibly be because of the increased inter-tube spacing caused by the increased length of the poly-T spacer. When n went up to more than 12, defects started to appear on DNA bundles, and from n=18, no well-assembled DNA bundles could be observed. When n>20, only aggregations could be observed. Thus, we conclude that with certain binding affinity, the linker length should also be in an appropriate range to enable well-formed DNA bundle assembly. The linkers which are too long may disturb the orderliness of nanotube alignment, rendering loose and defect areas on DNA bundles.

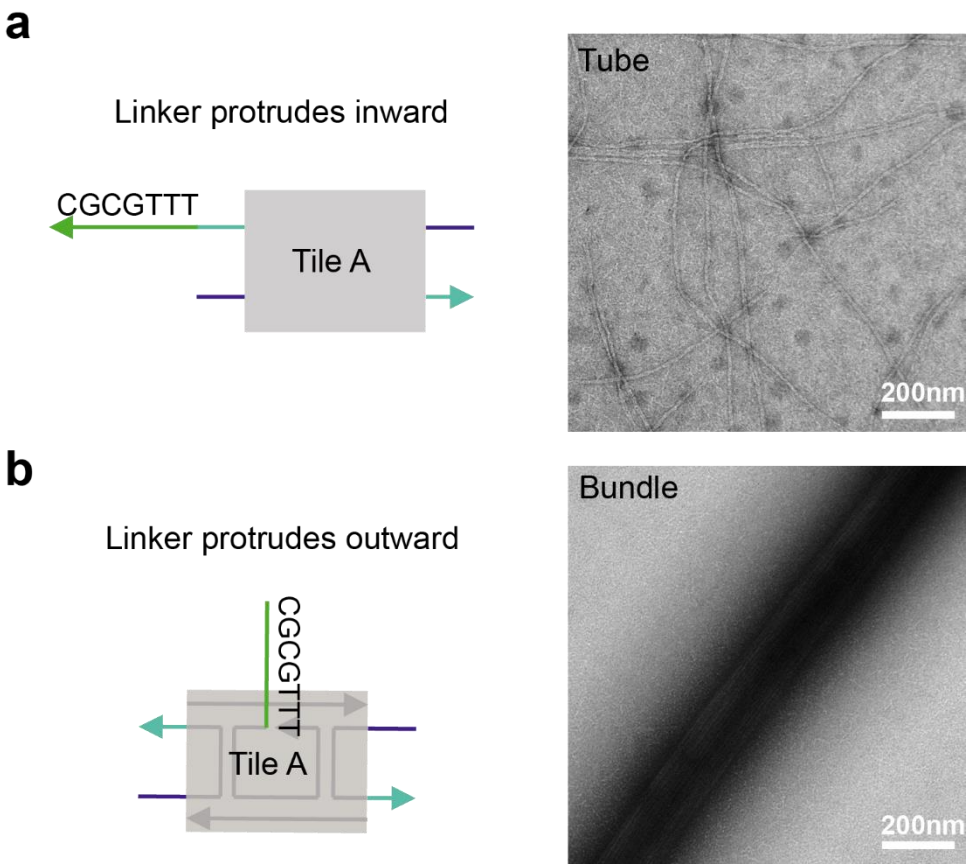

Figure 3-4. Linker position affects DNA bundle assembly. (a) DNA tubes were formed if linker is positioned on the 3' end of S2 strand that protruding inward towards the tube tunnel. (b) DNA bundles were formed if linker is positioned on the 5' end of S3 strand that protruding outward from tube outer surface.

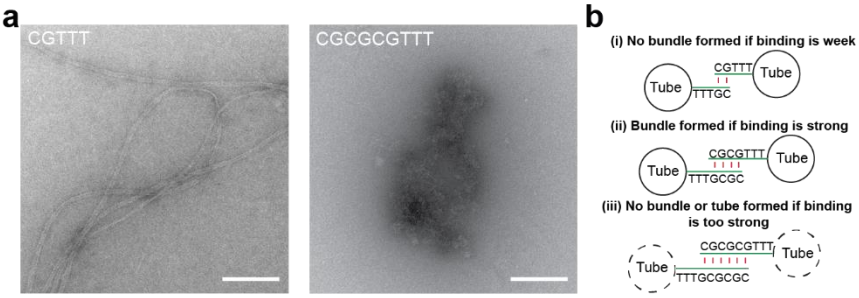

Figure 3-5. Effect of linker binding strength on DNA bundle assembly. (a) TEM images of assembled structures with linkers of CGTTT or CGCGTTT at 20 mM of Mg2+. For these linker designs, the binding strength was varied by tuning the number of CG on the binding domain while keeping the same spacer length. Scale bars: 200nm. (b) The influence pattern of binding strength CG pair binding on DNA bundle assembly. Appropriate binding strength of the linker is critical to bundle formation. Weak linker leads to little inter-tube binding, while too strong linker disrupts tube assembly.

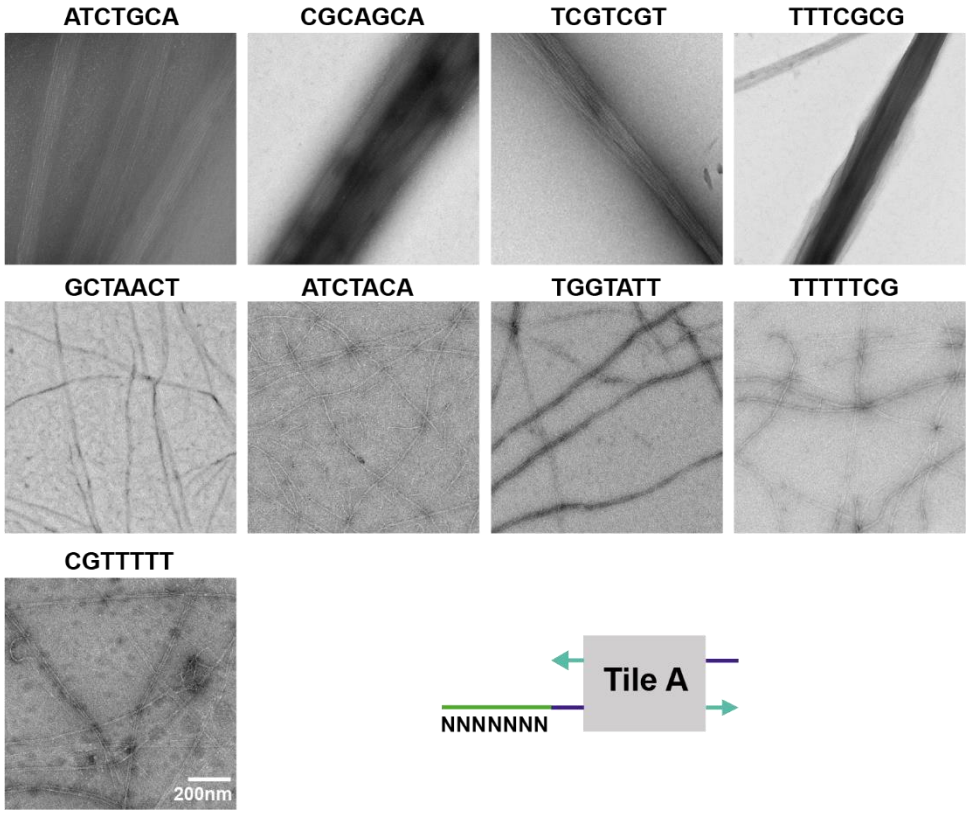

Figure 3-6. TEM images of assembly results for some linker designs in Figure 3-7. The designs included in other figures are not presented here, and the designs that does not yield DNA tubes or bundles are not included. All images share the same scale bar of 200 nm.

Forms bundle?	Sequence 5'-3'	Base pair number	Binding Pattern	NUPACK Simulation
Yes	ATCTGCA	4bp	ATCTGCA | | | | ACGTCTA	Delta G = -7.11kcal/mol
	CGCAGCA	4bp	CGCAGCA | | | | ACGCAGC	Delta G = -8.10kcal/mol
	CGCGTTT	4bp	CGCGTTT | | | | TTTGCGC	Delta G = -9.30kcal/mol
	TCGTCGT	4bp	TCGTCGT | | | | TGCTCGT	Delta G = -7.56kcal/mol
	TTTCGCG	4bp	TTTCGCG | | | | GCGCTTT	Delta G = -9.69kcal/mol
	AAAAAAA + TTTTTTT	7bp	AAAAAAA | | | | | | | TTTTTTT	Delta G = -8.70kcal/mol
No	ACGTACGT	8bp	ACGTACGT | | | | | | | | TGCATGCA	Delta G = -14.09kcal/mol
	CGCGCGT	6bp	CGCGCGT | | | | | | TGCGCGC	Delta G = -14.67kcal/mol
	GCTAACT	4bp	GCTAACT | | | | TCTAACG	No self-binding
	ATCTACA	4bp	ATCTACA | | | | ACATCTA	No self-binding
	TGGTATT	2bp	TGGTATT | | TTATGGT	No self-binding
	CGTTTTT	2bp	CGTTTTT | | TTTTTGC	No self-binding
	TTTTTCG	2bp	TTTTTCG | | GCTTTTT	No self-binding
	TTTTTTT	0bp	N/A	No self-binding

Figure 3-7. All linker sequences designed and studied for further investigation. Simulations are done under the condition with 100 mM of Na+ and 20 mM of Mg2+. By comparing the NUPACK simulation result, the conclusion can be drawn that the self-binding strength (delta G) of a linker should be in a certain range to enable the assembly of DNA bundle structure with certain Mg^{2+} concentration.

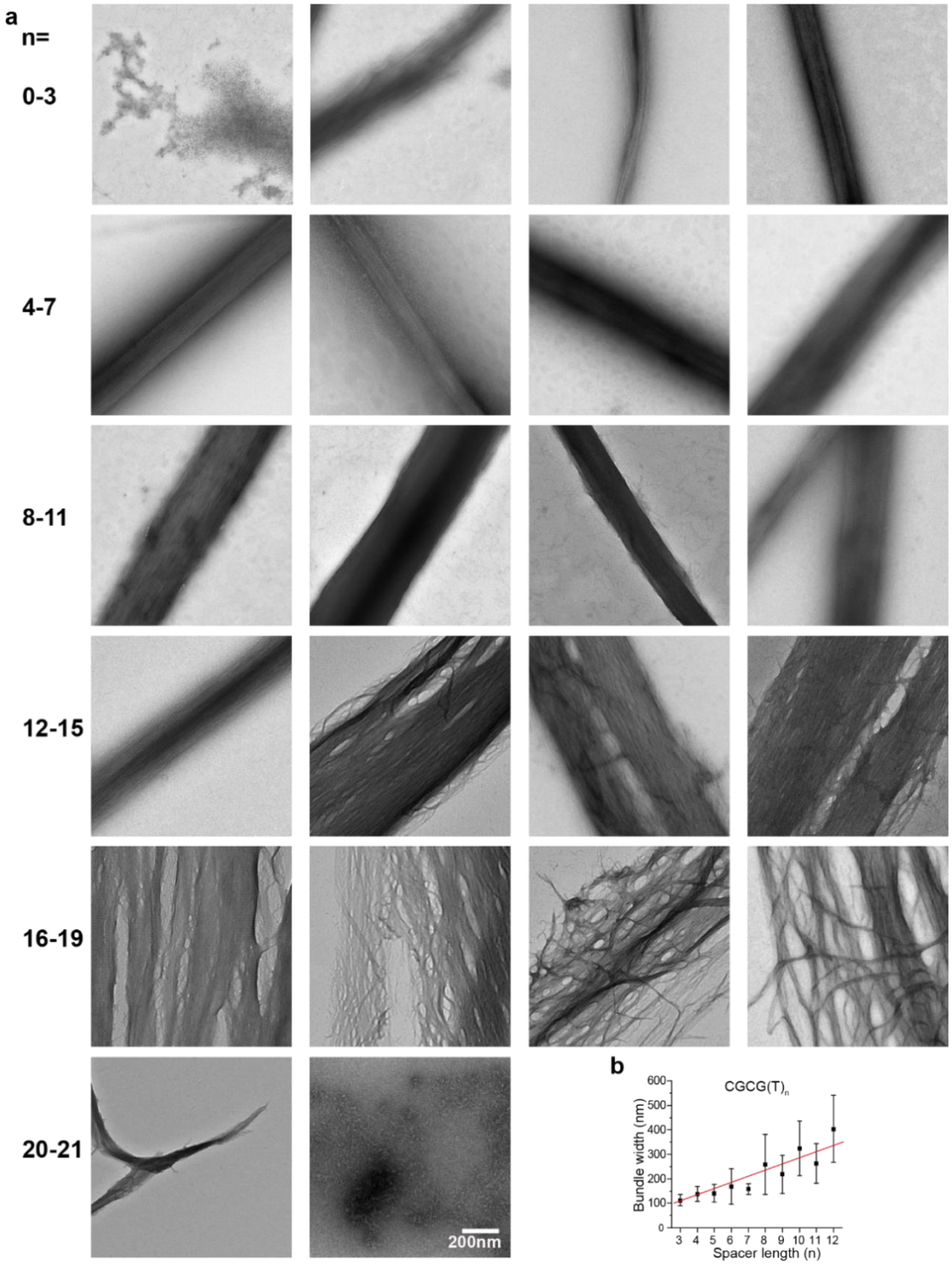

Figure 3-8. The spacer length on linkers also influences DNA bundle assembly. (a) Representative TEM images illustrating the assembly product of DX tiles with designed set of linkers. The linker sequences used here are 5'-CGCG$(T)_n$-3', where n varies from 0-21. All groups are assembled with 20 mM of Mg2+. All figures share the same scale bar. (b) Measured width of bundles with varied spacer length when n=3-12.

3.3.3 Reaction condition's influence on DNA bundle assembly

We next sought to verify the influence of reaction conditions on DNA bundle assembly. In this part, we investigated the annealing temperature's influence and the divalent ion concentration in reaction buffer's influence.

First, we investigated the influence of annealing temperature. As we hypothesized in Figure 3-1, if the assembly pathway is indeed a hierarchical pathway, we should be able to observe different inter-state of assembly products under TEM during different annealing stages. DX tile A with 5'-CGCGTTT-3' was used for this investigation. As the annealing process is designed to be a gradual cooling process from 65 °C to room temperature, we intentionally stopped the assembly process at a series of temperature points during the annealing process at 60, 50, 45, 35, 30, and 25 °C. The reaction tube was quickly taken out from the thermal cycler and subjected to TEM imaging (Figure 3-9). As revealed, no large assemblies were observed at 60 °C. However, individual tubes began to show up at 50 °C exhibiting minimal inter-tube interactions. This result corresponds to previous literature's result well, where only DNA nanotubes are constructed (34). At 45 °C, tubes showed enhanced interactions as they began to bind and align with others. At 35 °C, loosely linked bundles of tubes were observed. And finally at 25 °C, long, wide, and compact DNA bundles with expected spatial features were formed. This experimental result not only supports our hypothesis of the hierarchical nature of the DNA bundle assembly process, but also indicates that the bundling process of nanotubes generally occurs when the annealing temperature is rather low. This may be interpreted by the low T_m of the linker sequences, as the self-complementary binding of linkers is the main driving force of nanotube bundling.

Next, a comprehensive examination of how cationic strength affects the assembly of DNA bundles was conducted. In DNA nanotechnology, although all cations in the assembly buffer

may play a role in the assembly process, divalent ions, however, are usually the more important ones. Thus, we mainly focused on the influence of divalent ions on DNA bundle assembly, and Mg^{2+} was selected for investigation as it is commonly used in DNA nanotechnology. As shown in previous results in DNA nanotechnology, Mg^{2+} plays pivotal roles in DNA self-assembly by shielding the negative charge of DNA backbones to facilitate DNA hybridization and self-assembly of complex DNA structures, while also promoting nonspecific or unwanted interactions between DNA strands (e.g., causing random aggregation of DNA structures). Thus, we hypothesized that only an appropriate range of Mg^{2+} is capable of promoting the formation of DNA bundles. To test this hypothesis, we systematically investigated a series of Mg^{2+} concentrations from 5 to 200 mM using DX tile A with the linker of 5'-CGCGTTT-3' (Figure 3-10). Nanotubes were unable to bundle at 5 mM of Mg^{2+}, possibly due to the low binding strength of linkers under this condition. From 10mM of Mg^{2+}, nanotubes started to bundle with defects, and well-formed DNA bundles started to appear from 20mM Mg^{2+}. While the concentration of Mg^{2+} increased, a general trend that higher cationic strength led to DNA bundles of larger width was observed and statistically measured (Figure 3-10b). However, specific DNA self-assembly was severely impaired at 200 mM of Mg^{2+} where neither tubes nor bundles were formed.

This result confirmed our hypothesis that for DX tiles with 5'-CGCGTTT-3' sequence, 20-150mM concentration of Mg^{2+} is an appropriate range for DNA bundle formation. However, it is also important to mention that for different cohesive linkers, such appropriate Mg^{2+} concentration range may vary. For example, we went on to test the minimal Mg^{2+} concentration that allows the DX tiles with 5'-CGTTT-3' and 5'-CGCGCGTTT-3' linkers to form DNA bundles (Figure 3-11a). These two linkers were used in previous investigations as linkers with lower and higher binding strength. As experimentally revealed, DX tiles with 5'-CGTTT-3' linker were able to form DNA bundles at an elevated Mg^{2+} concentration of 50 mM. On the

other hand, DX tiles with 5'-CGCGCGTTT-3' linker were only found to be capable of forming bundles at 5 mM concentration of Mg^{2+}. Both of them were unable to induce bundle assembly at 20mM Mg^{2+} concentration used by previous routinely used annealing protocol. We also further tested the assembly result of DX tiles without cohesive linkers and with pure poly-T linkers (Figure 3-11b, 3-11c). DX tiles without cohesive linkers, which will normally form DNA nanotubes without linkers protruding on the surface, were also found to be able to align and bundle together at a high Mg^{2+} concentration. In contrast, DX tiles with poly-T linkers were not able to induce inter-tube bundling even at high cationic strength. Therefore, as the linkers used in the investigation are different, their required Mg^{2+} concentration to induce successful bundling varies a lot. Generally speaking, a linker of relatively weak binding strength is required in high cationic strength conditions, and vice versa, in order to promote DNA bundle assembly of high quality.

It is also worth noting that in a similar report by Burns (32), DNA nanotubes are bundled solely by divalent ion Mg^{2+}. However, in this report, a rather high concentration of Mg^{2+} was required (>40mM), which may hinder the future application of this bundle system in biomedical and nanofabrication areas. In our method, a Mg^{2+} concentration as low as 10mM is enough for the formation of DNA bundle structure, thus bypassing the hindrance of the application of such system. This is truly one of the merits of our method compared to previous reports.

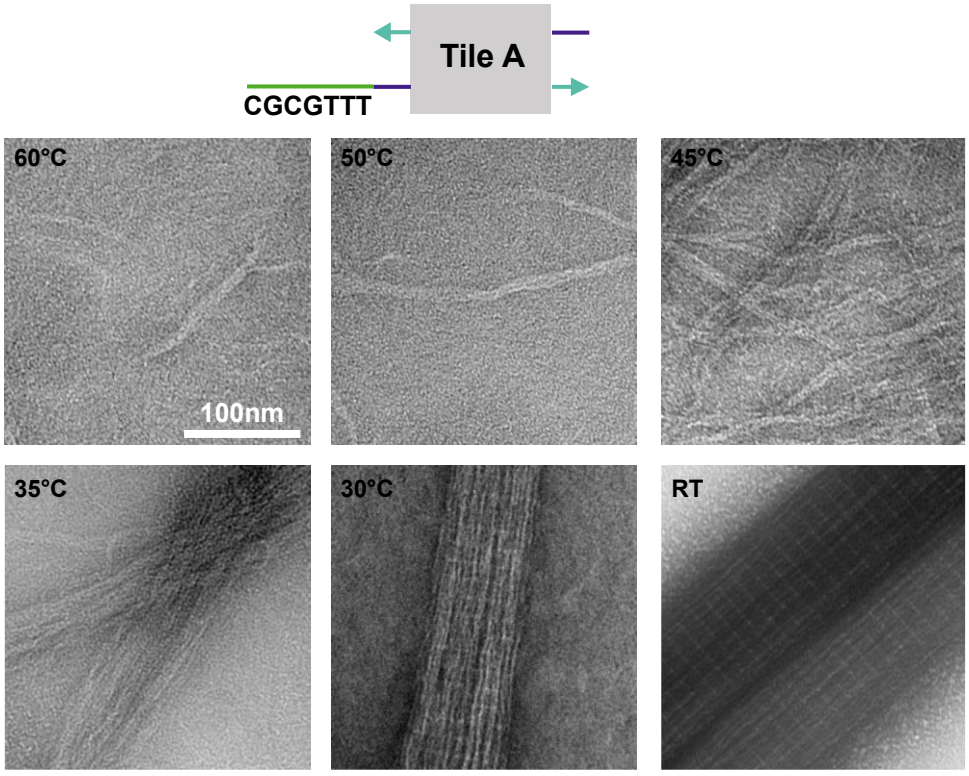

Figure 3-9. DNA bundles are hierarchically assembled. Representative TEM images show the assembly product of DX tiles at different temperature point. The DNA tiles are heated to 85°C, then gradually cooled down to designated temperatures for characterization. All images share the same scale bar.

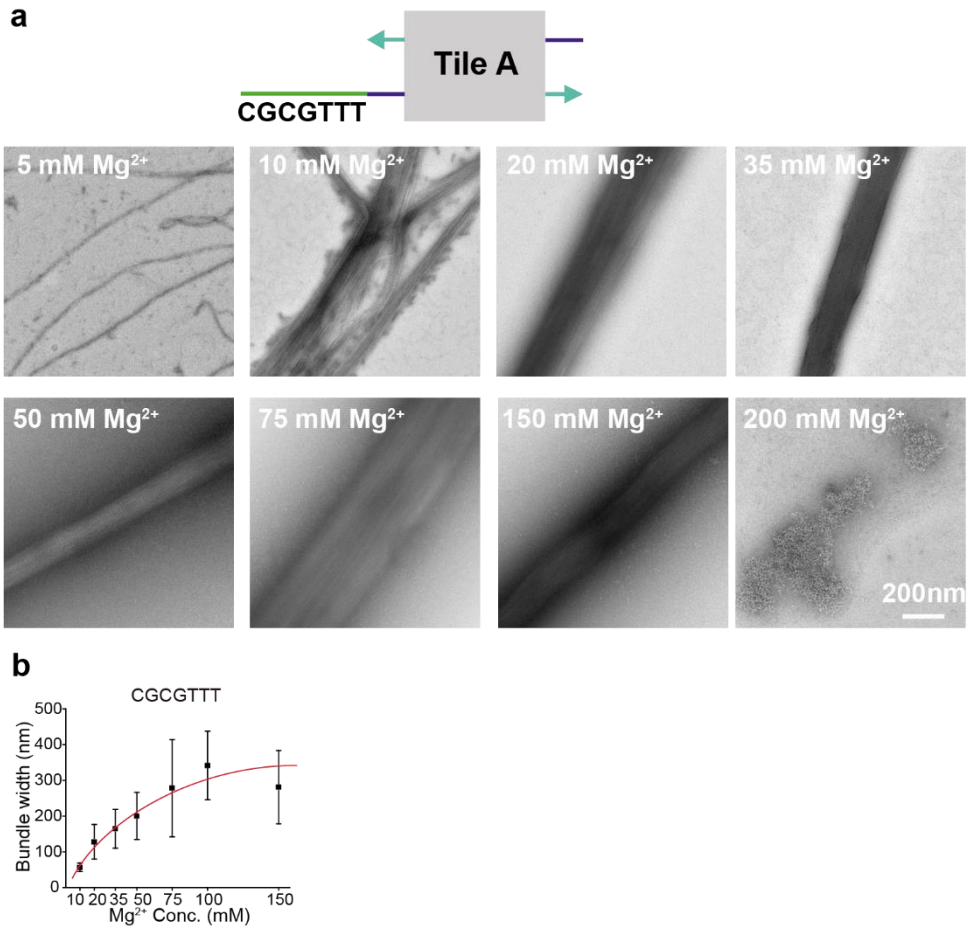

Figure 3-10. The influence of divalent ion concentration on DNA bundle assembly. DX tile A with 5'-CGCGTTT-3' linker was used for this investigation. (a) Representative TEM images illustrated the assembly results of DX tiles with different Mg^{2+} concentration. (b) Measured width of DNA bundles assembled at different Mg^{2+} concentrations. The measurements were conducted and averaged based on multiple bundles on TEM images. The decrease of average bundle width at 150 mM Mg^{2+}, compared to 100 mM Mg^{2+}, is likely due to aggregation of wider bundles at this high concentration of Mg^{2+}.

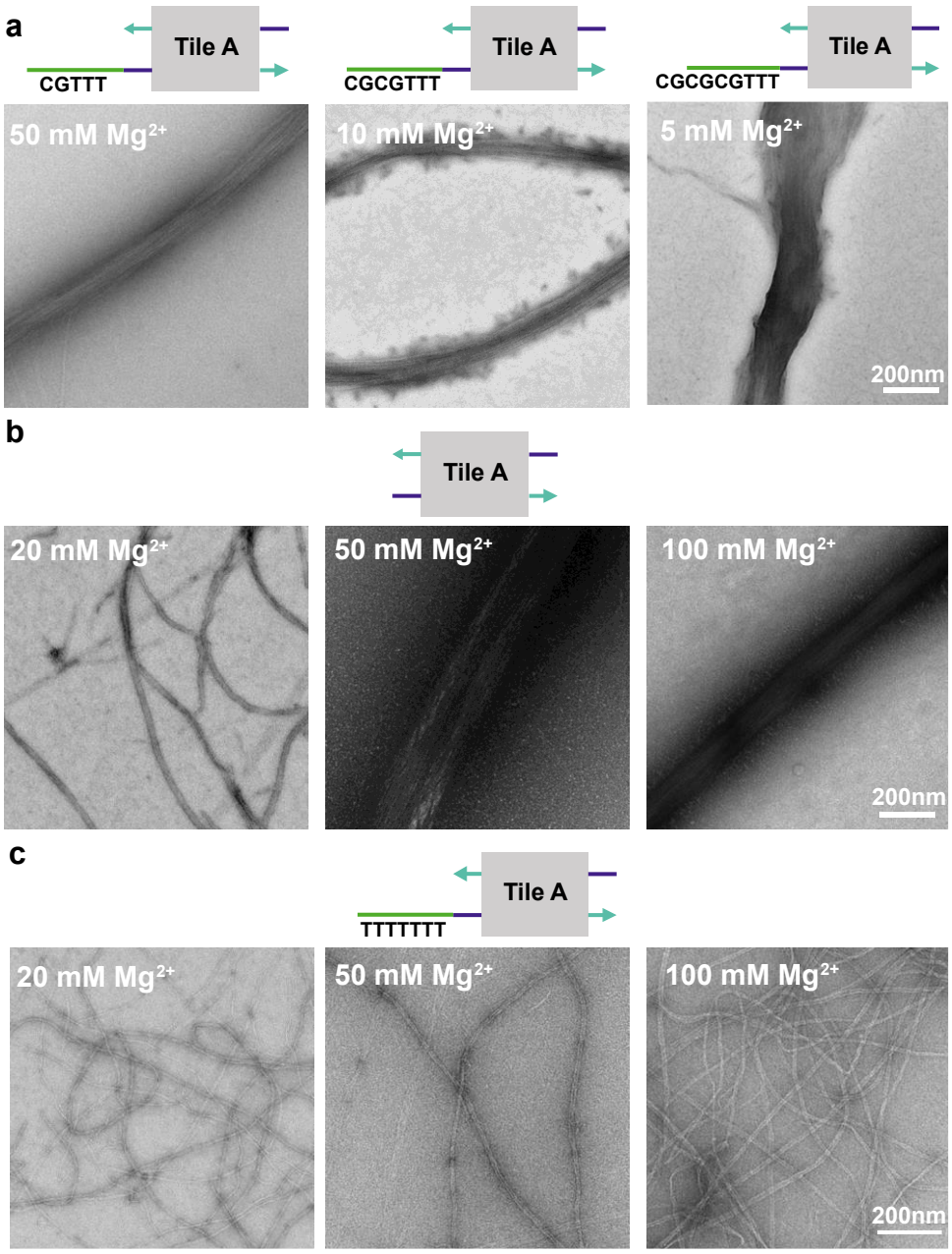

Figure 3-11. Cationic concentration needed for DNA bundle assembly is highly dependent on the binding strength of linkers. (a) Higher cationic strength is needed for weaker linkers, while lower cationic concentration is demanded by stronger linkers. (b) DNA tile with no linker can even form DNA bundles at sufficiently high concentrations of Mg2+. (c) DNA tile with a non-cohesive linker of TTTTTTT is unable to form DNA bundles even at 100 mM of Mg2+. All figures share the same scale bar of 200 nm.

3.3.4 DNA bundles of prescribed features assembled from multiple components

In above experiments, all DNA bundles were assembled with a single kind of DX tile (Tile A) with homogenous constitution. As one of the most stunning merits of DNA technology being the high programmability, here we aim to construct DNA bundles using different kinds of DX tiles with heterogeneous constitution. This will largely enlarge the versatility and functionality of our system.

First of all, we realized the heterogenous assembly of two different types of tubes with tunable bundle width and composition (Figure 3-12). Tube A, colored in blue, was assembled from Tile B with the linker 5'-AAAAAAA-3', and tube T, colored in grey, was assembled from Tile A with the linker 5'-TTTTTTT-3'. All the 5 strands (S1-S5) used to construct these DX tiles are unique and were simulated to have minimal unwanted cross-talking. As indicated in previous result, neither tube A nor tube T are self-cohesive to form DNA bundles. However, if both tubes present in the solution, the heterogeneous bundling between tube A and tube T will allow the formation of DNA bundles. We hypothesized that for this system, by adjusting the stoichiometric ratio between two tubes, which can be realized by adjusting the concentration of both DX tiles, the resulting bundle width and composition may be rationally modulated. To test this hypothesis, the one-pot reaction, where all strands for both DX tiles are annealed together directly from the beginning, was first carried out (Figure 3-12b). Different tube A: tube T ratios were tested, and at the ratio of 1:1, the resulting DNA bundle is the widest and most compact condition. A general trend of DNA bundle width can also be observed when statistically measured and plotted (Figure 3-12c). Besides one-pot reaction, a stepwise assembly protocol was also employed by separately assembling different tubes first, and then mixing them together with varied ratios at room temperature (Figure 3-12d). By using this assembly protocol, DNA bundles at all ratios showed similar morphology compared to the ones assembled from the one-pot protocol. Furthermore, similar general trend of DNA bundle width

was also observed for stepwise assembly protocol (Figure 3-12e). Thus, we conclude that this method is capable of the assembly of multicomponent DNA bundles with different properties with distinct types of tubes.

The abovementioned DNA bundle is assembled from two types of nanotubes, while each nanotube consists of one type of DX tile. On the other hand, we also wanted to construct a DNA bundle that is assembled from a single type of nanotube, but such nanotube consists of multiple types of DX tiles. Thus, we further fabricated a multi-tile DNA bundle homogenously assembled from Tile C, D, and E (Figure 3-13). All strands on these tiles are specifically designed to enable the sequential assembly of C-D-E multi-tile DNA nanotubes. Furthermore, each type of tile has its own unique cohesive linker that only allows homogeneous binding to linkers on the same type of tile. For example, the linker on Tile C can only bind to the linker on another Tile C, and the same for the linker on Tile D and E. In this case, the binding pattern of the nanotubes can be tuned, and multi-tile DNA bundles were then assembled after inter-tube binding was completed. With different sets of linkers being present or missing on the bundle, different white stripe features on the bundle surface with 1x, 2x, and 3x distance between adjacent stripes could be observed (Figure 3-13a). This result not only demonstrates the high programmability of our system, but also confirms the identity of white stripes to be the rendering of surface linker strands under TEM. It is also worth mentioning that when the number of remaining linkers was decreased, certain defects started to show up in the resulting DNA bundle (Figure 3-13b), possibly due to the bundling force being unable to counter the flexibility of nanotubes.

Finally, we also realized the multicomponent DNA bundles assembled by simultaneously using the above two strategies, as illustrated in Figure 3-14. Two types of tubes consisting of distinct tiles F, G, H and I heterogeneously bind to form DNA bundles. Linkers on tiles were designed specifically to enable the binding between Tile F and Tile H, and Tile G and Tile I. Similar to

abovementioned results, by independently modulating the presence of the linkers, the fabricated DNA bundles could result in various width and white stripe patterns (Figure 3-14d). This ultimately complex constitution of DNA bundles clearly demonstrates the inheritance of high programmability and versatility from structural DNA nanotechnology of our system.

In structural DNA nanotechnology, versatility and programmability usually come along with functionality. The white stripe patterns on the DNA bundle surface inspired the nanofabrication application of our system. To further verify the spatial features of DNA bundles and to demonstrate their utility in assembling other materials, large assemblies of gold nanoparticles (AuNPs) and streptavidin (STV) with prescribed patterns were fabricated by using DNA bundle templates. In order to realize this, a DNA bundle assembled from a single multi-tile DNA nanotube was designed. Such DNA nanotube consists of four distinct tiles with all strands' sequence different (Tile J in blue, tile K in orange, tile L in green, and tile M in grey. Figure 3-15). The linkers on tile J and L are designated to work as handles for docking guest materials, while the linkers on tile K and M are serving as normal cohesive linkers for nanotube bundling. Two different kinds of materials are used as guest materials: Inorganic nanoparticle 10nm gold nanoparticle (AuNP. Figure 3-15a), and small protein streptavidin (STV. Figure 3-15b). For the binding of AuNP, -HS group was added to the 5' end of linkers on tile j and L, and AuNP was added after DNA bundle assembly under room temperature. For the binding of STV, linkers on tile J and L were biotinylated at 5' end, and STV was added after DNA bundle assembly under room temperature. These two payloads were designed to produce two kinds of patterns by including or omitting the handles on designated tiles, and TEM images revealed the successful assembly of AuNPs and STV with prescribed patterns and band distance. This result further confirmed the spatial feature of DNA bundles and showed its versatility in assembling guest materials into large structures of defined patterns.

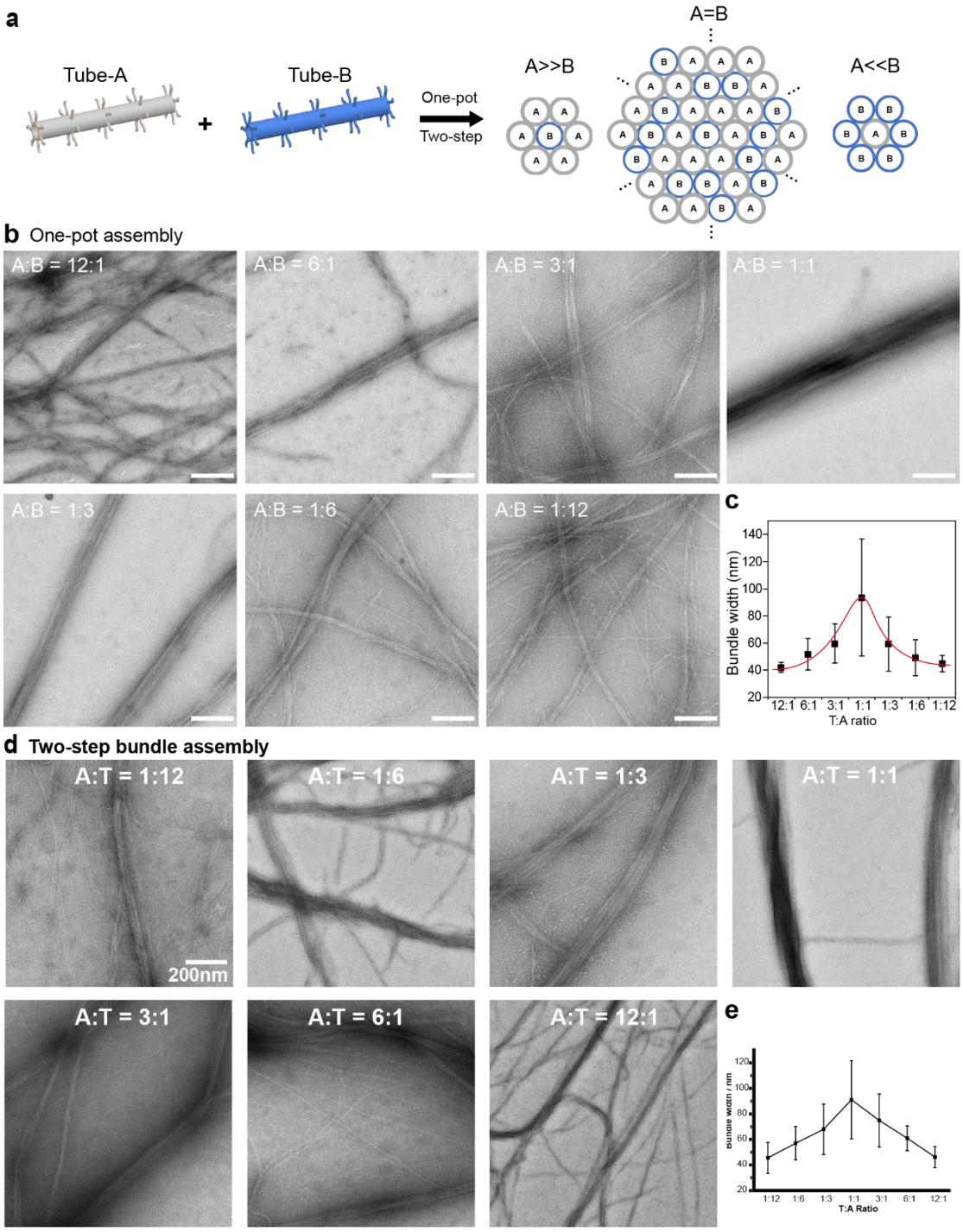

Figure 3-12. Heterogenous assembly of two different types of nanotubes. (a) Design of DNA bundles assembled from two distinct types of tubes. Tube-A was assembled from Tile B with a linker of AAAAAAA, while Tube-T was assembled from Tile A with a linker of TTTTTTT. DNA bundles are formed via heterogenous binding between Tube-A and Tube-T. The bundle width and composition can be modulated by adjusting the ratio between Tube-A and Tube-T.

(b) Representative TEM images of DNA bundles assembled at various A: T ratios in one-pot reaction. Scale bars: 200 nm. (c) Measured width of DNA bundles assembled in one-pot reaction. (d) Representative TEM images of DNA bundles assembled at various A: T ratios in stepwise assembly reaction. All figures share the same scale bar: 200nm. (e) Measured width of DNA bundles assembled in stepwise assembly reaction.

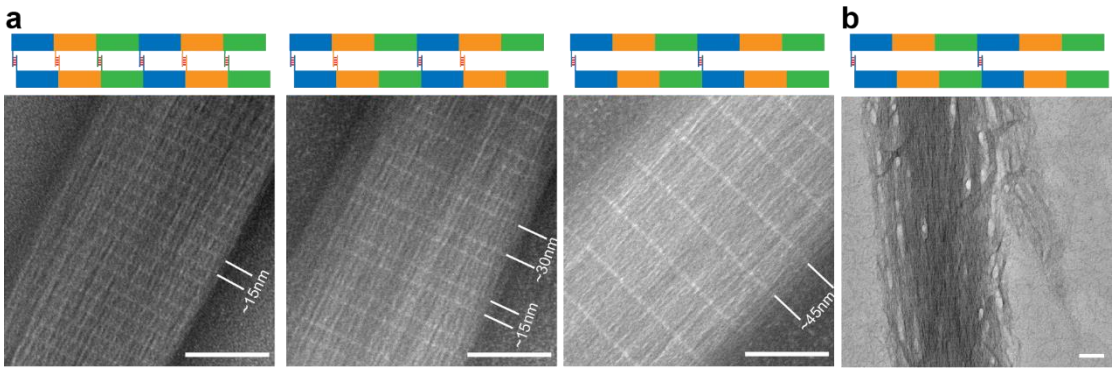

Figure 3-13. Multi-tile DNA bundle fabrication. (a) Multi-tile DNA bundles of prescribed features assembled from three distinct tiles. Three types of tiles (blue, Tile C; orange, Tile D; green, Tile E) alternatively assemble into tubes first, while the homogeneous assembly of tubes led to the formation of multi-tile DNA bundles. Each tile contains a unique linker that can only bind to another linker from the same type of tile. The white stripes on bundles were controlled by including or omitting the linkers of designated tiles. Scale bars: 100 nm. (b) DNA bundles cannot be well formed at 20 mM of Mg^{2+} if only Tile C having the linker given the binding strength may not be sufficient at this low cationic strength. Scale bar: 100nm.

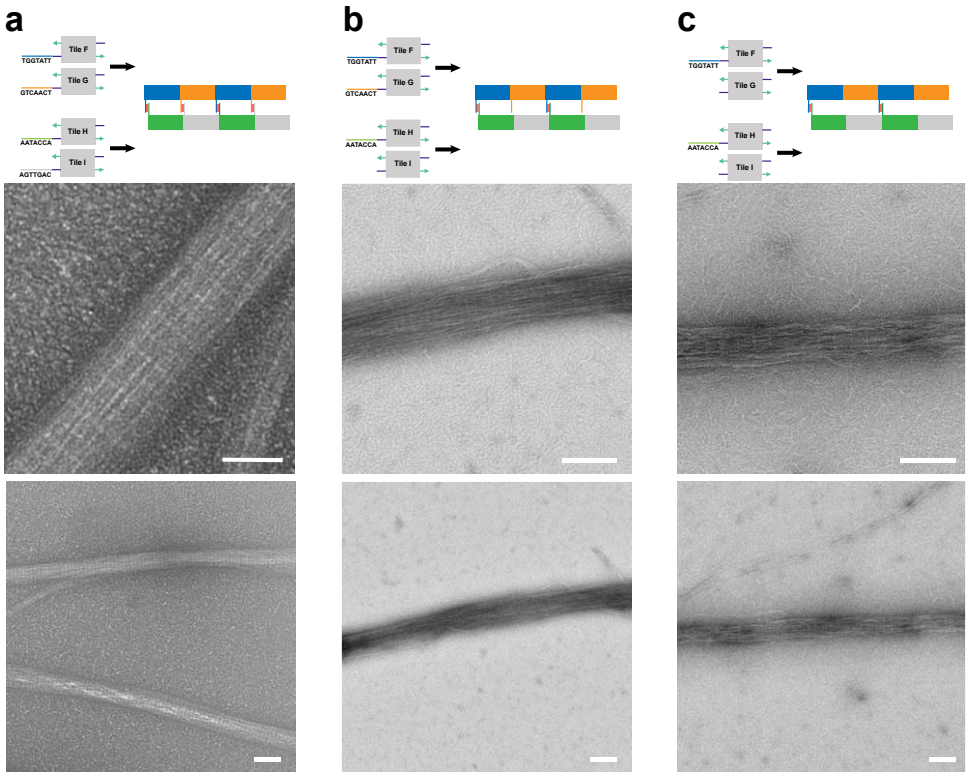

d

Bundle type	a	b	c
Average width / nm	73.2	57.4	51.6
Interval / nm	15	15	30

Figure 3-14. Multicomponent DNA bundles assembled from distinct tubes consisting of distinct tiles. (a-c) Assembling schemes and TEM images for DNA bundles. Scale bars: 100 nm. (d) Morphology data of DNA bundles in three experimental groups. Lower number of linkers led to DNA bundles of smaller width. Besides, the white stripe features agree well to the designs.

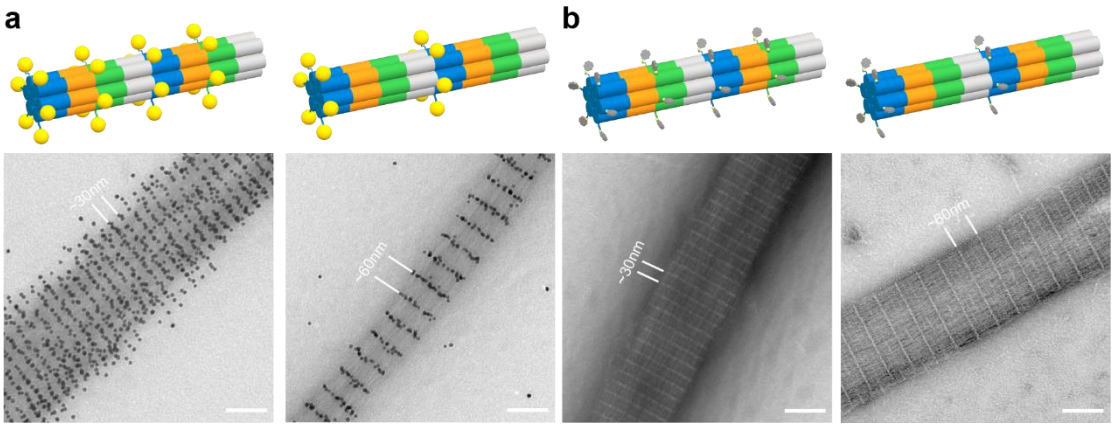

Figure 3-15. Assembly of guest materials on DNA bundles. (a) Assembly of 10nm gold nanoparticles on DNA bundles. Tile J (blue) and Tile L (green) are designed to hold the capture handles for AuNP docking. Tile K (orange) and Tile M (grey) are designed to hold the cohesive linkers for DNA tube bundling. (b) Assembly of STV on DNA bundles. The capture handles are functionalized with biotins for streptavidin (STV) binding. Note that the dimmer white stripes between the bright STV stripes shall attribute to cohesive linkers. Scale bars: 100 nm.

3.3.5 Reconfiguration of DNA bundles

In nature, dynamic reconfiguration of fiber or bundle structures, like muscle fibers, is critical to perform cell or organ function. To mimic such processes, dynamic reconfiguration of artificial tubular nanostructures has been realized to fulfill various applications in previous work (36, 37). As our DNA bundle system may find certain applications in biomedical areas, herein we also want to integrate dynamic reconfigurability into our DNA bundle structures. We envision that by incorporating this reconfigurability, our system may further enrich the toolbox of dynamic DNA systems for future structural DNA nanotechnology research.

In our work, reconfigurability was implemented by using toehold-mediated strand displacement reactions to inhibit/activate binding between linkers and/or between sticky-ends. Tuning the binding between linkers can further tune the bundle assembly, and tuning the binding between sticky-ends can further tune the nanotube assembly. Figure 3-16 shows the basic scheme of this strategy. With the help of three sets of inhibitors (I) and anti-inhibitors (AI), three types of reversible transformations were demonstrated, which are between tube and tile, bundle and tube, or bundle and tile. All the transformations were carried out by first assembling the starting structure, then adding the corresponding I or AI strands to the reaction under room temperature. Agarose gel electrophoresis was first used to verify the transformation reactions, as the mobility change of corresponding bands is able to suggest the successful reconfigurations between DNA structures (Figure 3-16d). TEM was then used to directly visualize the structures before and after reconfigurations (Figure 3-17). Representative TEM images were chosen to reveal that all three types of reconfigurations were executed in a reversible manner. However, it is necessary to point out that the restored bundles had an average width of 91.3 nm (Restored from nanotubes. Figure 3-17b) or 80.2 nm (Restored from DX tiles. Figure 3-17c), both being slightly narrower than normally assembled bundles with an average width of 112.0 nm. We hypothesize that this difference is because the reconfiguration and

restoration process of DNA bundles was carried out under room temperature, which was less efficient than the normal thermal annealing process for DNA bundle assembly. Nevertheless, this result still demonstrates the successful incorporation of dynamic process into our DNA bundle system.

Furthermore, we combined this dynamic system with multi-component DNA bundle design to demonstrate the reconfiguration process' potency. Similar to the multi-component DNA bundle design previously, we designed distinct invader/anti-invader systems for each DX tile (Figure 3-18). Compared to the single-component DNA bundle system in the last paragraph, here the invader only blocked the linker, so the dynamic assembly process occurred between nanotube and DNA bundle stage in a stepwise manner. All three distinct cohesive linkers on DNA tiles (Tile C in blue, Tile D in orange, and Tile E in green) were initially inhibited by inhibitors, so only tubes were produced in the first place. When only the blue linker was activated by adding one anti-invader, due to the low bundling strength, only loose DNA bundles with defects were formed. Further activation of the orange and green linkers induced stronger inter-tube binding forces, and generally DNA bundles yielded after each activation became wider and more compact. TEM imaging was used to confirm the successful transformation, and an obvious difference between each stage was observed. These results demonstrate the potential of involving dynamic process in aforementioned applications on multi-component DNA bundle systems, including dynamic nanofabrication and nano-device.

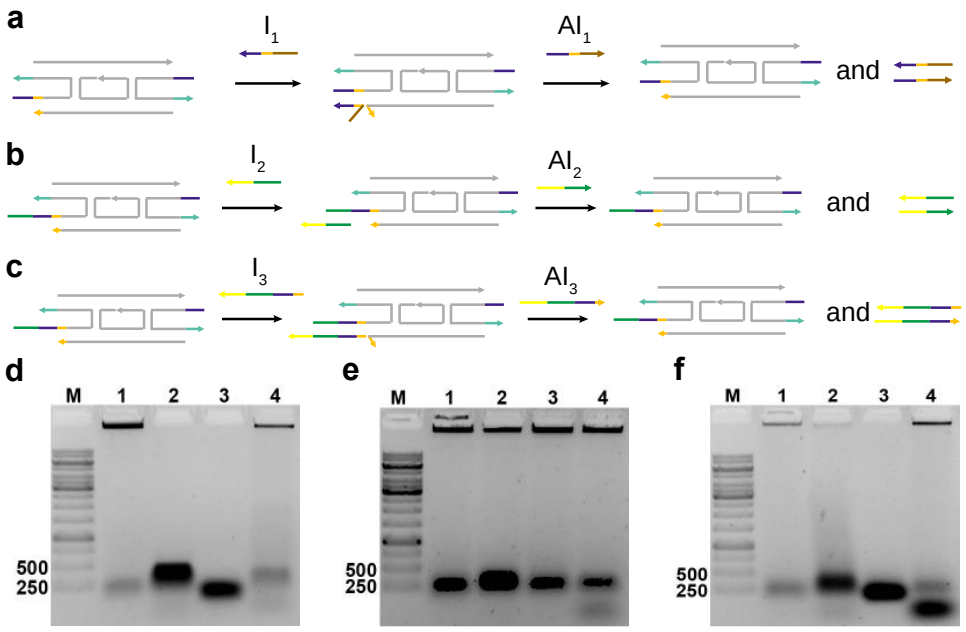

Figure 3-16. Schematics and gel electrophoresis for DNA bundle reconfigurations. (a, d) Reversible reconfigurations between DNA tubes and DNA tiles. An inhibitor strand (I1) is designed to disrupt sticky-end cohesion between tiles, which can be dislocated from the tile by the anti-inhibitor strand (AI1) via strand displacement reaction. (b, e) Reversible reconfigurations between DNA bundles and DNA tubes. An inhibitor strand (I2) is designed to disrupt linker binding between tubes, whose disruptive effect can be reversed by the anti-inhibitor strand (AI2). (c, f) Reversible reconfigurations between DNA bundles and DNA tiles. An inhibitor strand (I3) is designed to disrupt both sticky-end cohesion and linker binding, whose deconstructive effect can be neutralized by the anti-inhibitor strand (AI3). All gels share the same sample setup among all 5 lanes. M: DNA marker. Lane 1: Original assembly. Lane 2: Pre-annealed original assembly mixed with inhibitors and incubated under RT. Lane 3: original assembly annealed together with inhibitors. Lane 4: Lane 3's product mixed with anti-inhibitors and incubated under RT.

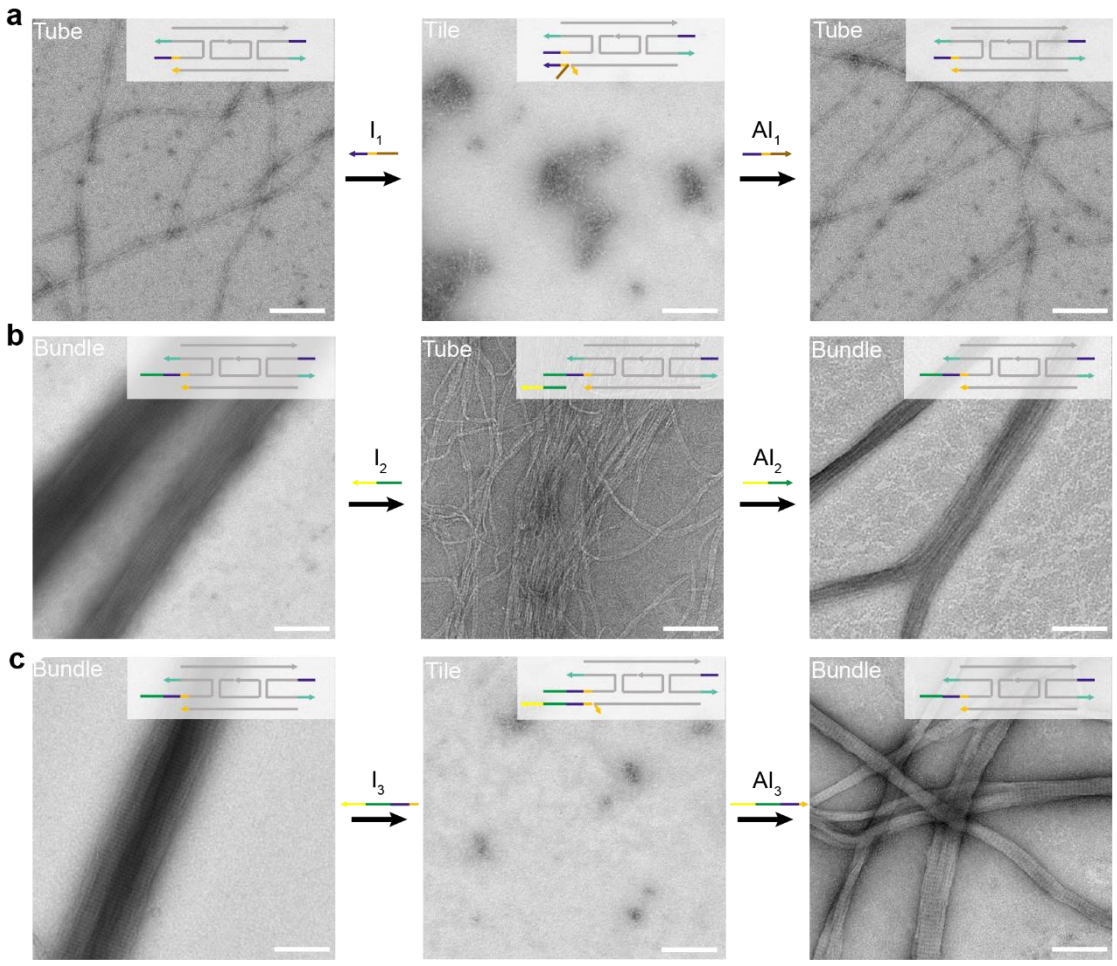

Figure 3-17. Representative TEM images showing the successful reconfiguration of DX tiles, nanotubes and bundles. (a) Reversible reconfiguration between tubes and tiles. (b) Reversible reconfiguration between bundles and tubes. (c) Reversible reconfiguration between bundles and tiles. Note: Tile A was used for these above experiments.

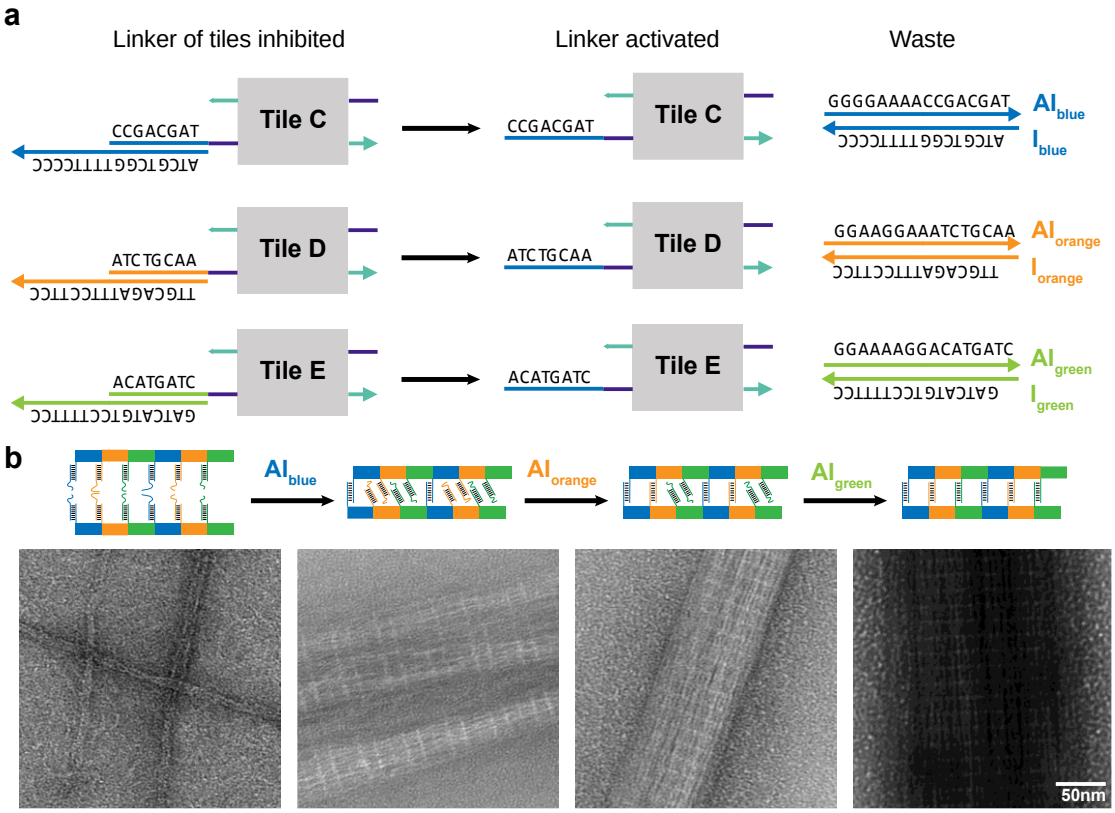

Figure 3-18. Sequentially activation of linkers for the transformation from DNA tubes to DNA bundles with prescribed features. (a) Schematics for linker inhibition and activation on various DNA tiles. (b) Representative TEM images showing the transformation result at each stage. Note that the assembly stage, the bundle compactness, and width are different among all figures. All figures share the same scale bar of 50 nm.

3.4 Conclusion

In this project, we developed a novel method for the self-assembly of DNA macro-structures that can be used to mimic naturally occurring fiber structures. The basic building block of this self-assembly process is the DX tile with a linker sequence. The assembly from DX tile to nanotube is tuned by sticky ends, and the assembly from nanotube to bundle is tuned by both linkers and Mg^{2+} concentration. The influence of linker's position, poly-T spacer length, and self-binding affinity on bundle assembly was investigated. Divalent metal ions, like Mg^{2+}, and annealing temperature were also tested to show synergistic influence on bundle assembly. Furthermore, several DX tiles with different backbone and linker sequence were designed to form multi-component bundles with higher complexity. Using such multi-component DNA bundle system, we confirmed that the white line crossing the bundle under TEM was rendered by linkers. These multicomponent DNA bundles were also employed in the fabrication of large AuNP and STV structures with prescribed patterns as determined by the bundle templates. Finally, we designed a reaction pathway where inhibitor and anti-inhibitor strands were used to dynamically control the assembly process from DX tile to bundle. Such dynamic reconfiguration process was also able to combine with the multi-component bundle design.

Recent research has shown the diverse applications of DNA nanotubes, including drug delivery , nanomachine , and nanofabrication (26, 29, 31). However, the use of DNA nanotubes is still confined by their low radial size and high flexibility (13). The self-assembled DNA bundle in this paper can serve as an alternative scaffold for such applications due to its several advantages. First of all, our strategy is simple and cost-effective, given that only five short DNA strands are needed for DNA bundle assembly. Previously reported large one-dimensional structures of comparable dimensions and controllability were mostly assembled from DNA origami or DNA brick units that are complex and expensive (21, 38). Secondly, DNA bundles with prescribed features constructed in this project may be readily achieved by inducing slight changes into

DNA tile designs owing to our strategy's high robustness and versatility. Thirdly, our DNA bundles exhibit versatile dynamic capability that can readily reconfigure among various conformations by using beforementioned novel molecular triggers. To our best knowledge, this might represent the first example of DNA tubular structures with such large dimensions that are capable of executing reversible transformations. Alongside the applications we demonstrated in this project, the DNA bundles still hold enormous application potential in various other fields. For example, the linkers on the bundle surface can serve as tracks for DNA walkers to simulate 3D walking process on the substrate. The high rigidity of the bundle also makes it an ideal scaffold for payloads when distance and relative position among them need precise control. We believe that our work not only develops a novel method to construct large-scale DNA macro-structure, but also provides inspiration for further research to produce next-generation micrometer-sized materials and machines.

3.5 Material and Methods

DNA strand preparation. All DNA strands involved in this paper were directly purchased either from Integrated DNA Technologies (IDT) or from Sangon Biotech (Shanghai) Co., Ltd. Strands ordered from these two companies were tested to show minimal difference in tests. For strands longer than 60nt, PAGE purification was ordered from the company. All strands were dissolved in deionized water to a final concentration of 100 uM for later use.

DNA sequence design. There are 3 parts in one DX tile: Backbone, sticky ends and linker. For Backbones, they are designed using a free software called DNA-Uniquimer, following the publisher's guideline (39). For sticky ends, they are generated as random sequences and ensured to be able to connect to the next tile. For linkers, they are designed according to the result of the investigation of linkers' length and binding affinity in the paper. Their orthogonality was tested using an online software called NUPACK (35).

NUPACK and oligoanalyzer simulation. The simulation on NUPACK was performed using the analysis tool on the website. Parameters were chosen to meet the actual reaction condition. This simulation is used to check the binding pattern of linkers and the orthogonality of DX tile strands. The simulation on oligoanalyzer was performed referencing to the guidance posted on IDT website. Parameters were chosen to meet the actual reaction condition. This simulation is used to check the binding pattern of linkers and their binding delta G value.

Annealing process. The assembly for all trials was carried out in 1× TE buffer with corresponding concentration of $MgCl_2$. The annealing process to assemble DX tiles, nanotubes and bundles for most trials in this paper was:

Step 1: Stay at 85°C for 10min.

Step 2: From 65°C to 25°C, decrease 0.1°C for every 10 min.

For specific trials, like the investigation of nanotube and bundle formation under different temperature, modifications were made accordingly. The annealing was carried out using Bio Rad C1000 Touch Thermal Cyclers.

One-pot and 2-step assembly of A-T bundles. For one-pot assembly, both DX tiles for A-tube and T-tube were mixed together in one tube and underwent the annealing process above-mentioned. For 2-step assembly, DX tiles for A-tube and T-tube were annealed in different tubes respectively. After annealing, the products were mixed into one tube and shaken under room temperature overnight.

Gold nanoparticle (AuNP) and Streptavidin (STV) conjugation on DNA bundles. The DNA bundle consisting of Tile J, K, L and M with corresponding cohesive linker and handle sequence was first annealed with normal annealing protocol. Then the annealed DNA bundle was then mixed with payloads and shaken under room temperature for 2 hours. For AuNP

conjugation, the functionalization of AuNP with Thiol-labeled single-strand DNA was carried out as in the previous reference (40). The thiol-DNA was first reduced with enough TCEP, then mixed with 10nm AuNP in 300:1 ratio. The mixture was frozen in -20 °C overnight, then thawed under room temperature for 1 hour. The solution was then centrifuged under 12000xg for 20min, then the supernatant was removed. The AuNP pallet was washed with water twice and additional centrifuge steps were used to remove water after each washing. The recovered AuNP was dissolved in 1xTE 20mM Mg^{2+} buffer and used at the ratio of 1:10 to DX tiles. For STV conjugation, STV was diluted into 1xTE 20mM Mg^{2+} buffer and used at the ratio of 1:5 to DX tiles.

10nm AuNP was ordered from Ted Pella. STV was ordered from New England Biolabs.

Dynamic control of the assembly process. For all inhibitor and anti-inhibitor reactions, two kinds of methods were tested. The first method was to mix the DX tile and the inhibitor/anti-inhibitor together, then underwent the annealing process. The second method was to anneal the starting structure (Tile, Tube or Bundle) first. Then inhibitor/anti-inhibitor was added and the tube was shaken under room or corresponding temperature overnight. The concentration of inhibitor added was 2 times of DX tile's, and the concentration of anti-inhibitor added was 2 times of invader's.

Transmission electron microscopy (TEM) imaging. For the sample preparation for TEM imaging, 3 μL sample was deposited on the surface charged carbon film coated copper EM grids for 30 seconds, then a filter paper was used to remove the excess liquid on the grid. 8 μL 1% uranyl formate (UF) solution was used for negative staining, and excess liquid was also removed with a filter paper after 20 seconds. The samples were imaged using a Hitachi HT-7700 120 kV W (Tungsten) TEM with AMT CCD camera. Note that the number of nanostructures shown on the images does not represent the actual yield of them, and the

brightness of the figures solely depend on the staining and imaging technique. To prepare the 1% UF solution, 10mg UF powder was dissolved in 1 mL DI water and heated to the point when no changes further appeared. Then 1 μL of 5 M NaOH was added to the solution and mixed well. The solution was further filtered using a 0.2 μm syringe filter with cellulose acetate membrane and the filtrate was collected. Copper EM grids were charged using Pelco easiGlow Glow Discharge Cleaning System. UF powder was purchased from Electron Microscopy Sciences. 5 M NaOH was purchased from Fisher Scientific. EM grids were purchased from Electron Microscopy Sciences, and the model of grids was CF400-CU. 0.2 μm syringe filter was purchased from VWR International.

Agarose gel electrophoresis. Nondenaturing agarose gel was prepared according to the standard protocol provided by Thermo Scientific. An 1% agarose gel was prepared with 0.5× TBE and 10mM Mg^{2+} for the separation of DX tiles and assembled nanotubes and bundles. 100ng sample was loaded in each well. The electrophoresis was carried out at 60V for 90 minutes and used ethidium bromide for staining. The gel was imaged using Bio-Rad Gel Doc EZ Imager.

Confocal microscopy imaging. Confocal images were obtained by confocal microscopy (Leica TCS SP8) with 63×/1.40 NA oil immersion objectives. For sample preparation, a 5 μL droplet (200 nM for bundles and 20nM for tubes) of sample were pipetted onto a glass slide and then covered by a coverslip. Tubes with fluorophores were imaged using corresponding laser exciter and filter.

Measuring the size of nanostructures using ImageJ. The size of the structures in TEM images was analyzed using ImageJ and plotted to exhibit the trend. A TEM image is evenly divided into 9 squares (3 by 3), and width of the bundle near the center of each square is measured. At least 25 data points were randomly selected for each group and their average

value was calculated and plotted. See Figure 3-19 for more details.

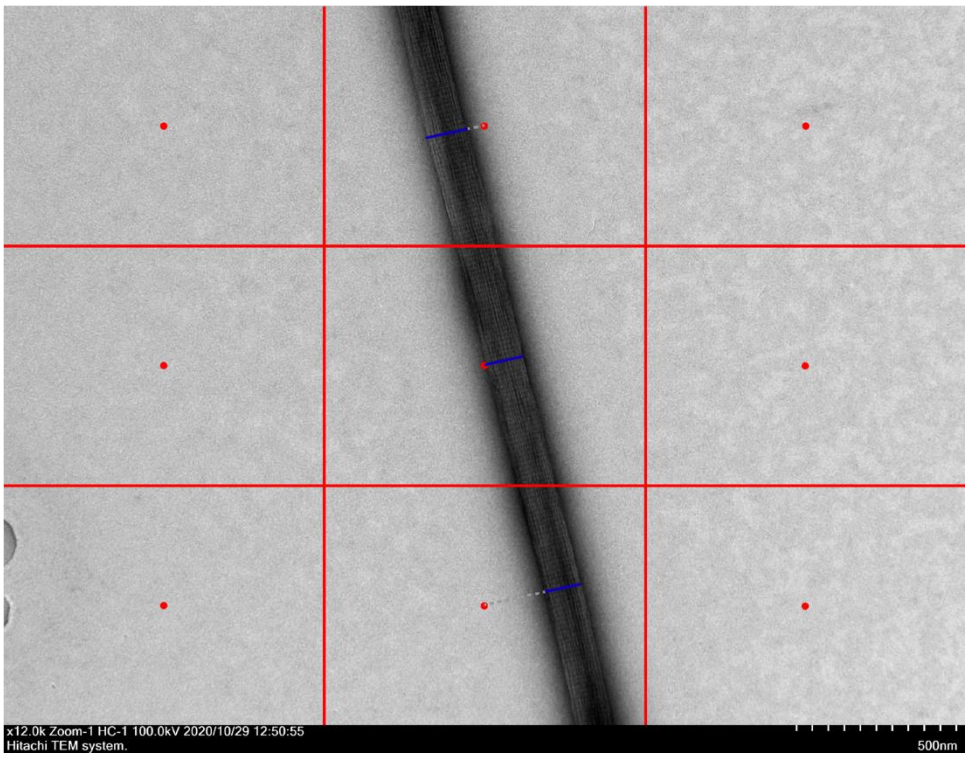

Figure 3-19. Measurement of bundle width using ImageJ. The original TEM image is evenly divided into 9 segments (Indicated by red lines). The center of each segment is labeled using red dots. In each segment, the bundle segment which is nearest to the center red dot (Indicated by grey dashed lines) is selected, and the width of selected bundle segment is measured (Indicated by blue lines). For each experimental group, at least 25 data points are collected through out multiple TEM images.

3.6 References

1. Fletcher DA, Mullins RD. Cell mechanics and the cytoskeleton. Nature. 2010;463(7280):485-92.

2. Hall A. The cytoskeleton and cancer. Cancer Metastasis Rev. 2009;28(1-2):5-14.

3. Han W, Chen S, Yuan W, Fan Q, Tian J, Wang X, et al. Oriented collagen fibers direct tumor cell intravasation. Proc Natl Acad Sci U S A. 2016;113(40):11208-13.

4. Gardner MK, Charlebois BD, Janosi IM, Howard J, Hunt AJ, Odde DJ. Rapid microtubule self-assembly kinetics. Cell. 2011;146(4):582-92.

5. Brieher W. Mechanisms of actin disassembly. Mol Biol Cell. 2013;24(15):2299-302.

6. Mukund K, Subramaniam S. Skeletal muscle: A review of molecular structure and function, in health and disease. Wiley Interdiscip Rev Syst Biol Med. 2020;12(1):e1462.

7. Zhang N, Milbreta U, Chin JS, Pinese C, Lin J, Shirahama H, et al. Biomimicking Fiber Scaffold as an Effective In Vitro and In Vivo MicroRNA Screening Platform for Directing Tissue Regeneration. Adv Sci (Weinh). 2019;6(9):1800808.

8. Zhan P, Jahnke K, Liu N, Gopfrich K. Functional DNA-based cytoskeletons for synthetic cells. Nat Chem. 2022;14(8):958-63.

9. Derr ND, Goodman BS, Jungmann R, Leschziner AE, Shih WM, Reck-Peterson SL. Tug-of-war in motor protein ensembles revealed with a programmable DNA origami scaffold. Science. 2012;338(6107):662-5.

10. Ke Y, Castro C, Choi JH. Structural DNA Nanotechnology: Artificial Nanostructures for Biomedical Research. Annu Rev Biomed Eng. 2018;20:375-401.

11. Zhan P, Peil A, Jiang Q, Wang D, Mousavi S, Xiong Q, et al. Recent Advances in DNA Origami-Engineered Nanomaterials and Applications. Chem Rev. 2023;123(7):3976-4050.

12. Hong F, Zhang F, Liu Y, Yan H. DNA Origami: Scaffolds for Creating Higher Order Structures. Chem Rev. 2017;117(20):12584-640.

13. Xin Y, Shen B, Kostiainen MA, Grundmeier G, Castro M, Linko V, et al. Scaling Up DNA Origami Lattice Assembly. Chemistry. 2021;27(33):8564-71.

14. Wang P, Gaitanaros S, Lee S, Bathe M, Shih WM, Ke Y. Programming Self-Assembly of DNA Origami Honeycomb Two-Dimensional Lattices and Plasmonic Metamaterials. J Am Chem Soc. 2016;138(24):7733-40.

15. Liu W, Zhong H, Wang R, Seeman NC. Crystalline two-dimensional DNA-origami arrays. Angew Chem Int Ed Engl. 2011;50(1):264-7.

16. Wagenbauer KF, Sigl C, Dietz H. Gigadalton-scale shape-programmable DNA assemblies. Nature. 2017;552(7683):78-83.

17. Tikhomirov G, Petersen P, Qian L. Fractal assembly of micrometre-scale DNA origami arrays with arbitrary patterns. Nature. 2017;552(7683):67-71.

18. Zhang Z, Yang Y, Pincet F, Llaguno MC, Lin C. Placing and shaping liposomes with reconfigurable DNA nanocages. Nat Chem. 2017;9(7):653-9.

19. Liu W, Halverson J, Tian Y, Tkachenko AV, Gang O. Self-organized architectures from assorted DNA-framed nanoparticles. Nat Chem. 2016;8(9):867-73.

20. Ong LL, Hanikel N, Yaghi OK, Grun C, Strauss MT, Bron P, et al. Programmable self-assembly of three-dimensional nanostructures from 10,000 unique components. Nature. 2017;552(7683):72-7.

21. Yao G, Zhang F, Wang F, Peng T, Liu H, Poppleton E, et al. Meta-DNA structures. Nat Chem. 2020;12(11):1067-75.

22. Fu TJ, Seeman NC. DNA double-crossover molecules. Biochemistry. 1993;32(13):3211-20.

23. Jorgenson TD, Mohammed AM, Agrawal DK, Schulman R. Self-Assembly of Hierarchical DNA Nanotube Architectures with Well-Defined Geometries. ACS Nano. 2017;11(2):1927-36.

24. Mohammed AM, Sulc P, Zenk J, Schulman R. Self-assembling DNA nanotubes to connect molecular landmarks. Nat Nanotechnol. 2017;12(4):312-6.

25. Green LN, Subramanian HKK, Mardanlou V, Kim J, Hariadi RF, Franco E. Autonomous dynamic control of DNA nanostructure self-assembly. Nat Chem. 2019;11(6):510-20.

26. Yang D, Wang P. A DNA-Based Molecular System That Can Autonomously Add and Extract Components. ACS Appl Mater Interfaces. 2021;13(34):41004-11.

27. Del Grosso E, Prins LJ, Ricci F. Transient DNA-Based Nanostructures Controlled by Redox Inputs. Angew Chem Int Ed Engl. 2020;59(32):13238-45.

28. Gentile S, Del Grosso E, Pungchai PE, Franco E, Prins LJ, Ricci F. Spontaneous Reorganization of DNA-Based Polymers in Higher Ordered Structures Fueled by RNA. J Am Chem Soc. 2021;143(48):20296-301.

29. Liang L, Shen JW, Wang Q. Molecular dynamics study on DNA nanotubes as drug delivery vehicle for anticancer drugs. Colloids Surf B Biointerfaces. 2017;153:168-73.

30. Lin C, Ke Y, Liu Y, Mertig M, Gu J, Yan H. Functional DNA nanotube arrays: bottom-up meets top-down. Angew Chem Int Ed Engl. 2007;46(32):6089-92.

31. Ranasinghe DR, Aryal BR, Westover TR, Jia S, Davis RC, Harb JN, et al. Seeding, Plating and Electrical Characterization of Gold Nanowires Formed on Self-Assembled DNA Nanotubes. Molecules. 2020;25(20).

32. Burns JR. Introducing Bacteria and Synthetic Biomolecules along Engineered DNA Fibers. Small. 2021;17(25):e2100136.

33. Zhang Y, Yang D, Wang P, Ke Y. Building Large DNA Bundles via Controlled Hierarchical Assembly of DNA Tubes. ACS Nano. 2023;17(11):10486-95.

34. Rothemund PW, Ekani-Nkodo A, Papadakis N, Kumar A, Fygenson DK, Winfree E. Design and characterization of programmable DNA nanotubes. J Am Chem Soc.

2004;126(50):16344-52.

35. Zadeh JN, Steenberg CD, Bois JS, Wolfe BR, Pierce MB, Khan AR, et al. NUPACK: Analysis and design of nucleic acid systems. J Comput Chem. 2011;32(1):170-3.

36. Zhang DY, Hariadi RF, Choi HM, Winfree E. Integrating DNA strand-displacement circuitry with DNA tile self-assembly. Nat Commun. 2013;4:1965.

37. Agarwal S, Klocke MA, Pungchai PE, Franco E. Dynamic self-assembly of compartmentalized DNA nanotubes. Nat Commun. 2021;12(1):3557.

38. Ke Y, Ong LL, Sun W, Song J, Dong M, Shih WM, et al. DNA brick crystals with prescribed depths. Nat Chem. 2014;6(11):994-1002.

39. Wang W, Chen S, An B, Huang K, Bai T, Xu M, et al. Complex wireframe DNA nanostructures from simple building blocks. Nat Commun. 2019;10(1):1067.

40. Hao Y, Li Y, Song L, Deng Z. Flash Synthesis of Spherical Nucleic Acids with Record DNA Density. J Am Chem Soc. 2021;143(8):3065-9.

Chapter 4. Summary and perspectives

4.1 Summary for the thesis

Structural DNA nanotechnology is the art of using synthetic or biological DNA strands as basic building blocks for the construction of artificial nanostructures through self-assembly. After tens of years of development, structural DNA nanotechnology has demonstrated unprecedented capability in constructing nanostructures with high complexity, versatility, and programmability. Besides, the capability to endow environment-responsive properties on nanostructures has highlighted structural DNA nanotechnology upon other construction methods (1, 2). These self-assembled DNA nanostructures have been extensively utilized in various research areas, including nanomachine, nanofabrication, and biomedical research (3). However, despite the extraordinary strength of structural DNA nanotechnology, there are still several directions that require further improvement, and such improvement sometimes could be challenging. In this thesis, we focused on the following challenges: Novel DNA nanostructure construction and DNA nanostructure scaling.

In chapter 2, we focused on the novel DNA nanostructure construction. In a large number of previously assembled DNA nanostructures, the main body of the structure is built by sole DNA or oligonucleotides. On the other hand, by conjugating DNA strands to other molecules or particles to become DNA block copolymers (DBCs), new interactions can be introduced to DNA strands, which may result in novel assembly mechanisms. In this project, we extensively investigated the assembly of cholesterol-DNA (chol-DNA) block copolymer. We discovered that under acidic conditions, chol-DNA with certain DNA sequences could form micellular nanostructures, including spherical micelles and nanorods. Extensive study was carried out to confirm that the morphology of the assembly was mainly controlled by salt concentration, solution pH, and DNA sequence. The assembly process of chol-DNA DBC was revealed to be

a hierarchical pathway, where nanorods were the result of incomplete merging of spherical micelles. To our best knowledge, this is the first report to show the assembly of sole chol-DNA DBC and the novel hierarchical merging pathway. Thinking of the popularity of using DBC to construct amphiphilic nano-vehicle for drug delivery in recent years, we believe that our work can provide valuable reference on new design principles and assembly mechanisms for future DBC investigations. This project was published on Bioconjugate Chemistry (4).

In chapter 3, we focused on DNA nanostructure scaling. One of the major merits of structural DNA nanotechnology is the unrivaled capability of building nanoscale artificial structures. However, a simple but versatile constructing method to assemble large-scale DNA structures, for example, from nanoscale to microscale, is still challenging. In this work, we designed a simple yet straightforward nanostructure scaling system where double-crossover (DX) tiles first assemble into nanotubes, then nanotubes further assemble into micrometer-scale rigid DNA bundles. The assembly mechanism of this system is a hierarchical pathway mainly enabled by the flanking cohesive linker design. Along with the buffer conditions, such cohesive linkers provide the capability to better control the major assembly parameters including width, compactness, constitution, and reconfigurability. DNA bundles with high complexity on constitution and reversible assembly process were also presented, and these two properties were able to be further combined into one design. We also included one illustration of this system's application by fabricating gold nanoparticles and streptavidin on DNA bundles with prescribed patterns. We envision that this project can provide strategies for future rational design on constructing macro-sized biomimetic functional materials, and the DNA bundle structure fabricated in this project can potentially find various applications in materials science, synthetic biology, and biomedical research. This project was published on ACS Nano (5).

4.2 Future perspectives of the thesis

4.2.1 Hierarchical Self-Assembly of Cholesterol-DNA Nanorods

In chapter 2, we reported a novel self-assembly of micelles and nanorods from Cholesterol-DNA block co-polymers under acidic conditions. During the investigation, the identity of the black gaps periodically appeared on the nanorods was extensively researched, and it was believed to be caused by incomplete merge of the spherical micelles. We hypothesized that the relatively small volume of the cholesterol hydrophobic cores and the interactions between DNA strands led to this incomplete merge. However, this hypothesis still requires further investigation.

In the future, based on the same system, we will design experiments to confirm this hypothesis. However, currently, we don't have other candidates that can show the same assembly pathway as cholesterol-DNA block copolymer. Thus, we will firstly try other hydrophobic modifications on DNA strands to check if such novel assembly pathway can be applied to a wider range of DBC constitutions and reaction conditions. After this, the comparison of the size difference between hydrophobic core and hydrophilic DNA shell among all candidates will possibly demonstrate a trend for the black gap appearance, which will ultimately validate our hypothesis.

We envision that our current work not only further proves the versatility of amphiphilic DBCs, but also provides insights on new design principles and assembly mechanisms for future investigations. If the previously proposed experiment works in the follow-up investigations, we believe that such design principle could even become a widely used standard in structural DNA nanotechnology towards biomedical research.

4.2.2 Building Large DNA Bundles via Controlled Hierarchical Assembly of DNA Tubes

In chapter 3, we developed a simple yet versatile molecular assembling strategy for the rational fabrication of long and wide DNA bundle structures of defined spatial features and dynamic

capabilities. The current assembling system exhibits several noteworthy advantages in terms of fabricating DNA bundle structures with such large dimensions and versatile functionalities. First, it is simple and cost-effective, given that only five short DNA strands are needed for DNA bundle assembly. Previously reported large one-dimensional structures of comparable dimensions and controllability were mostly assembled from DNA origami or DNA brick units that is complex and expensive (6). The work by Burns employed high concentrations of cations to condense tubes into bundles, which lacks rational control over bundle features, and a high cationic strength may limit the subsequent applications of bundles (7). Second, DNA bundles of prescribed features may be readily achieved via inducing slight changes into DNA tile designs, which is simple, robust, and versatile. Third, our DNA bundles exhibit a versatile dynamic capability that can readily reconfigure among various conformations by using specific molecular triggers (5).

During the investigation, we also found that by substituting the inserted cohesive linkers with other moieties, interesting phenomena will occur on the final assembled structures. For example, by substituting the cohesive linkers with poly-T hairpins, and move the insertion spots to strand 5, although the bundling process is interrupted due to the low binding strength between poly-T hairpins, the assembly of DNA nanotubes are significantly changed. Compared to normal assembly pattern of DX tiles on DNA nanotubes, where DX tiles are aligned parallelly to the longitude of DNA nanotubes, in the situation where poly-T hairpins are inserted, the assembly pattern of DX tiles rotate 90 degrees to become perpendicular to the longitude of DNA nanotubes. This change on the assembly pattern results in a much wider DNA nanotube product, with white stripes on nanotube surface rendered by the alignment of poly-T hairpins (Figure 4-1). To our best knowledge, this is the first time that such novel assembly pattern is reported. Currently, we are still putting much effort into the investigation of this phenomenon.

With their large sizes and capability of reversible transformations, the DNA bundles and wide DNA nanotubes reported hold great application potential in various fields. For example, they may serve as biomimetic cellular skeletons for constructing artificial cells or organelles for synthetic biology studies. Or they may be used as templates to direct the assembly of functional materials forming macroscopic materials with emerging properties. They may also find utility in building artificial tissues such as muscle fibers (5). We believe that our work not only develops a novel method to construct large-scale DNA macro-structure, but also provides inspirations for further research to produce next generation micrometer sized materials and machines.

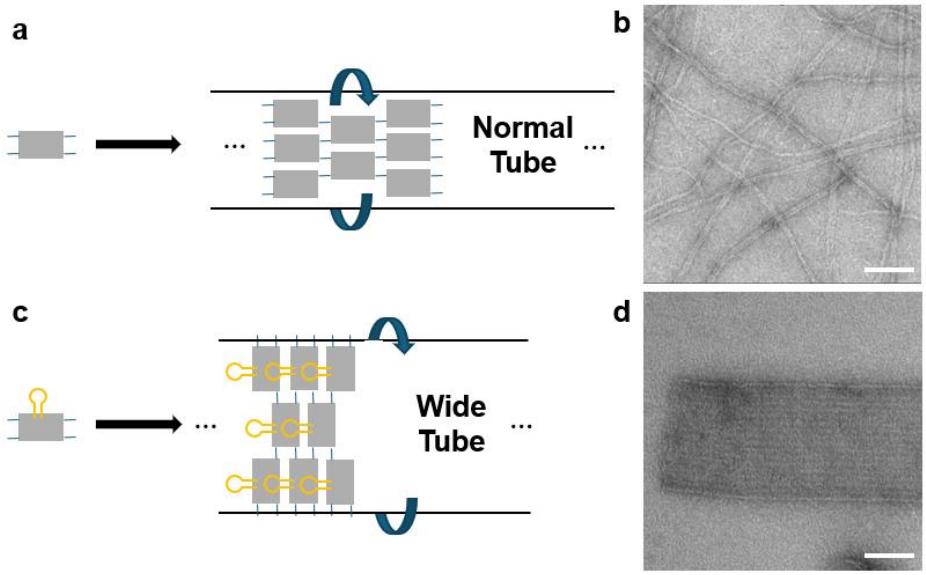

Figure 4-1. Assembly of wide nanotube from DX tiles with poly-T hairpin insertion. (a) Normal nanotube assembly pattern. The grey rectangles are DX tile backbones. The blue lines are sticky ends. The DX tiles are aligned parallelly to the longitude of nanotubes. (b) Representative TEM images of normal nanotubes. (c) Wide nanotube assembly pattern. The grey rectangles are DX tile backbones. The blue lines are sticky ends. The yellow lines are inserted poly-T hairpins. The DX tiles are aligned perpendicularly to the longitude of nanotubes. (d) Representative TEM images of wide nanotubes. All TEM images share the same scale bar: 100nm.

4.3 Other projects related to the application of structural DNA nanotechnology in biomedical research

Besides these two works, during my graduate study, we also conducted other research focusing on other challenges, including the optimization of drug delivery and cancer targeting of DNA nanostructures, the combination of structural DNA nanotechnology with other enzyme-based molecular biology techniques, and the transfer from DNA nanostructure to RNA nanostructure. These projects were either unfinished, discontinued, or only partially contributed by me. Thus, they are not discussed in this thesis in detail. In the following sections, some of these projects will be briefly introduced.

4.3.1 Development of novel dual-targeting immune checkpoint inhibitors for cancer therapy using DNA nanotechnology

Cancer immunotherapy is a powerful treatment that stimulates immune system to attack tumors (8). One recent development of promising strategies to activate antitumor immunity is the blockade of immune checkpoints by DNA aptamers (9). Although the antibody-based checkpoint inhibitors have shown reasonable antitumor effects in several types of cancers, the therapeutic efficacy of these antibodies is still suboptimal and needs new research to more potential novel strategies. Compared to antibodies, DNA aptamers have a wider target range due to the ease of producing a large variety of strands with different lengths and sequences. However, the therapeutic efficacy of these aptamers was hindered by their limited in vivo stability, sometimes low affinity, and the lack of efficient in vivo delivery systems to overcome biological barriers (i.e., entering circulation or target tissue) (10, 11).

To address these challenges, this project will use DNA-aptamer nanoparticles (DANPs) formulated via DNA nanotechnology to deliver DNA aptamers blocking PD-L1 and PD-1 interaction for potential immunotherapy (Figure 4-2). We have two long-term goals for this

project: One is to develop a DANP system with more effective immunotherapy with low or minimal cytotoxicity, and another one is to employ the newly exploited geometry and multi-valency effect on the formulation of DANP system to enhance the overall therapeutic effect (12-15).

This is currently an ongoing project. At the current stage, we have selected PD-1/PD-L1 aptamers as payloads, and the binding affinity to their corresponding targets has been extensively tested. Besides, we have formulated a library of DNA nanoparticles to conjugate with aptamers to form DANPs. These DNA nanoparticles and resulting DANPs were characterized using various analytical techniques. In our future plan, we will start testing these DANP's binding affinity to T cells and CD11b+ myeloid cells. We envisage the project to have a transformative impact beyond the project, because such a system can not only be utilized in the treatment of certain cancer types in clinical trials, but also be promoted to investigate other drug delivery-related goals and provide valuable feedback for future DNA nanostructure design with complex morphology and function.

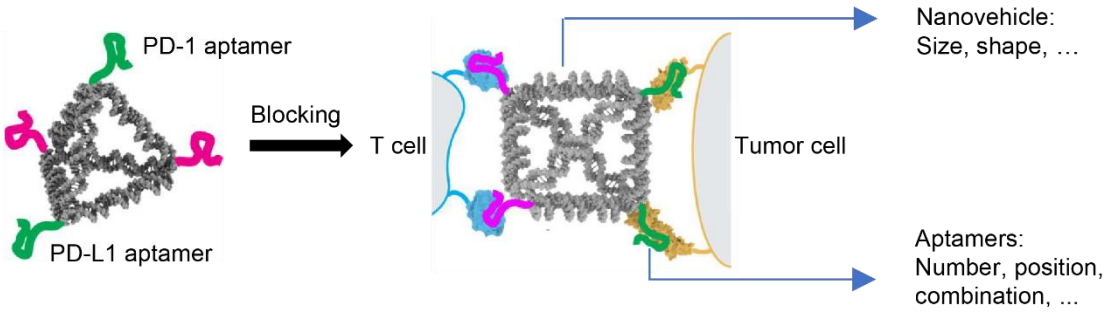

Figure 4-2. Development of dual-targeting immune checkpoint inhibitors based on DNA-aptamer nanoparticles for cancer therapy.

4.3.2 Programmable site-specific functionalization of DNA origami with polynucleotide brushes

DNA nanostructures, including DNA origami, have been extensively utilized in various biomedical applications (2). However, the utilization of DNA nanostructures in real biological environments, such as cells and mouse models, is usually compromised by the tendency of denaturation caused by unfavorable buffer conditions, nuclease degradation, and innate immune response (16). A potential strategy to walk around this challenge is by coating the DNA nanostructure with other shielding reagents, including lipid bilayers, proteins, and synthetic polymers (17-19). However, the shielding capability of these reagents is still limiting confronting the changing and disrupting of biological environments. Furthermore, the tunable and site-specific functionalization of these shielding reagents on DNA nanostructures is still challenging.

In this project, we realized the site-specific functionalization and shielding of DNA nanostructures by employing a novel enzyme-based method: Terminal deoxynucleotidyl polymerase (Tdt) catalyzed enzymatic polymerization of nucleotides and nucleotide analogues (Figure 4-3). By employing this method, the patterned "polynucleotide brush" grown under the catalysis of Tdt was precisely controlled over multiple parameters, resulting in a set of shielded DNA nanostructures. These shielded nanostructures demonstrated substantially higher enzymatic degradation resistance compared to their unshielded counterparts. We envision that this work can provide valuable references for future design of DNA nanostructure-based drug delivery systems. Furthermore, this Tdt-based system may find interesting applications in the construction of next-generation biosensors and microreactors.

This work was published on Angewandte Chemie (20). In this project, I contributed to the design of DNA origami core structures and the test of Tdt polymerizations on DNA origami.

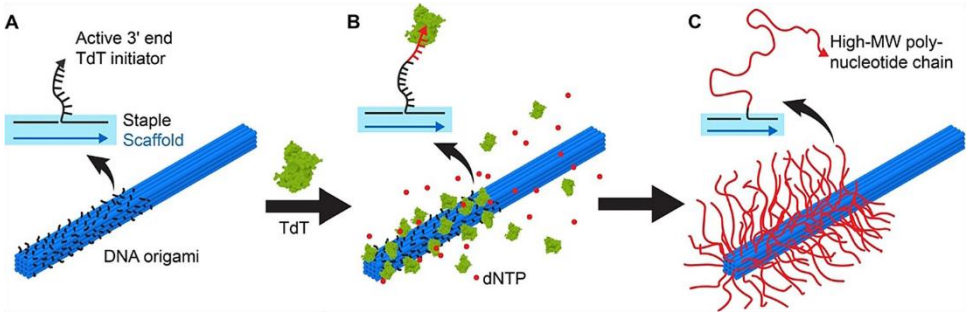

Figure 4-3. Programmable site-specific functionalization of DNA origami with polynucleotide brushes. Reprinted with permission.

4.3.3 Systemic delivery of Bcl2-targeting shRNA by single-stranded RNA nanoparticles

RNA interference (RNAi) is a promising cancer therapy process in which short RNA molecules are utilized to suppress target gene expression by forming sequence-specific double-stranded RNA (21). One of the most commonly used RNAi agents is the short interfering RNA (siRNA); However, limited success has been achieved in the systemic administration of siRNA due to a set of biological barriers, such as kidney filtration and nuclease degradation (22). In one of the previous projects in Ke lab, DNA nano-vehicles bearing Bcl2-targeting siRNA were designed and demonstrated successful uptake and target gene silencing in cancer cells (23). Owing to the homogeneous and versatile nature of DNA nanostructures, this work offered great potential for future systemic delivery of RNAi agents.

Based on this work, we further came up with a new strategy using single-stranded RNA nanoparticles (ssRNPs) as the delivery vehicle for small hairpin RNA (shRNA) (Figure 4-4a). An shRNA can be treated as a siRNA linked with a tight hairpin turn that can still be used to silence target gene expression while possessing higher stability (24). When delivering shRNA, compared to conventional DNA-based vehicles, ssRNPs' constitution is more homogeneous and seamless, thus increasing the resistance of RNA interference agents to degradation (25). Furthermore, the single RNA strand used for the self-folding into tetrahedron was produced by one-step *in vitro* transcription from DNA templates. Thus, compared to multi-stranded DNA nanostructures, the cost for strands and the workload for assembly preparation may be decreased.

For this project, we have successfully transcribed the single-stranded RNA for self-folding. We did preliminary characterization of the folded RNA nanostructure and western blotting to show the silencing effect of shRNA-bearing RNA nanostructure. However, this project was

discontinued due to the difficulty of solving the low enzymatic resistance issue of RNA nanostructure.

During the investigation, we also noticed that sometimes the transcription efficiency of RNA single strand is not satisfying due to the high complicity of the template sequence. Inspired by alphavirus genome-based self-amplifying mRNA vaccine, we proposed a method to fast produce RNA single strands for ssRNP construction (Figure 4-4b). Owing to its unique replicase, alphavirus possesses an RNA-to-RNA amplification process, which has been realized in both mammalian and bacterial cells (26, 27). We anticipate that by substituting the capsid protein gene with the ssRNP sequence of interest, we can gain improved efficiency in producing complex RNA single strands. Up to now, we have successfully constructed the plasmid with alphavirus replicase gene and the RNA tetrahedron sequence. We have also successfully transfected reconstructed plasmids into bacterial cells. However, due to the discontinuation of single-stranded RNA nanostructure project, this project was also discontinued.

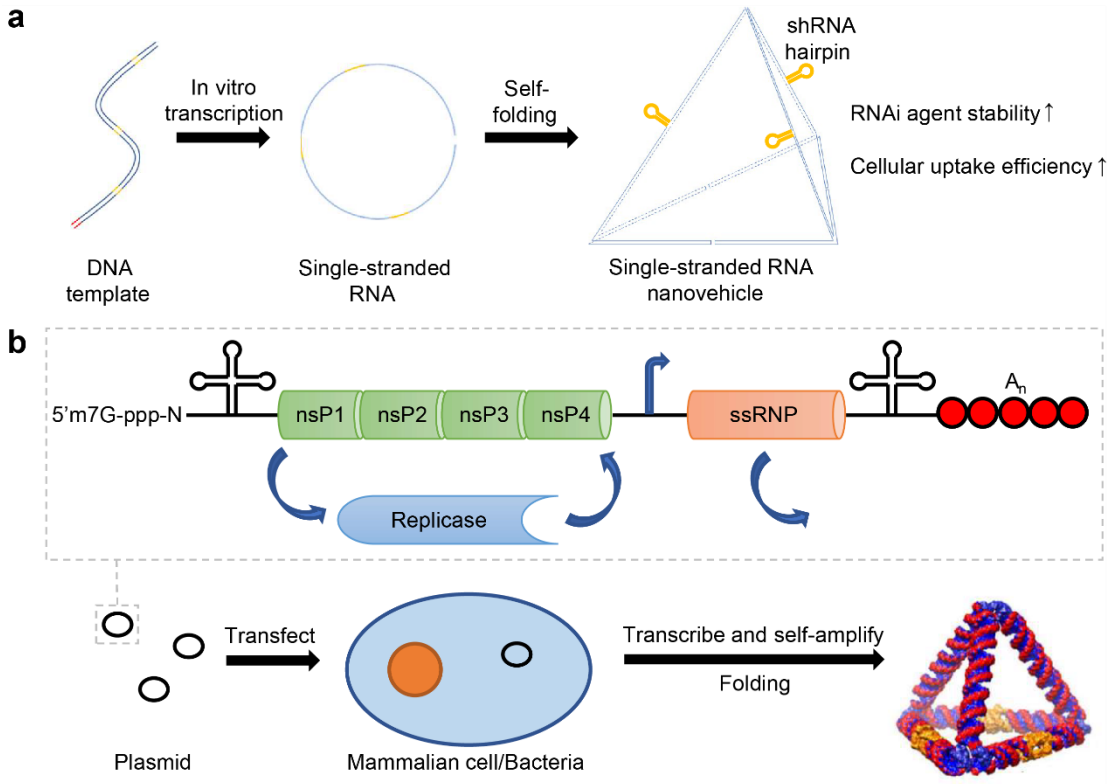

Figure 4-4. From DNA nanostructure to RNA nanostructure. (a) Development of single-stranded RNA nanostructure through in vitro transcription for shRNA hairpin delivery. (b) Fast production of RNA nanostructure inspired by alphavirus genome-based self-amplifying mRNA vaccine.

4.4 References

1. Hong F, Zhang F, Liu Y, Yan H. DNA Origami: Scaffolds for Creating Higher Order Structures. Chem Rev. 2017;117(20):12584-640.

2. Ke Y, Castro C, Choi JH. Structural DNA Nanotechnology: Artificial Nanostructures for Biomedical Research. Annu Rev Biomed Eng. 2018;20:375-401.

3. Zhan P, Peil A, Jiang Q, Wang D, Mousavi S, Xiong Q, et al. Recent Advances in DNA Origami-Engineered Nanomaterials and Applications. Chem Rev. 2023;123(7):3976-4050.

4. Zhang Y, Peng R, Xu F, Ke Y. Hierarchical Self-Assembly of Cholesterol-DNA Nanorods. Bioconjug Chem. 2019;30(7):1845-9.

5. Zhang Y, Yang D, Wang P, Ke Y. Building Large DNA Bundles via Controlled Hierarchical Assembly of DNA Tubes. ACS Nano. 2023;17(11):10486-95.

6. Wang PF, Meyer TA, Pan V, Dutta PK, Ke YG. The Beauty and Utility of DNA Origami. Chem-Us. 2017;2(3):359-82.

7. Burns JR. Introducing Bacteria and Synthetic Biomolecules along Engineered DNA Fibers. Small. 2021;17(25):e2100136.

8. Schuster M, Nechansky A, Kircheis R. Cancer immunotherapy. Biotechnol J. 2006;1(2):138-47.

9. Zhang Y, Lai BS, Juhas M. Recent Advances in Aptamer Discovery and Applications. Molecules. 2019;24(5).

10. Lakhin AV, Tarantul VZ, Gening LV. Aptamers: problems, solutions and prospects. Acta Naturae. 2013;5(4):34-43.

11. Hu Q, Li H, Wang L, Gu H, Fan C. DNA Nanotechnology-Enabled Drug Delivery Systems. Chem Rev. 2019;119(10):6459-506.

12. Simone EA, Dziubla TD, Muzykantov VR. Polymeric carriers: role of geometry in drug delivery. Expert Opin Drug Deliv. 2008;5(12):1283-300.

13. Wang P, Ke Y. Attack on the Cell Membrane: The Pointy Ends of DNA Nanostructures Lead the Way. ACS Cent Sci. 2018;4(10):1298-9.

14. Wang P, Rahman MA, Zhao Z, Weiss K, Zhang C, Chen Z, et al. Visualization of the Cellular Uptake and Trafficking of DNA Origami Nanostructures in Cancer Cells. J Am Chem Soc. 2018;140(7):2478-84.

15. Talevi A. Multi-target pharmacology: possibilities and limitations of the "skeleton key approach" from a medicinal chemist perspective. Front Pharmacol. 2015;6:205.

16. Jiang Q, Liu S, Liu J, Wang ZG, Ding B. Rationally Designed DNA-Origami Nanomaterials for Drug Delivery In Vivo. Adv Mater. 2019;31(45):e1804785.

17. Perrault SD, Shih WM. Virus-inspired membrane encapsulation of DNA nanostructures to achieve in vivo stability. ACS Nano. 2014;8(5):5132-40.

18. Ponnuswamy N, Bastings MMC, Nathwani B, Ryu JH, Chou LYT, Vinther M, et al. Oligolysine-based coating protects DNA nanostructures from low-salt denaturation and nuclease degradation. Nat Commun. 2017;8:15654.

19. Wang ST, Gray MA, Xuan S, Lin Y, Byrnes J, Nguyen AI, et al. DNA origami protection and molecular interfacing through engineered sequence-defined peptoids. Proc Natl Acad Sci U S A. 2020;117(12):6339-48.

20. Yang Y, Lu Q, Huang CM, Qian H, Zhang Y, Deshpande S, et al. Programmable Site-Specific Functionalization of DNA Origami with Polynucleotide Brushes. Angew Chem Int Ed Engl. 2021;60(43):23241-7.

21. Agrawal N, Dasaradhi PV, Mohmmed A, Malhotra P, Bhatnagar RK, Mukherjee SK. RNA interference: biology, mechanism, and applications. Microbiol Mol Biol Rev. 2003;67(4):657-85.

22. Setten RL, Rossi JJ, Han SP. The current state and future directions of RNAi-based therapeutics. Nat Rev Drug Discov. 2019;18(6):421-46.

23. Rahman MA, Wang P, Zhao Z, Wang D, Nannapaneni S, Zhang C, et al. Systemic Delivery of Bc12-Targeting siRNA by DNA Nanoparticles Suppresses Cancer Cell Growth. Angew Chem Int Ed Engl. 2017;56(50):16023-7.

24. Paddison PJ, Caudy AA, Bernstein E, Hannon GJ, Conklin DS. Short hairpin RNAs (shRNAs) induce sequence-specific silencing in mammalian cells. Genes Dev. 2002;16(8):948-58.

25. Brummelkamp TR, Bernards R, Agami R. A system for stable expression of short interfering RNAs in mammalian cells. Science. 2002;296(5567):550-3.

26. Pietila MK, Hellstrom K, Ahola T. Alphavirus polymerase and RNA replication. Virus Res. 2017;234:44-57.

27. Atkins GJ, Fleeton MN, Sheahan BJ. Therapeutic and prophylactic applications of alphavirus vectors. Expert Rev Mol Med. 2008;10:e33.